Selective oxidation of methane in a trickle bed reactor over a platinum-based catalyst

Dissertation submitted in partial fulfilment of the requirements for the degree of

Master of Science in Engineering in Chemical Engineering

Prepared by:

Nasseela Hytoolakhan Lal Mahomed

Supervised by:

Professor Eric van Steen

Catalysis Institute

Department of Chemical Engineering

University of Cape Town

February 2022

Declaration

I know the meaning of plagiarism and declare that all the work in the document, save for that which is properly acknowledged, is my own. This thesis/dissertation has been submitted to the Turnitin module (or equivalent similarity and originality checking software) and I confirm that my supervisor has seen my report and any concerns revealed by such have been resolved with my supervisor.

Signed by candidate

Nasseela Hytoolakhan Lal Mahomed

13 February 2022

Acknowledgements

First and foremost, praises and thanks to God, the Almighty for his blessings and guidance throughout my journey in completing this dissertation.

I would like to gratefully acknowledge the efforts and support of the following individuals and institutions who were instrumental in the development of this research endeavour:

Professor Eric van Steen for the constant guidance provided and knowledge shared throughout this research project. I am extremely thankful for being given the extraordinary opportunity to conduct this research under his supervision. Thank you sincerely, Professor Eric van Steen, for believing in me when I did not myself, for always being supportive and patient. All the invaluable interactions and discussions we had together have instilled in me the confidence and passion for continuing research

My Parents and family for their unconditional love and support throughout my entire academic journey without whom this research project would not have been possible. I am beyond grateful to my parents for all their sacrifices, for always believing in me and encouraging me in all of my pursuits

Adam Oodally for always being by my side, cheering me up whenever things went south and for being so understanding and supportive of my endeavours. The completion of this project would certainly not have been possible without your contributions. I cannot thank you enough for that and I will forever be in your debt

Friends and colleagues for all the support, care and love throughout this journey. A special thanks to Naomi Harrisankar who made my days at UCT filled with enjoyable moments and for always feeding me with chocolate croissants, cakes and snacks during tea breaks. Thank you to Dominic de Oliveira for helping me fix my electrical issues in the laboratory. I would like to extend my gratitude to Junfeng Guo, a great reactor engineering mentor and for assisting me in the design stage of this project. Thank you Sinqobile Vuyisile Mahlaba, the best laboratory partner for always willing to help and for being a godmother to Neptune (nickname of the TBR)

Technical staff at the Catalysis Institute specifically Ms Portia Johnston, Ms Chantal Le Roux and Ms Rachel Cupido for their assistance and providing a safe working space in the laboratory. A special thanks to Mr Waldo Koorts for his expertise and always being available whenever I needed help, as well as for allowing me to salvage spare parts from old unused rigs

Cape Catalytix workshop for their tremendous help and assistance with regards to the construction of the trickle bed reactor system, as well as for the supply of the various Swagelok fittings and components required in this project

The University of Cape Town and the Department of Chemical Engineering for financial support and the use of laboratory facilities and other resources

The National Research Foundation of South Africa (NRF) and the South African Research Chairs Initiative (SARChI) for providing financial support

Synopsis

The direct on-site conversion of methane to methanol could provide a more cost-effective and less energy-intensive utilization of natural gas compared to the industrial two-step syngas-based route. Despite the numerous approaches investigated for direct methane to methanol (DMTM) conversion in the last century such as homogeneous gas-phase, homogeneous liquid partial oxidation and heterogeneous catalytic partial oxidation, none of them were deemed successful for commercialization due to either the use of expensive reagents such as H_2O_2 and H_2SO_4, low yields and conversions, or inefficient system requirements. This has been mainly attributed to the thermodynamic challenge of breaking the strong C-H bond (bond dissociation energy of 435 kJ/mol) in the highly stable methane molecule and due to the higher reactivity of the product methanol leading to the formation of CO_x products.

Based on density functional theory (DFT) calculations, it was postulated that the selective oxidation of methane to methanol was possible with weakly adsorbed oxygen species over transition metal surfaces such as Ag and Pt at high oxygen and water partial pressures. Recent experimental studies also indicated that the presence of water through site blocking action had beneficial effects on catalytic activity and methanol selectivity. Since the role of liquid water in a single continuous-flow reactor has not been well established, evaluating its effect on catalytic performance and product selectivity in the direct conversion of methane over platinum-based catalysts was the prime focus of this research.

Therefore, a specifically designed trickle bed reactor (TBR) system capable of operating continuously and safely at high pressures was constructed to investigate the selective oxidation of methane over platinum-based catalysts in the presence of liquid water. Methane, oxygen and helium were pressurized and flow-metered prior to entering the reactor while the flow of deionized liquid water was controlled through a pump. The reactor assembly consisted of a quartz tube liner sealed at the top with a fluorocarbon O-ring in a stainless-steel shell (545 mm in length and 15.8 mm in inside diameter). A central thermowell fixed along the reactor tube which shielded an internal thermocouple was also quartz-sheathed to prevent undesired side reactions on the metal surface. Pelletized platinum catalyst supported on titania (ca. 1.5 g, d_p = 150-250 µm) was packed in the isothermal region (ca. 100 mm) of the reactor with silicon carbide granules (d_p ~ 1000 µm) filling the top and bottom void spaces. The reactor body was heated through a five-zone electric furnace. Pressure-controlled argon was allowed to flow between the annular region of the quartz liner and reactor shell at the same pressure as inside the quartz tube liner. The flowrate of argon was set approximately 2-3 times higher than the total gas flowrate through the catalyst bed to completely vaporize the effluent stream. The reactor effluent was throttled to atmospheric pressure and heated via heating cords to ensure no condensation of products prior to analysis via an existing online GC-Polyarc™-FID system.

Long-term catalytic experiments were performed on platinum impregnated TiO_2(P25) and TiO_2(rutile) in the newly constructed trickle bed reactor at 220 °C and 30 bar. The inlet partial pressures of methane and oxygen were kept constant at 0.5 bar and 1.5 bar, respectively, while

the feed rate of liquid water was varied from 0 - 0.3 ml/min with intermittent return to baseline condition (i.e., at P_{H_2O} = 6.9 bar) to monitor catalyst activity. The results of this investigation indicated that co-feeding liquid water has beneficial effects on the activity of these catalysts as well as the selectivity towards C_1 oxygenated products. Both catalysts were able to selectively convert methane to C_1 oxidation products in the trickle bed reactor with the highest activity and selectivity obtained while operating in the flooding region whereby water exists in the liquid phase (P_{H_2O} > 23.1 bar). Pt/TiO_2(P25) selectively formed methanol and methoxy methanol with a maximum selectivity of ca. 10% at a methane conversion of 0.6%, corresponding to an average turnover frequency of 0.25 h^{-1}. Carbon dioxide was the major product formed over Pt/TiO_2(P25). Conversely, over Pt/TiO_2(rutile), formaldehyde was the exclusive selective oxidation product formed with a remarkable selectivity of 90% at a methane conversion of 1%, corresponding to an average turnover frequency of 0.43 h^{-1}. Carbon dioxide and carbon monoxide were also detected in the product spectrum. Thus, under similar operating conditions, Pt/TiO_2(rutile) exhibited a significantly higher activity and improved selectivity, greatly favouring the formation of C_1 oxygenates compared to Pt/TiO_2(P25).

The novel trickle bed reactor system has demonstrated great ability in operating continuously at steady state for long-term runs for the selective oxidation of methane in the presence of liquid water at high pressure (< 50 bar) and moderate temperature (< 400 °C). Although the findings in this research indicate that liquid water facilitates the direct conversion of methane to selective oxidation products such as methanol and formaldehyde, the role of liquid water is not still obvious and has not been explicitly studied. Therefore, it is recommended that more catalytic testing with optimised reactor conditions and/or addition of promoters (such as Ag, Ni, Pd, Mo, Co and Cu) should be done in order to improve methane conversion, as well as yield for C_1 oxidation products. Furthermore, to enhance the performance of the reactor and better understand the interaction of liquid water with the solid catalysts in the tri-phasic system, hydrodynamics studies should be performed.

Table of Contents

List of Illustrations

List of Tables

List of Figures

Abbreviations

AFT	Adiabatic flame temperature
BPR	Back-pressure regulator
CAGR	Compound annual growth rate
DBD	Dielectric barrier discharge
DFT	Density functional theory
DME	Dimethyl ether
DMTM	Direct methane to methanol conversion
FI	Flow indicator
FIC	Flow indicator and controller
FID	Flame ionization detector
GC	Gas chromatography
HPLC	High pressure liquid chromatography
ID	Inside diameter
LFL	Lower flammability limit
MFC	Mass flow controller
MMO	Methane monooxygenase
MS	Mass spectrometry
MTBE	Methyl tertiary-butyl ether
MTG	Methanol to gasoline
MTO	Methanol to olefins
OD	Outside diameter
PI	Pressure indicator
PIC	Pressure indicator and controller
SS	Stainless steel
TBR	Trickle bed reactor
TIC	Temperature indicator and controller
TOF	Turnover frequency
UFL	Upper flammability limit
VCR	Vacuum coupling radiation

Symbols

a_v	Specific external area of packing
ε_B	Bed porosity
β_T	Total liquid hold-up
β_R	Residual liquid hold-up
β_D	Dynamic liquid hold-up
D	Reactor tube diameter
d_p	Particle diameter
D/uL	Dispersion number
ρ	Density
Eö	Eotvos number
g	Acceleration due to gravity
Ga	Galileo number
L	Length
ΔP	Pressure drop
Pe	Peclet number
Re	Reynolds number
S_i	Selectivity of any carbon-containing product, i
Sc	Schmidt number
u	Actual mean velocity
μ	Viscosity
u_g	Mean interstitial gas velocity
Ug	Gas flowrate
v_g	Superficial gas velocity
χ_C	Electronegativity value of carbon
χ_H	Electronegativity value of hydrogen
X_{CH_4}	Conversion of methane
Y	Yield of any carbon-containing product, i
γ_{gl}	Gas-liquid surface tension

1. Introduction

Natural gas, with methane as main constituent is an abundant and clean source of energy with its reserves standing approximately at 199 trillion cubic metres [1]. Natural gas accounted for 24% of the global energy consumption in 2020 [2] and the demand growth is expected to increase at an average rate of 1.7%/year for the 2022-2024 period [3]. Natural sources of methane can be found for example: encapsulated in salt caverns, in porous rocks, as gas hydrates, associated with oil wells while anthropogenic sources are from landfill sites and livestock farming. This valuable gas can be used directly for heating purposes and electricity generation. However, in some cases, a large portion of the natural gas is being flared due to difficulties associated with its transportation from remote reserves, resulting in increasing greenhouse gas emissions.

Methane can also be used as a green and cheap carbon feedstock for the chemical industry and even be transformed into fuels. However, as methane is a gas having a lower density than oil, it cannot be readily transported and stored as compared to oil, unless it can be fed into an accessible pipeline network in the areas. Consequently, transportation of natural gas to the markets over large distances poses an economic risk making the prices of its derivatives less competitive in relation to those of oil [4]. Transportation of natural gas after liquefaction is possible but methane has a very low boiling point (-164 °C); it is thus expensive to refrigerate, which is required throughout its transportation [5]. Therefore, a desirable alternative would be the conversion of methane into useful liquid fuels at the point of extraction for ease of transportation and storage. The conversion of methane into a liquid fuel is energetically demanding and capital cost-intensive, but it does not only make the material transportable; it can even further increase the value of this raw material by converting it into more valuable products such as chemicals.

Methane can be converted into liquid hydrocarbons via the Fischer-Tropsch synthesis or methanol synthesis. Methanol is a highly versatile building block for the manufacture of numerous everyday products. The latter can be used directly as a fuel, it can be converted into olefins (MTO) and gasoline (MTG) or used in the chemical industry as either a feedstock or solvent. Approximately 30% of the methanol produced globally is used to produce formaldehyde and the remaining portion is converted into methyl tertiary-butyl ether (MTBE), acetic acid, methyl methacrylate, fuel additives and other chemicals [6]. Methanol has recently been regarded as a promising fuel in the automotive sector [7] due to environmental and energy considerations. It can be blended directly with gasoline or converted to dimethyl ether (DME) and biodiesel. Furthermore, methanol has been in great demand as an intermediate, green and clean source to produce electricity via fuel cells [8]. Methanol can also be used in wastewater treatment plants as an external carbon source to maximise the denitrification process [9].

The wide application of methanol is motivated by its large scale production which is ever increasing, for instance, the global methanol demand is anticipated to increase at a compound

annual growth rate (CAGR) of 5.66% between 2019 and 2027 [10]. At present, the most widely commercialised process of converting methane to methanol is a two-step process whereby natural gas is first reformed into synthesis gas (a mixture of hydrogen and carbon monoxide), which is subsequently transformed selectively into methanol. The production of syngas via steam reforming is nevertheless an energy-intensive and costly process since it involves high temperatures (~ 900 °C). It was reported that the steam reforming stage in the indirect process accounts for approximately 60-70% of the overall process costs [5], [11]. For this reason, there has been significant interest in developing a direct route that would be more economically attractive for methane conversion into methanol for the past decades. Furthermore, a direct methane-to-methanol (DMTM) process makes it possible for on-site conversion at the isolated natural gas reserves for more efficient utilization and thus creating competitive prices for the end products [7].

The direct conversion of methane to methanol via partial oxidation has been studied extensively for the past century since it was first discovered by Bone and Wheeler in 1902 [5]. To be able to compete with the commercialized two-step process, DMTM must achieve a methanol selectivity of 80% at a single pass of methane conversion of 10% according to technical economic assessments performed in the past [5], [12]. Numerous studies were carried out to investigate the range of optimal conditions and the different catalytic and non-catalytic systems for DMTM. However, up to now there has still been no breakthrough since the reported methanol yields from reproducible experiments were considered too low for commercialization [6]. This has been attributed to the low reactivity of methane (it being a highly stable and symmetrical bearing no dipolar moment) and the tendency for the products to undergo over-oxidation to CO and CO_2. Hence, the control of the selectivity in the partial oxidation of methane to the point of methanol requires a highly active and selective catalytic system [5], [13].

2. Literature review

2.1 Thermodynamics of partial oxidation of methane

Gas phase oxidation of methane may yield various oxygenated hydrocarbons namely, methanol (CH_3OH), formaldehyde (CH_2O) and formic acid (CH_2O_2), as well as deep oxidation products (CO_x) such as carbon dioxide (CO_2) and carbon monoxide (CO) (see Table 2-1).

Table 2-1: Standard Gibbs free energy change of reaction and standard enthalpy change of reaction for the oxidation of methane [14]

Reaction	$\Delta_{rxn}G°$ (kJ/mol)	$\Delta_{rxn}H°$ (kJ/mol)
$CH_4 + 2\ O_2 \rightarrow CO_2 + 2\ H_2O$	-801	-803
$CH_4 + 1.5\ O_2 \rightarrow CO + 2\ H_2O$	-544	-520
$CH_4 + \ O_2 \rightarrow CH_2O + 2\ H_2O$	-281	-276
$CH_4 + 0.5\ O_2 \rightarrow CH_3OH$	-112	-126

The challenge in converting methane to methanol lies in the activation of the C-H bond, the strongest aliphatic C-H bond amongst alkanes. Activation of this bond has been studied intensively and is often regarded as one of the 'Holy Grails' in catalytic chemistry [15]. This is due to the high energy for dissociation of the C-H bond in the symmetric methane molecule of 435 kJ/mol and its low polarity due to the comparable electronegativity values of the carbon (χ_C = 2.55) and hydrogen (χ_H = 2.20) atoms [16].

Compared to methane, the C-H bonds in methanol and formaldehyde have lower dissociation bond energies, implying that they have a higher relative reactivity (see Table 2-2). This means that under similar conditions, these oxygenated products are easier to activate and oxidise than methane, which results in the production of stable, deep oxidation products such as CO and CO_2. As indicated by the standard change in Gibbs free energy of reactions ($\Delta_{rxn}G°$) in Table 2-1, though the oxidation of methane to methanol is thermodynamically favoured, the formation of CO_2 and CO is even more favoured. Furthermore, the combustion reaction to CO_2 has the most negative $\Delta_{rxn}G°$, and CO_2 is thermodynamically the most favoured product [5]. Therefore, to control the partial oxidation of methane to methanol and cease further oxidation, a highly active catalyst is required to readily activate the H-CH_3 bond and to selectively form methanol but does not have a high activity for the subsequent oxidation steps.

Table 2-2: Bond dissociation energy of methane, methanol and formaldehyde [17]

C-H Bond	$\Delta_{dis}H°$ (kJ/mol)
H-CH_3	435
H-CH_2OH	402
H-CHO	369

2.2 Indirect processes for the conversion of methane to methanol

2.2.1 Conversion of methane to methanol via synthesis gas

The conventional industrially used route to transform methane into methanol is a two-step process. It involves the production of synthesis gas (syngas) which is a mixture of H_2 and CO, followed by the catalytic conversion of syngas to produce methanol selectively. Syngas can be widely produced by the endothermic steam reforming (SR) of natural gas. Combusting some of the methane fed into the steam reformer generates heat to obtain an autothermal process, whilst at the same time generating some steam required for steam reforming step; the reverse water-gas shift (RWGS) regulates the CO/H_2 ratio of the syngas [18]. Syngas can also be obtained by reacting methane with CO_2 (dry reforming) and with O_2 (partial oxidation) generating different H_2/CO stoichiometries (see Table 2-3). The reforming reactions are often combined to generate the ideal methanol synthesis gas (metgas) with a H_2/(CO+CO_2) ratio of 2.5 [19]. It was reported that a 3:2:1 mixture of CH_4, H_2O and CO_2 can be directly converted into metgas with H_2:CO ratio of 2 over a NiO/MgO catalyst at 5–30 bar and 800–950 °C through a process called bi-reforming which combines both the steam and dry reforming routes [20].

Table 2-3: Standard enthalpy change of reaction for the different processes in syngas production

Reaction		$\Delta_{rxn}H°$ (kJ/mol)
Steam reforming	$CH_4 + H_2O \rightarrow CO + 3\ H_2$	206 kJ/mol
Methane combustion	$CH_4 + 2\ O_2 \rightarrow CO_2 + 2\ H_2O$	-801 kJ/mol
RWGS	$CO_2 + H_2 \rightarrow CO + H_2O$	41 kJ/mol
Dry reforming	$CH_4 + CO_2 \rightarrow 2\ CO + 2\ H_2$	247 kJ/mol
Partial oxidation	$CH_4 + 0.5\ O_2 \rightarrow CO + 2\ H_2$	-36 kJ/mol

The syngas mixture of varying ratios can be converted into useful liquid hydrocarbons through the Fischer-Tropsch synthesis or directly into an equilibrium limited reaction to methanol. Methanol is synthesized via the hydrogenation of CO and CO_2 by means of the ICI (Imperial Chemical Industries) process using an active Cu/ZnO/Al_2O_3 catalyst at pressures of 50-100 bar and temperatures between 250-300 °C [4], [16].

$$CO + 2\ H_2 \rightarrow CH_3OH \quad (2\text{-}1)$$

$$CO_2 + 3\ H_2 \rightarrow CH_3OH + H_2O \quad (2\text{-}2)$$

Steam reforming of methane is an energy demanding process due to its highly endothermic nature necessitating extreme temperatures (~ 900 °C). It implies that special infrastructures and materials are required. Moreover, the amount of steam needed results in the corrosion of reactors and challenges with handling and maintenance. This requires massive capital investment making syngas production the most expensive step of the indirect methanol production chain accounting for approximately two thirds of the overall process costs [5], [11].

2.2.2 Homogeneous catalysis in solution

Periana *et al*. [21] developed a homogeneous catalytic system for the selective oxidation of methane to methanol via the electrophilic displacement [21] of methane using concentrated sulfuric acid (H_2SO_4) as oxidant and mercury bisulphate ($Hg(OSO_3H)_2$) as the catalyst. Using Hg(II) ions, the low-temperature reaction was performed in batch mode at 180 °C achieving 43% single-pass yield. It involved the synthesis of an intermediate methyl bisulphate (CH_3OSO_3H) species and sulphur dioxide (SO_2) as a by-product at a methane conversion of 50% with 85% selectivity towards CH_3OSO_3H. Methanol can then be produced by the subsequent hydrolysis of CH_3OSO_3H while SO_2 was re-oxidised in presence of water to regenerate diluted H_2SO_4 (which needs to be concentrated in an additional step). The net reaction results in the selective oxidation of CH_4 to CH_3OH. Other ions such as Au(II), Pt(II), Tl(III) and Pd(II) were also reported to promote the oxidation of methane to CH_3OSO_3H in strong oxidizing acids [21], [22].

$$CH_4 + 2H_2SO_4 \xrightarrow{Hg(II)} CH_3OSO_3H + 2\,H_2O + SO_2 \quad (2\text{-}3)$$

$$CH_3OSO_3H + H_2O \rightarrow CH_3OH + H_2SO_4 \quad (2\text{-}4)$$

$$SO_2 + 0.5\,O_2 \rightarrow H_2O + H_2SO_4 \quad (2\text{-}5)$$

$$CH_4 + 0.5\,O_2 \rightarrow CH_3OH \quad (2\text{-}6)$$

Based on their previous work and the chemistry originally developed by Shilov, the Periana group later reported that the overall yield could be improved to 72% (81% selectivity towards methyl bisulphate at 90% methane conversion) using a platinum complex, (bipyrimidyl platinum chloride - $(bpym)PtCl_2$) as a catalyst in the presence of H_2SO_4 at 220 °C. Moreover, the more stable and effective Pt-based catalyst can oxidise methane at temperatures as low as 100 °C [23], [24]. It is believed that this is to date the most active catalytic system in terms of conversion, yield and selectivity. It should however be noted, that this homogeneous system is still rather slow with a turnover frequency (TOF) value of ca. $10^{-3}\,s^{-1}$, implying that the catalyst activity has to be increased a thousand-fold to achieve a TOF of $1\,s^{-1}$ for noble metal-based catalysts in order to be cost-effective [16], [25]. Recently, it was shown that the catalyst potassium tetrachloroplatinate (K_2PtCl_4) in controlled concentrations of SO_3 managed to reach TOFs higher than the $(bpym)PtCl_2$ system by three orders of magnitude, which authors claimed are comparable to industrial processes [26]

Though the high selectivity in the Pt(II) systems is attributed to the electron withdrawing effect of the sulphate group providing stabilization against further oxidation to combustion products, the challenges lie in the difficult separation of the methanol derivative from the reaction solution as well as the H_2SO_4 and SO_2 recycle [26], [27]. Furthermore, the utilization of precious or toxic metals as homogeneous catalysts in these indirect processes entails additional separation steps for catalyst recovery from the acidic medium. Besides, due to the highly acidic nature of the reagents used, expensive corrosion-resistant equipment is required adding more to the capital costs. This makes the scale-up of these homogeneous catalytic systems cost-intensive and economically not feasible for industrialization [28], [29].

2.3 Direct methane to methanol (DMTM) conversion processes

Both the syngas-based and acid-assisted homogeneous catalysis routes mentioned above are indirect processes which are highly energy-dependent and capital-intensive due to the multiple reactor units involved. For this reason, the direct conversion of methane to added-value chemical products has been of increased industrial and academic interest since the 20th century, more specifically to a liquid fuel such as methanol which can be easily transported and stored. Thus, the direct methane to methanol (DMTM) conversion in a single reactor may constitute a far more economically viable solution and make it possible for on-site conversion at the isolated natural gas reserves.

2.3.1 Enzymatic conversion of methane to methanol

In nature, the bioconversion of methane to methanol occurs in methanotrophic bacteria, also known as methanotrophs, which use methane as a sole carbon and energy source [30]. These bacteria employ methane monooxygenase (MMO) enzymes, capable of oxidising methane to selectively produce methanol in a single step at ambient conditions using oxygen as oxidant. Figure 2-1 below illustrates the two forms of MMO enzymes that can biologically perform this reaction: a soluble MMO (sMMO) and a membrane bound particulate MMO (pMMO). The active site in the sMMO is constituted of a diiron group whereas that in the pMMO is a dinuclear copper center [31], [32].

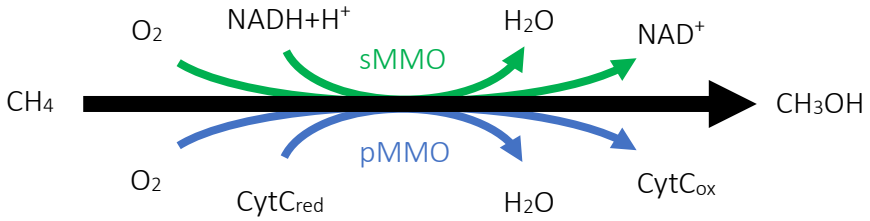

Figure 2-1: Biological pathways for the oxidation of methane to methanol adapted from Hanson & Hanson [30]

An experimental study showed that about 0.95 g/L methanol was produced from methane in a membrane aerated reactor after 40 hours using a methanotroph culture of 17 dry cell g/L *Methylosinus trichosporium* OB3b [33]. These biocatalytic systems are however difficult to implement on an industrial scale because they require the use of expensive reductants such as nicotinamide adenine dinucleotide (NADH) [34] and due to the relatively slow gas-liquid mass transfer attributed to low methane solubility in aqueous culture [35], [36]. Furthermore, methanol is toxic to most methanotrophs, consequently it must be removed immediately from the reaction medium before growth which hampers methanol synthesis [35].

2.3.2 Homogeneous gas phase conversion of methane to methanol

The partial oxidation of methane to methanol in the absence of a catalyst can occur directly in a single reactor, in which the reaction is governed by a free radical mechanism. Methane is usually fed in excess while the oxygen concentration is kept low in order to prevent the

complete combustion of methane as well as the avoidance of the explosion region. This gas phase free radical process involves more than 1000 elementary reaction steps with 60 reactive species [37]. The homogeneous reaction is extremely difficult to control using variation in the operational reactor conditions [5]. Numerous experimental and theoretical studies on the homogeneous partial oxidation of methane to methanol have shown that methanol selectivity decreased significantly with an increase in methane conversion which can be explained by the higher reactivity of methanol compared to methane [12], [38], [39].

In the non-catalytic reaction, methanol does not form until the reaction temperature reaches a transition point (400-420 °C) at which methanol selectivity is optimized and remain stable in a small temperature range of about 40 °C. However, upon further increase in reaction temperature the methanol selectivity drops while the selectivity towards CO increases [12], [40]. Elevated reaction pressure, typically between 30-60 bar was observed to favour the conversion of methane to methanol whereas decreasing the pressure resulted in the improved yield of CO and CO_2 [12], [40]–[42]. Other process parameters such as reactor design, feed gas composition and residence time have been investigated to improve the efficiency of the catalyst-free homogeneous process. For instance, Zhang *et al.* [40] showed that by insulating the ringed gap between the inner quartz liner and the stainless steel reactor wall, the yield and selectivity of methanol increased dramatically while the production of undesired CO_2 was suppressed. This indicates that the formation of deep oxidation products catalysed by the metal reactor surface can be minimised by preventing the reactants from getting in contact with the stainless steel reactor [40]. Though these non-catalytic reaction systems were extensively studied, reproducible results could not be achieved [5].

2.3.3 Heterogeneous catalytic conversion of methane using oxygen

In an effort to enhance the overall performance of the partial oxidation of methane to methanol, the participation of solid catalysts was studied comprehensively. However, under the homogeneous reaction conditions, that is, at high pressures (30-60 bar) and temperatures (350-450 °C) and using oxygen as oxidant, the heterogeneous catalysts showed no positive improvements on the methanol yield and selectivity [43], [44]. For instance, an experiment carried out to compare the homogeneous oxidation and catalytic oxidation of methane using a Mo-V-Cr-Bi-P oxide catalyst under the same reactor conditions (50 bar and 380-500 °C) showed that methanol selectivity was still very low and comparable to that obtained in the homogeneous gas phase reaction [45]. Under similar conditions, no methanol was formed using Mo/ZrO_2 catalysts but instead formaldehyde was the main oxygenated product [5].

At low pressures (~ 1 bar) the presence of a catalyst could be more effective. For example Alptekin *et al*. [46] reported the production of 25 $g/kg_{cat}/h$ of methanol over a $FePO_4/SiO_2$ catalyst in the methane oxidation in the presence of water at 600 °C. Otsuka & Wang [43] obtained formaldehyde as the major product in the partial oxidation of methane at atmospheric pressure (T > 500 °C) over metal oxide catalysts. It was suggested that intermediate CH_3 and CH_3O species would more likely be attacked by active surface oxygen

species formed via the fast dissociative adsorption of oxygen, favouring the formation of HCHO and CO_x compounds over CH_3OH. Besides, the high temperatures might also be responsible for the low methanol selectivity (the initially formed CH_3OH formed could decompose almost instantaneously into HCHO or CO_x under these conditions [43].

As mentioned above, MMO enzymes do not need high temperatures to catalyse the selective oxidation of methane to methanol with atmospheric oxygen. Inspired by the nature of the active metal centers found in these enzymes, a research has been focussed on the development of catalysts using Fe or Cu complexes embedded in the micropore structure of zeolites to mimic these bio-enzymatic systems. Copper-containing zeolites can convert methane to methanol in a single reactor through a process involving three distinct steps (see Figure 2-2). This is a cyclic process consisting of the catalyst activation in O_2 at high temperatures (> 450 °C), followed by the reaction of CH_4 over the oxygenated catalyst at a lower temperature (≤ 200 °C). The resulting adsorbed CH_3O intermediate is subsequently extracted from the catalyst surface as methanol using water completing the catalytic cycle [27], [47]–[50].

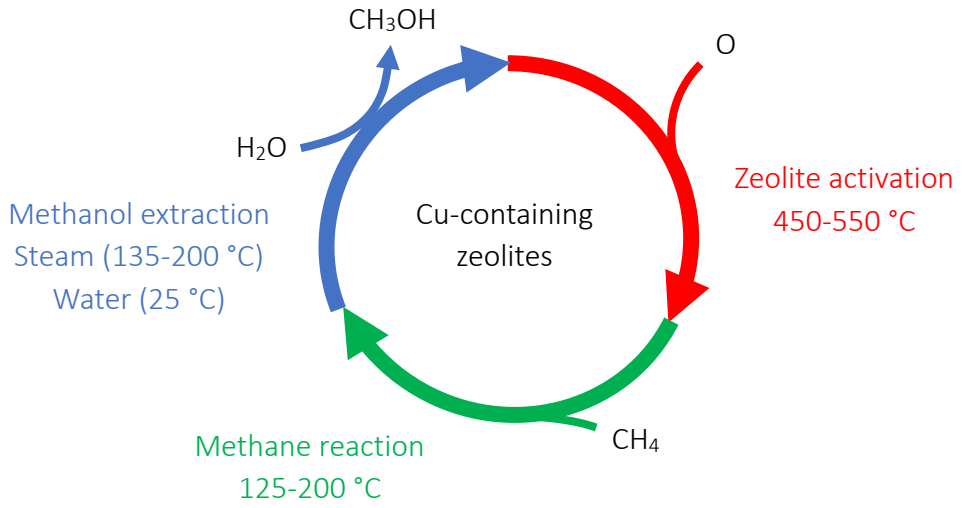

Figure 2-2: Three-step direct conversion of methane to methanol over copper-exchanged zeolites adapted from Tomkins *et al.* [49]

An early study by Groothaert *et al.* [51] using Cu-ZSM-5 as a catalyst showed a low methanol yield of 8.2 µmol/g_{cat} with a selectivity of 98%. Higher methanol yields of 125 µmol/g_{cat} and 169 µmol/g_{cat} were recently achieved over Cu-SSZ-13 [50] and Cu-MOR [52] with high methanol selectivity (> 85%). The main drawback of the stepwise process is the operating at a different temperature for each cycle which requires cyclic heating/cooling. This reduces both the thermal and production efficiency; thus, it cannot be upscaled for commercialisation. It was also reported that this process can be carried out in a two-step route in which methane is converted to methanol in the presence of oxygen and water using Cu-ZSM-5 catalysts [53] or isothermally at 200 °C over a Cu-MOR catalyst [54]. Despite the significant contribution for the advancement in this field, the methanol yields are still quite low, and the methane conversions are far from industrial practice.

2.3.4 Heterogeneous catalytic conversion of methane using hydrogen peroxide

Besides oxygen, hydrogen peroxide (H_2O_2) can also be used as the oxidant in the direct conversion of methane to methanol at lower temperatures. A single atomic Rh catalyst dispersed on ZrO_2 (Rh_1/ZrO_2) [55] and bi-metallic $AuPd/TiO_2$ catalyst [56] have shown to selectively oxidise methane to methanol in autoclave reactors at low temperatures (≤ 90 °C) and pressure of 30 bar in the gas-liquid phase using H_2O_2 ex-situ or also generated in-situ from H_2/O_2 mixtures. Under similar reactor conditions, the catalyst productivity could be increased by five times over using tri-metallic $AuPdCu/TiO_2$ catalyst, yielding methanol selectivities as high as 83% [57].

Likewise, zeolite catalysts such as copper and iron modified ZSM-5 catalysts have also demonstrated to catalyse the oxidation of methane to methanol in aqueous H_2O_2 at 50 °C. The primary product in these systems was reported to be methyl hydroperoxide (CH_3OOH) which could be possibly formed from the reaction of a methyl radical with H_2O_2 and which is subsequently transformed to methanol via hydrolysis [58], [59]. Other products such as formaldehyde, formic acid as well as carbon dioxide were also detected in the studies. These batch systems are capable of achieving a methanol selectivity of up to 93% at a maximum of 10% methane conversion [59]. Under continuous flow operation with H_2O_2 as oxidant, the selective oxidation of methane to methanol over Cu and Fe-ZSM-S catalysts yielded a 92% methanol selectivity at 0.5% methane conversion [60]. The use of expensive H_2O_2 as oxidant is nevertheless a significant limitation, considering the relatively high price of the reactant compared to the desired product CH_3OH. Thus, rendering this type of process less commercially viable [13].

2.3.5 Heterogeneous catalytic conversion of methane using nitrous oxide

Using other oxidants such as nitrogen oxide (N_2O) in the gas phase, methane can be activated over Fe-ZSM-5 catalysts for the partial oxidation of methane to methanol. It is suggested that upon decomposition of N_2O at temperatures below 300 °C, unique active oxygen species (α-oxygen) could be generated on Fe-sites. The α-oxygen species react with methane to form hydroxyl and methoxy surface species through a hydrogen abstraction mechanism. The methanol formed is strongly bonded to the active site and has to be extracted in a subsequent hydrolysis step [61], [62]. It was reported that the gas phase methane oxidation with N_2O over Fe-ZSM-5 produced methanol under continuous flow operation at 275 °C and that the co-feeding of steam improved the methanol selectivity from 2.7% to 62%. Although upon addition of water coke formation could be suppressed, the methane conversion however decreased by a factor of ten [63]. Copper-containing zeolites such as Cu-SSZ-13 and Cu-MOR have both shown to produce methanol using N_2O as oxidant at ambient pressure through either the continuous catalytic operation or via the three step cyclic process [64], [65]. The main issues regarding the usage of N_2O as an oxidant is that it is more expensive than the target product CH_3OH and is not environmentally friendly.

2.3.6 Novel technologies for direct methane to methanol conversion

There are a few novel and innovative processes besides the DMTM processes discussed previously that have been developed from clean technology. For instance, technologies such as plasma discharge and photocatalysis can also be used to produce methanol from methane.

2.3.6.1 Plasma discharge

Plasma is an ionised gas constituted of positive and negative ions, electrons and neutral species. Plasma technology can be categorised into thermal plasma and non-thermal plasma. The former can be described as a gas containing electrons, ions and neutral species in thermal equilibrium with each other whereas non-thermal plasma is composed of electrons having higher temperatures (energy) than the surrounding species [66]. Using the non-thermal plasma approach, plasma can be generated by creating a large potential difference between the inner and outer electrodes in a dielectric barrier discharge (DBD) reactor (see Figure 2-3). The filamentary micro-discharges generate high-energy electrons capable of initiating chemical reactions [67], [68]. The reactors can be used for the conversion of methane. For example, Nozaki *et al.* (2011) demonstrated that the single step methane to methanol conversion in an unpacked micro dielectric barrier discharge (DBD) reactor with oxygen as oxidant resulted in a conversion of methane of 12% with a selectivity towards methanol of 11% CH_3OH under ambient conditions; Chawdhury *et al.* (2018) reported a conversion of methane of 15% and a selectivity towards methanol of 35% when using glass beads as packing medium in the DBD reactor implying the need to reduce the residence time to obtain a good selectivity.

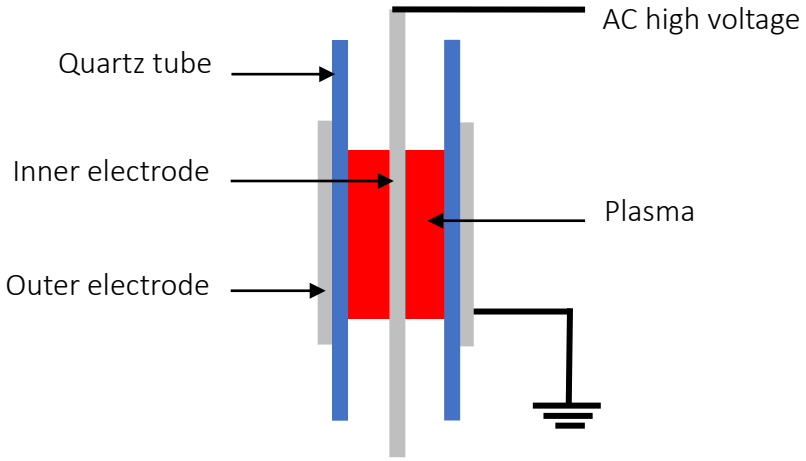

Figure 2-3: Schematic representation of a dielectric barrier discharge (DBD) reactor

It has been reported that combining plasma and catalysis can lead to enhanced methane conversion. For instance, plasma-assisted catalysis was studied over a Fe_2O_3–CuO/γ-Al_2O_3 catalyst using a DBD reactor under mild conditions in two configurations namely, in-plasma catalysis and post-plasma catalysis. Both configurations showed increased efficiency in CH_4 conversion (34-37%) compared to single plasma application, however the CH_3OH yields were very low (< 2%). Moreover, for the single in-plasma catalysis reactor the catalyst embedded in the discharge zone was more prone to coking and subsequent deactivation [69], [70].

2.3.6.2 Photocatalysis

Photocatalysis is the process in which a photo-induced chemical reaction is accelerated by the presence of a catalyst. Gonda *et al*. [71] showed that semiconductors such as tungsten oxide (WO_3), titanium oxide (TiO_2) and nickel oxide (NiO) can act as photocatalysts in the conversion of methane to methanol under UV laser radiation at room temperature. The experiment was carried out by suspending the photocatalyst in a water-containing glass cell which was afterwards saturated with a high flowrate of methane gas at 150 ml/min. The reactor was sealed at atmospheric pressure and illuminated with a 355 nm wavelength laser beam light. The absorption of photons through band gap excitation initiates the formation of hydroxyl radicals which can bind with the methane molecules to form methanol as follows.

$$\mathrm{CH_4} + \mathrm{OH^{\cdot}} \rightarrow \mathrm{CH_3OH} + \mathrm{H^{\cdot}} \qquad (2\text{-}7)$$

Hydrogen was also a major product during this photochemical reaction due to the degradation of the formed methanol by electron donation to valance band holes. The reported methane conversions for WO_3, TiO_2 and NiO, were 29%, 21% and 20%, respectively with WO_3 showing the highest methanol yield of 160 µmol [71]. The addition of electron scavengers (Fe^{3+}, Cu^{2+}, Ag^{+}) and H_2O_2 species to mesoporous WO_3 in an aqueous suspension at 55 °C under UVC–visible light irradiation was recently investigated by Villa *et al*. [72]. It was shown that the methanol selectivity was substantially increased to 58% with WO_3/Fe^{3+} which was attributed to the largely improved electron-hole pair separation in this system.

2.4 Summary of findings for current DMTM processes

An overview of the DMTM processes discussed above is given in Table 2-4, which compares the reactor conditions and performances of the different routes. According to technical economic assessments, in order for the DMTM conversion to be industrially attractive and compete with the commercialized two-step syngas process, it must achieve a methanol selectivity of at least 80% at a single pass of methane conversion of 10% or greater [5], [12]. Whilst some of the homogeneous gas phase systems have claimed to achieve this target, the experiments were irreproducible [5]. From an industrial point of view, the heterogeneously catalysed DMTM processes using oxidants such as N_2O and H_2O_2 cannot compete against O_2 which is abundant, cheap and environmentally friendly. Furthermore, to become more viable at large scale, a system in which methanol can be produced catalytically under continuous flow conditions would be more ideal as it can allow for the steady state conversion of large amounts of methane in comparison to batch mode operation. As previously mentioned, the heterogeneous stepwise processes are impractical for commercialisation since the intermediate heating and cooling cycles lower both the thermal and production efficiency. Heat integration is an important factor to consider in improving the energy efficiency in industrial plants. For DMTM processes operating at temperatures lower than 150 °C, heat recovery of the heat of reaction becomes quite challenging. Hence, a heterogeneous catalytic system operating at mild temperatures of 200-350 °C would be advantageous, allowing heat recovery via steam generation, in addition to increasing the kinetic rate of reaction.

Table 2-4: Summary of direct methane to methanol conversion processes

DMTM process	Catalyst	Oxidant	T (°C)	P (bar)	X_{CH4} (%)	S_{CH3OH} (%)	TOF (h^{-1})	Ref.
Homogeneous gas phase	-	O_2	450	50	8	81	-	[42]
		O_2	450	50	9.5	76	-	[73]
		O_2	450	50	5.2	38	-	[74]
		O_2	400	30	3.1	47	-	[75]
		O_2	430	34	7	53.6	-	[76]
		O_2	470	50	13	60	-	[40]
Heterogeneous with O_2	Mo-V-Cr-Bi-Oxide	O_2	470	50	11	43[a]	-	[45]
	$FePO_4/SiO_2$[b]	O_2	600	1	2	3	-	[46]
	NiO/CeO_2-ZrO_2[c]	O_2	450	1	14	19	50	[77]
	Cu-SSZ-13	O_2	200[d]	1	-	90	0.034	[50]
	Cu-MOR	O_2	200[e]	1	-	92.7	0.077	[52]
	Cu-MOR	O_2	200[f]	37	-	-	0.24	[54]
	Cu-ZSM-5	O_2	210[g]	1	0.0014	70.6	0.002	[53]
Heterogeneous with H_2O_2	Rh_1/ZrO_2	H_2O_2	70	30	-	72[h]	1.75	[55]
	$AuPd/TiO_2$	H_2O_2	70	30.5	-	79.4[h]	0.16	[56]
	$AuPd/TiO_2$	H_2/O_2	50	30.5	-	49.3[h]	0.77	[56]
	$AuPdCu/TiO_2$	H_2/O_2	50	30	-	82.7[h]	1.4	[57]
	Cu-ZSM-5	H_2O_2	50	30.5	0.3	83[h]	2110	[59]
	Cu-Fe-ZSM-5	H_2O_2	50	30.5	0.7	85[h]	31	[59]
	Fe-silicalite-1 and Cu/silicalite-1	H_2O_2	70	3	10.1	93	70	[59]
	ZSM-5	H_2O_2	50	10	0.91	11.6[i]	5.6	[58]
	Fe-Cu-ZSM-5	H_2O_2	50	20	0.5	92.2	0.3	[60]
Heterogeneous with NO_2	Fe-ZSM-5[j]	N_2O	275	< 1	0.19	62	0.006	[63]
	Cu-SSZ-A3	N_2O	270	1	0.022	39.7[a]	0.36	[65]
	Cu-MOR	N_2O	270	1	0.013	24[a]	0.26	[65]
	Cu-MOR	N_2O	150[k]	1	-	-	-	[64]
Plasma discharge	-	O_2	l	1	15.4	35.4	-	[67]
	-	O_2	m	1	12	11	-	[68]
	Fe_2O_3-CuO/Al_2O_3	O_2	< 250	1	36	-	-	[69]
Photocatalytic	WO_3	-	25[n]	1	29	-	-	[71]
	WO_3	-	55[o]	1	-	46	-	[72]
	WO_3/Fe^{3+}	-	55[o]	1	-	58.5	-	[72]

a Other products: CO and CO_2
b Co-feeding of steam at 3 vol%; HCHO as primary product
c Co-feeding of steam; C_2H_5OH as primary product
d Catalyst activation at 500 °C with O_2; reaction at 200 °C with CH_4; extraction of CH_3OH with steam at <135 °C
e Catalyst activation at 500 °C with O_2; reaction at 200 °C with CH_4; extraction of CH_3OH with steam at 200 °C

f Catalyst activation at 200 °C at 1 bar of O_2; reaction at 200 °C with CH_4; extraction of CH_3OH with water at 25 °C
g Catalyst activation at 550 °C at 1 bar of O_2; reaction at 210 °C with CH_4; extraction of CH_3OH with H_2O-O_2-CH_4 at 210 °C; Other product: CO_2
h Other products: CH_3OOH and CO_2
i Other products: CH_3OOH and HCOOH
j Catalyst pre-treated in air at 550 °C; Co-feeding of water at 30 vol%; Coke formation observed
k Catalyst activation at 600 °C with N_2O; reaction at 150 °C with CH_4; extraction of CH_3OH with steam at <135 °C
l Heating through plasma discharge; Other products: HCHO and HCOOH
m Heating through plasma discharge; Other products: H_2
n UV laser radiation; Other products: H_2
o UVC-visible light irradiation; Other products: CO_2 and C_2H_6

2.5 Platinum-catalysed partial oxidation of methane to methanol

Fratesi *et al*. [78] theorised from first principles that the direct partial oxidation of methane to methanol may occur over transition metal catalysts. The mechanism proposed involves methane reacting with an atomic oxygen adsorbed on the metal surface to directly form methanol in a single elementary step as described by Equation 2-8 (where * denotes an adsorbed state). Two competing reactions may also occur in which the dehydrogenation of methane can take place either in the absence (Equation 2-9) or presence (Equation 2-10) of adsorbed oxygen on the metal surface. Both side reactions can lead to the formation of deep oxidation products CO_x, if the adsorbed methyl species formed undergo further deprotonation and react with an active surface oxygen species. Methanol synthesis can still proceed when a methyl and hydroxyl species combine directly following Equation 2-10. However, the methyl species would more likely undergo further dehydrogenation, then react with oxygen to form formaldehyde, thus reducing the selectivity towards methanol [78].

$$\mathrm{CH_4 + O^* \rightarrow CH_3OH^*} \quad (2\text{-}8)$$

$$\mathrm{CH_4 \rightarrow CH_3{}^* + H^*} \quad (2\text{-}9)$$

$$\mathrm{CH_4 + O^* \rightarrow CH_3{}^* + OH^*} \quad (2\text{-}10)$$

DFT calculations indicated there that exists a linear relationship between the activation energy of the desired reaction and the difference in adsorption energy between OH and O on the metal surface, suggesting that methanol formation increases as the binding energy of oxygen on the surface decreases. Thus, by providing a more reactive O that is weakly bound to a catalyst surface compared to OH, the energy barrier between the adsorbed atomic oxygen and methane molecule will be lowered, favouring the direct methane to methanol formation pathway [78], [79]. Nørskov *et al*. [80] demonstrated that of all the pure noble metals investigated in their study, platinum had the highest catalytic activity for oxygen reduction in terms of both O and OH adsorption. This indicates that the binding of O and OH on platinum is at an optimal level and therefore it should be considered as a suitable metal catalyst for the partial oxidation of methane to methanol [81].

It was theoretically demonstrated that by increasing the oxygen coverage, the availability of vacant sites on the catalyst surface becomes limited. Consequently, the desired pathway for methanol formation (Equation 8) is favoured over the two competing side reactions (Equations 9 and 10), which could result in an increased methanol selectivity. This was observed on weakly reactive substrates such as Ag [78] and on Pt-Pd alloys [82]. Fellah & Onal [83] reported that

methane C-H cleavage was more facile over an atomic oxygen adsorbed on a metal (Ag, Au, Cu, Rh and Ru) compared to the metal itself. However, the saturation of a metal surface with adsorbing oxygen species is difficult to attain due to the lateral repulsive forces existing between them. For example, the saturation coverage on Pt(100) and Pt(111) surfaces was found to be limited to only 0.5 monolayer with either molecular or atomic oxygen [81], [84]. DFT calculations showed that saturation can be achieved via the co-adsorption of hydroxyl species (generated by co-feeding water), which can considerably reduce the repulsive interactions between the adsorbed oxygen atoms. For instance, a full coverage was attained with 2O/2OH on Pt(100) surfaces (see Figure 2-4) while on Pt(111) surfaces as illustrated in Figure 2-5, a full monolayer of OH species was achieved in the presence of high partial pressures of oxygen and steam [81]. The use of a promoter element can also help in achieving higher oxygen coverages and enhance catalytic activity such as the case of bismuth on Pd [85], [86] and Pt catalysts [85].

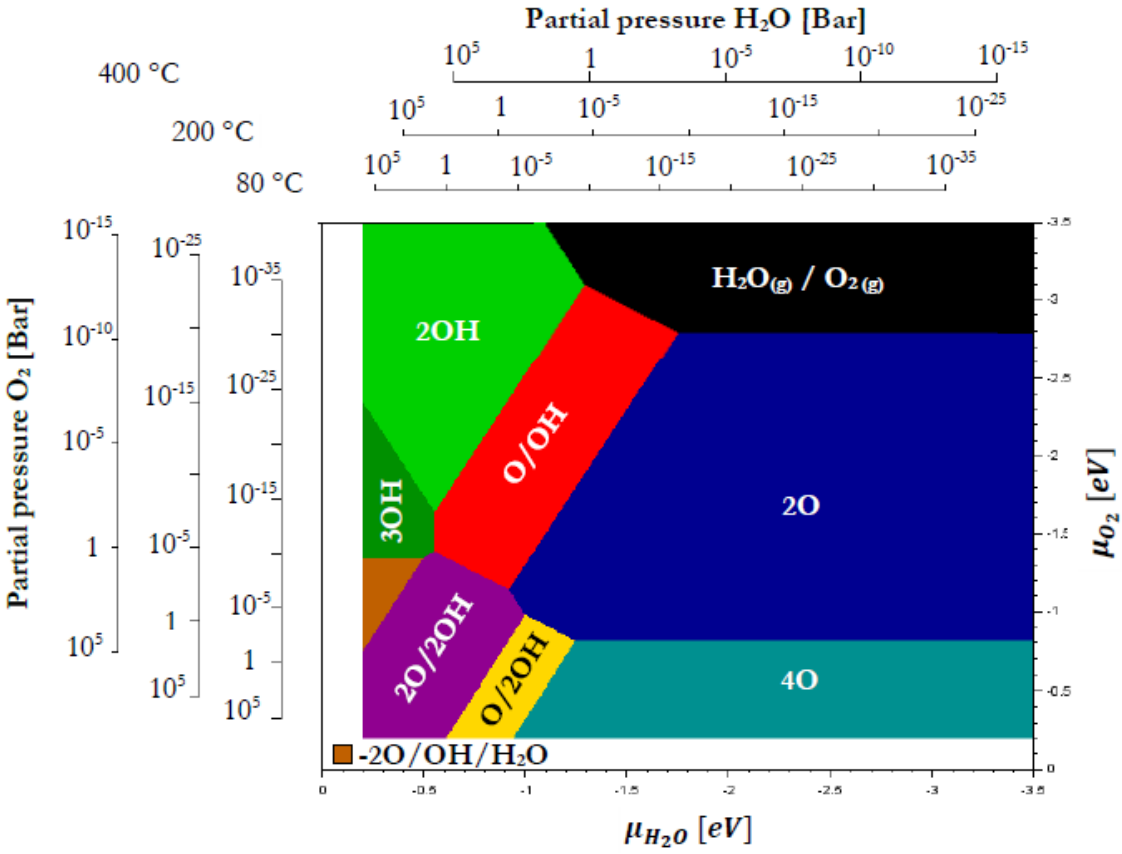

Figure 2-4: Phase diagram for the co-adsorption of O and OH on Pt(100) surfaces [81]

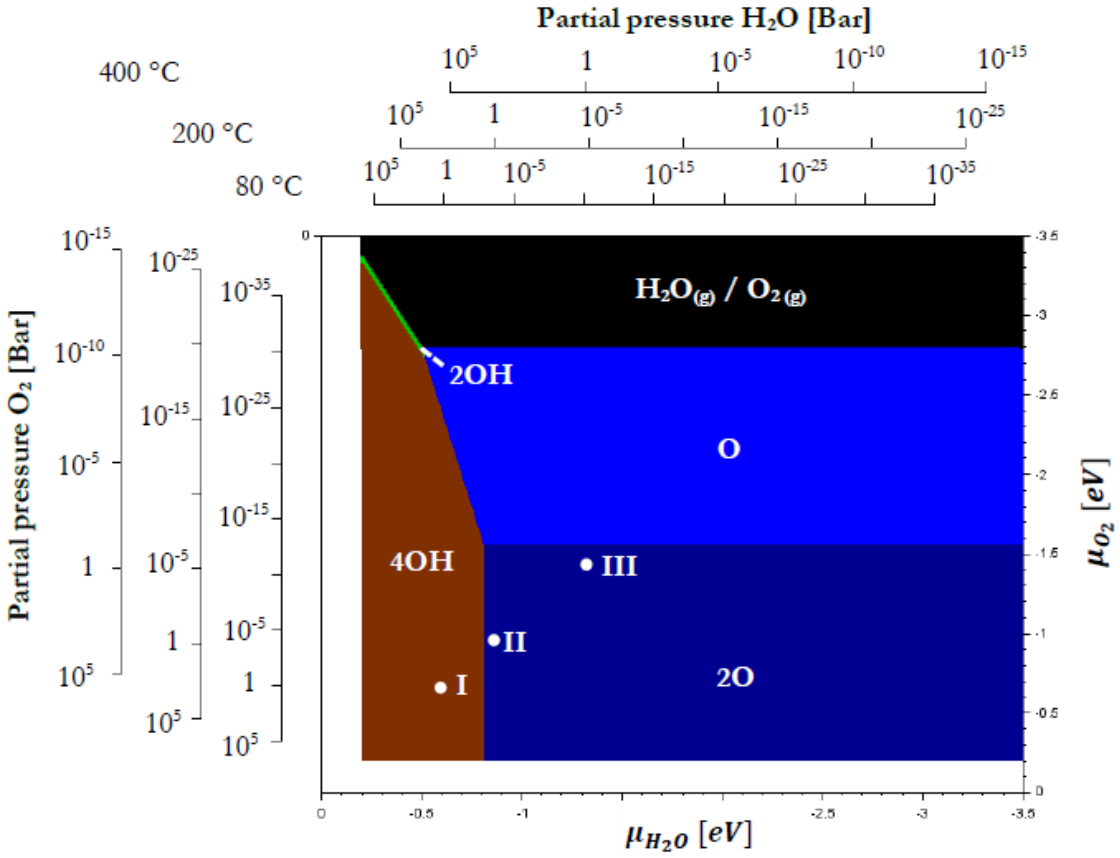

Figure 2-5: Phase diagram for the co-adsorption of O and OH on Pt(111) surfaces [81]

2.6 Effect of co-feeding water in direct methane to methanol conversion

2.6.1 Methanol yield and selectivity

Recent experimental and theoretical studies have shown that the presence of water, either as steam or in the liquid phase has a significant influence on the selective oxidation of methane to methanol process [46], [77], [87]–[89]. Molecular oxygen was used as the oxidant and the experiments were carried out at very low pressures, either at atmospheric pressure or under vacuum conditions. Despite the differing variables in each study such as reactor conditions and catalysts used, the same trend was observed towards the promotional effect of water on methanol selectivity upon the addition of water in the reactor systems.

Both Zuo *et al*. [87] and Lustemberg *et al*. [89] conducted experiments in a micro batch reactor at 175 °C on $CeO_2/Cu_2O/Cu(111)$ and Ni/CeO_2 catalysts, respectively, while Okolie *et al*. [77] performed reactions in a continuous packed bed reactor at 450 °C on NiO/CeO_2-ZrO_2 catalysts. Figure 2-6 below compares the amounts of CH_3OH and CO/CO_2 formed with and without water co-feeding whereby selectivity values were calculated on a carbon basis. These were reported for low methane conversions below 10% since above this threshold, methanol was no longer detected, as the latter reacted further to CO or CO_2. Under dry conditions, the corresponding selectivities towards CO/CO_2 for all three catalysts are above 90% while the amount of CH_3OH formed is minimal with a feed consisting of only O_2 and CH_4. However, in the presence of steam, there was a significant decrease in CO/CO_2 selectivity whereas the selectivity towards

CH_3OH improved considerably. For the inverse $CeO_2/Cu_2O/Cu(111)$ catalyst the methanol selectivity increased by fifteen times while for the Ni/CeO_2 and NiO/CeO_2-ZrO_2 catalysts, it increased to 35% and 19%, respectively [77], [87], [89].

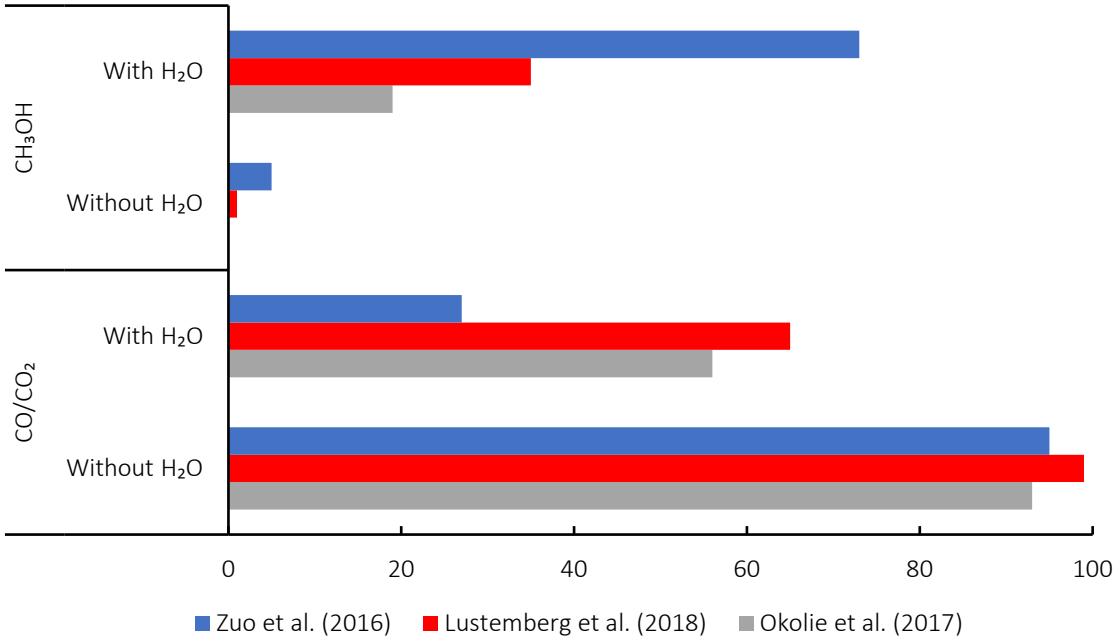

Figure 2-6: Selectivity towards carbon-containing compounds with and without water

From experiments carried out under vacuum conditions at low temperatures in batch reactors, the presence of steam (H_2O:CH_4 = 4:1) significantly improved methanol yield and selectivity [87], [89]. The addition of more water did not change the selectivity for methanol over Ni/CeO_2, but reduced methane conversion. The latter was ascribed to a surplus of OH groups that might saturate sites necessary for methane activation [89]. It has been proposed that water could help the partial oxidation of methane to methanol in two ways. Firstly, it blocks metal active sites with OH species generated from water dissociation. This results in CH_3 species combining with existing chemisorbed O to form OCH_3 species instead of fully decomposing to produce undesired deep oxidation products CO and CO_2. Secondly, by providing an OH species at the site from which methanol has desorbed, water enables methanol formation and desorption [87], [89].

It was shown that co-feeding water was essential to selectively form alcohols in continuous catalytic conversion of methane to methanol in packed bed reactors at atmospheric pressure and high temperature (450-600 °C), For instance, NiO/CeO_2-ZrO_2 [77] and $FePO_4/SiO_2$ [46] catalysts only produced CH_3OH in the presence of steam. The former even produced more of ethanol with a yield of 3.7% compared to that of methanol at 2.9%. Conversely, without water CO_2 was the main carbon-containing compound detected for both NiO/CeO_2-ZrO_2 and $FePO_4/SiO_2$ catalysts.

According to a kinetic model developed for the direct methane to methanol process, it was found that methanol selectivity was only observed at methane conversions below 0.001% at

50 °C under dry conditions. However, under aqueous conditions the selectivity increased by four orders of magnitude. The study proposed that it is due to the solvation free energy of methanol (−0.22 eV at 25 °C) whereby liquid water can possibly lower the difference in methane and methanol activation free energies up to this amount. Furthermore, the experimental values obtained for the selectivity in the presence of liquid water were higher than the predicted ones, suggesting that there may exist other factors in addition to solvation that can improve methanol selectivity [88].

2.6.2 Reactant activation and product desorption

DFT results on $CeO_2/Cu_2O/Cu(111)$ showed that the energy barrier for the activation of the C-H bond in methane was 49 kJ/mol but that of methanol formation was higher at 270 kJ/mol. This was possibly because of the strong interaction between the stable methyl species at the oxygen sites on the CeO_2 nanoparticles. This energy barrier was reduced to 118 kJ/mol once water was introduced, creating new active sites whereby OH adsorbed at Ce sites facilitated the direct formation of methanol from methane [87]. A similar promoting effect of water is observed with Ni/CeO_2 which was modelled using small flat Ni_4 clusters on a flat $CeO_2(111)$ surface partially covered with oxygen. For the $O/Ni_4/CeO_2(111)$ surface, it was found that the active methyl would rather dissociate into CH_2 and H species (97 kJ/mol) than forming OCH_3 species (112 kJ/mol). However, in the presence of surface OH groups from water, a lower energy pathway is provided. Water achieved this by blocking Ni sites to prevent methyl decomposition into CO/CO_2 and by donating an H atom to chemisorbed OCH_3 species to form CH_3OH while helping its desorption when OH is adsorbed onto same site [89]. Hence, water helps in the formation and desorption of methanol through site blocking action and by reducing the product binding to the active site by competitive adsorption of OH species.

Yan *et al*. [90] theoretically investigated the O_2 dissociation mechanism and the effect of water on nine transition metal surfaces (Co, Rh, Ir, Ni, Pd, Pt, Cu, Ag and Au). It was found that water not only enhances O_2 adsorption and facilitates its activation but also reduces the energy barrier for O_2 dissociation. For the purpose of this study, the focus is on pure Pt(111) surfaces as illustrated in Table 2-5. It was speculated that oxygen and water form a complex via hydrogen bonding and are co-adsorbed onto the metal surface. The corresponding standard adsorption free energy, $\Delta G_{ads}(O_2)$ of the complex was more negative than that of oxygen alone by 76 kJ/mol, which means that a more favourable adsorption of O_2 is observed in presence of water. Furthermore, the O-O bond length increases by 2.8% in presence of water, indicating that the activation of O_2 is more facile under such conditions on the Pt(111) surface. The study explained this behaviour by suggesting that water might inject electrons into the metal surface which are simultaneously transferred to the oxygen, resulting in a more negatively charged molecule and thus a more activated O-O bond. Thus, besides promoting O_2 adsorption through hydrogen bonding, water also helps in O_2 activation by altering the electronic structures of the metal surfaces. In terms of O_2 dissociation, the involvement of water on Pt(111) surface was found to lower the standard free energy barrier $\Delta_{dis}G°(O_2)$ by 26.1 kJ/mol while the reaction free energy was slightly reduced by 19.4% [90].

Table 2-5: Adsorption free energy and geometric characteristics of adsorbed oxygen with and without water on Pt(111) surface [90]

	Without water	With water
$\Delta_{ads}G°(O_2)$ (kJ/mol)	-56	-132
O-O Bond length (Å)	1.44	1.48
$\Delta_{dis}G°(O_2)$ (kJ/mol)	88.8	62.7

It can be concluded that the presence of water not only improves reactant-surface interactions but also promotes methanol desorption. Besides helping in the formation and desorption of methanol through its site blocking action, water via hydrogen bonding and electronic modification of the metal surfaces can create centres onto which CH_4 and O_2 activation as well as dissociation are facilitated [87], [89], [90]. As such, since the role of liquid water has not been well established, it would be of great interest to investigate its effect on catalytic performance and product selectivity in methane oxidation over platinum-based catalysts with molecular oxygen as oxidant.

2.7 Trickle bed reactor

Most experiments for the selective oxidation of methane to methanol involving liquid water co-feeding have been carried out in a batch reactor. However, as it is desired to investigate the effect of liquid water on the performance of platinum-based catalysts in a single reactor under continuous flow conditions, a trickle bed reactor (TBR) is a more suitable fit for this purpose. The trickle bed reactor is the most widely used three-phase contacting equipment in industry. It is another variation of the packed bed reactor, except liquid is introduced onto the top of the catalyst packing and trickles down through the bed. Conventional applications of the TBR include hydrocracking, hydrotreating and hydrodesulfurization in the petroleum and petrochemical industry, processes such as hydrogenation, alkylation and oxidation in the chemical industry and in wastewater treatment [91]–[93]. In a typical trickle bed reactor, gas and liquid phases introduced at the top of the column flow co-currently downwards over a packed bed of porous catalyst. It can be operated either in co-currently or counter-currently, however the most popular in industry is the co-current mode of operation because of a lower likelihood of flooding and it allows for larger volumes of each phase through the packed column [94], [95] and thus can accommodate larger flowrates. To be able to evaluate the performance of this type of reactor, it is important to acquire accurate understanding of the key hydrodynamics characteristics such as the prevailing flow regime, liquid hold-up, pressure drop, and knowledge of how these are influenced by design and operating parameters [96].

2.7.1 Flow-regime transition

Different flow patterns can be observed in the co-current trickle bed reactor as the gas and liquid flow over the catalyst bed. These flow patterns are influenced by numerous parameters such as the liquid and gas flowrates, density, viscosity of the fluids and packing properties. They

are generally classified into four distinct flow regimes that correspond to specific gas–liquid interactions with the packed solids [93], [97]:

a) Trickle flow regime
b) Pulse flow regime
c) Spray flow regime
d) Bubble flow regime

The trickle flow regime, also called the low interaction regime is observed when both the gas and liquid flowrates are relatively low. In this regime [see Figure 2-7(a)], the gas phase is continuous, and the liquid phase is semi-continuous whereby the liquid flows in the form of films or rivulets over the packed particles while the gas passes through the remaining void space. As the gas and liquid flowrates increase moderately, the interaction among the phases is higher. This is the pulse flow regime characterized by the formation of alternate liquid-rich and gas-rich zones throughout the packed bed [see Figure 2-7(b)]. The transition to the spray flow region occurs at low liquid and high gas flowrates. The liquid phase then becomes dispersed and travels down the column as droplets entrained by the continuous gas phase [see Figure 2-7(c)]. On the other hand, if the liquid throughput is relatively higher than the gas flow, the gas phase flows in the form of dispersed bubbles through the continuous liquid phase. For this case, the flow regime is described as the bubble flow regime [see Figure 2-7(d)]. Proper understanding of these transition regimes can help in tackling the main issues in the operation of trickle bed reactors such as liquid maldistribution and hot spot formation especially for the case of exothermic reactions [98].

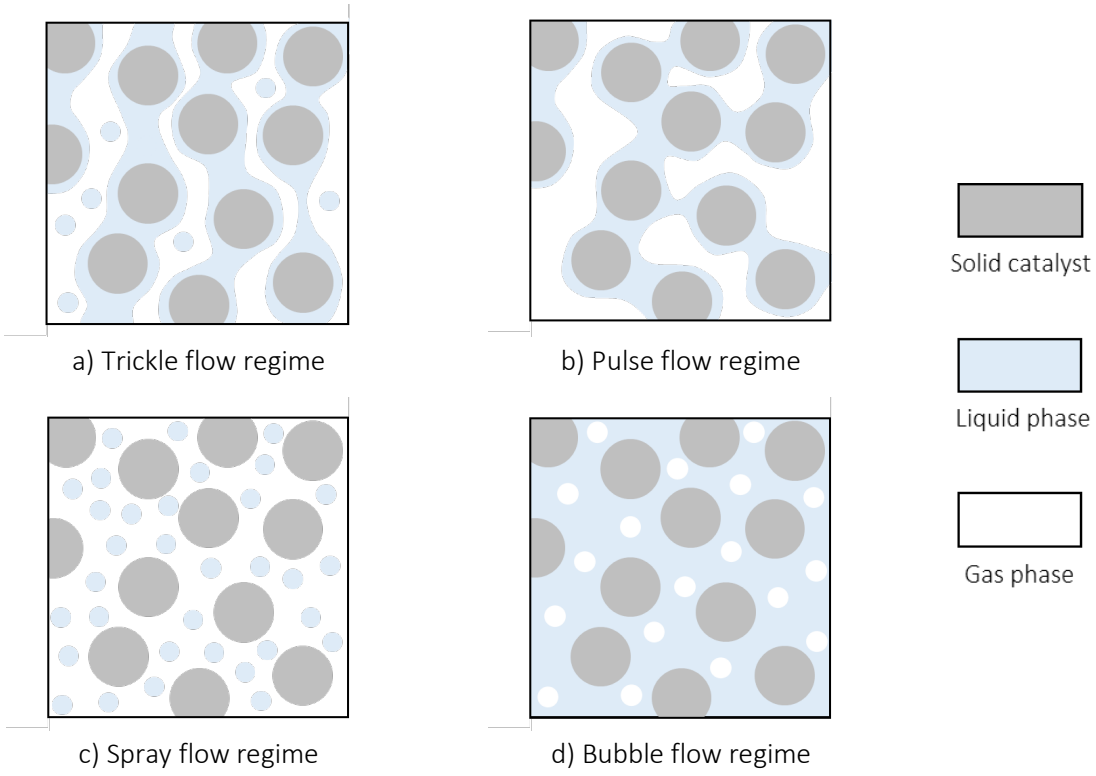

Figure 2-7: Schematic of the four distinct gas-liquid flow regimes in a trickle bed reactor adapted from Gunjal *et al*. [91]

2.7.2 Liquid hold-up and pressure drop

The total liquid hold-up (β_T) in a TBR can be defined as the fractional volume of the reactor that is occupied by the liquid. The liquid hold-up relates to the wetting effectiveness of the solid catalyst, which consequently can affect the reaction selectivity [99]. It also often determines the mean liquid residence time distribution in trickle bed reactors [93]. For porous particles, the total liquid hold-up can be divided into internal and external liquid hold-up. The internal hold-up consists of liquid contained inside a porous catalyst particle whereas the external hold-up refers to the liquid occupying the void volume between the catalyst particles in the packed bed. The external hold-up can, in turn, be further classified into residual or static hold-up (β_R) and dynamic hold-up (β_D). When a pre-wetted catalyst bed is drained, the volume fraction retained is called the residual hold-up. This term can be calculated using Equation 2-11 relating to the dimensionless Eotvos number, Eö (Equation 2-12), which represents the ratio of gravitational to surface tension forces [96], [100], [101]:

$$\beta_R = \frac{1}{20 + 0.9\,\text{Eö}} \qquad 2\text{-}11$$

$$\text{Eö} = \frac{d_p^2 \rho_l g}{\gamma_{gl}} \qquad 2\text{-}12$$

where d_p is the particle diameter, ρ_l the liquid density, g the acceleration due to gravity and γ_{gl} the gas-liquid surface tension.

The volume fraction of liquid trickling out of a packed column after immediate shut-off of liquid feed is known as the dynamic hold-up. It can be calculated using empirical correlations, for instance for an nitrogen-water system under atmospheric conditions with low gas velocities, the Equation 2-13 developed by Wammes *et al*. [101] can be used:

$$\beta_D = 3.8\,\text{Re}_l^{0.55}\text{Ga}_l^{-0.42}\left(\frac{a_v d_p}{\varepsilon_B}\right)^{0.65} \qquad 2\text{-}13$$

$$\text{Ga}_l = \frac{d_p^3 \rho_l^2 g}{\mu_l^2} \qquad 2\text{-}14$$

where Re_l is the liquid phase Reynolds number, a_v the specific external area of the packing, d_p the particle diameter, ε_B the bed porosity. Ga_l, the liquid phase Galileo number can be calculated using Equation 2-14 where ρ_l is the liquid density and μ_l is the liquid viscosity [101]. The pressure drop (ΔP) through a trickle bed reactor is an important design parameter which is affected by the particle packing characteristics and properties of the fluids. This phenomenon arises as a consequence of frictional forces at gas-liquid, gas-solid and solid-liquid interfaces as the gas flows downward through the catalyst bed, which causes resistance to flow and energy dissipation [102], [103]. It is thus essential to maintain a stable pressure drop across the reactor for smooth operation.

Most of the pressure-drop correlations are based on the semi-empirical Ergun equation, which is generally used to estimate the pressure drop in a single-phase packed bed reactor. However, it does not predict pressure drop in a trickle bed reactor accurately due to the varying changes in packing void fraction [104]. Although there has been considerable amount of work found in literature to determine the pressure drop in a trickle bed reactor, the vast majority of the correlations are derived from experimental data obtained in laboratory and are restricted to narrow ranges of operating conditions, solid packing and fluid properties [99]. For instance, Wammes & Westerterp [95] studied the hydrodynamics for two-phase systems operating at elevated pressures (up to 75 bar) with nitrogen and helium in the gas phase and various liquids such as water, ethanol and ethylene glycol in a co-current trickle bed reactor. They developed the inter-related empirical correlations below for pressure drop (Equation 2-16) and dynamic hold-up (Equation 2-17) for systems in the trickle flow regime with $\beta_T > 0.25$ and dimensionless groups ranges between $200 < Re_g < 5000$, $2 < Re_l < 55$ and $3200 < Ga_l < 320000$:

$$u_g = \frac{v_g}{\varepsilon_B(1-\beta_T)} \qquad 2\text{-}15$$

$$\frac{\Delta P}{0.5\,\rho_g u_g^2}\left(\frac{d_p}{L}\right) = 155\left(\frac{Re_g \varepsilon_B}{1-\varepsilon_B}\right)^{-0.37}\frac{1-\varepsilon_B}{\varepsilon_B(1-\beta_T)} \qquad 2\text{-}16$$

$$\beta_D = 3.8\,Re_l^{0.55}\left(Ga_l\left[1+\frac{\Delta P}{\rho_l g L}\right]\right)^{-0.42}\left(\frac{a_v d_p}{\varepsilon_B}\right)^{0.65} \qquad 2\text{-}17$$

where u_g the mean interstitial gas velocity, v_g the superficial gas velocity, ρ_g is the gas density, d_p the particle diameter, L the packing length, Re_g the gas phase Reynolds number, ρ_l the liquid density and g the acceleration due to gravity [95]. Since gas flow in the packed bed is restricted by the presence of the liquid, the porosity term is corrected by $(1-\beta_T)$ to account for the two-phase pressure drop in Equation 2-16. The dynamic liquid hold-up was found to be affected at higher pressures, which is illustrated in Equation 2-17 by the addition of the ratio $\Delta P/\rho_l gL$ to Equation 2-14. This is because an increase in reactor pressure, causing an increase in gas density, which results in a higher pressure gradient due to the increased gas-liquid interaction. With the gas phase occupying more of the void volume between the packed solid, the liquid is pushed out, subsequently reducing the dynamic liquid hold-up [95], [99].

3. Research aims and objectives

3.1 Problem statement

Methane gas is often flared on site instead of being used effectively due to the geo-economic difficulties associated with its transportation from the natural gas reserves through pipelines over long distances. This results not only in a waste of a potential source of energy but also in an increase in the greenhouse gas emissions. Therefore, a desirable alternative would be the conversion of methane into a versatile liquid fuel such as methanol. This would not only make the material transportable, but it can further add value to natural gas by converting it into methanol which is often used as a precursor to various end-products in the chemical industry. However, the present industrial process of manufacturing methanol from methane takes place via the indirect syngas-based route which is energy-intensive and expensive since it involves extreme temperatures. For this reason, the direct synthesis of methanol from methane using molecular oxygen as oxidant with water co-feeding in a single step may constitute a far more economically viable solution and make it possible for on-site conversion at the isolated natural gas reserves. Platinum-based catalysts are anticipated to favour the selective partial oxidation of methane to methanol as they are highly effective in increasing the saturation coverage of oxygen by producing reactive surface oxygen and hydroxyl species in the presence of water and high oxygen partial pressures. This ultimately results in an increase in the selectivity towards methanol and limiting the occurrence of competing side reactions. The co-adsorption of water in this reaction is expected to be essential in blocking active sites for the selective formation of methanol while the use of a promoter is speculated to help in attaining higher saturation coverages over the platinum catalyst surface. It is therefore of interest to evaluate the performance of platinum-based catalysts in the selective oxidation of methane with oxygen as oxidant as well as investigating the involvement of water in enhancing catalyst activity, C_1 oxygenate yield and selectivity.

3.2 Scope of study

The scope of this project will focus on the direct selective conversion of methane over platinum-based catalysts using molecular oxygen as oxidant in the presence of water. This will be achieved by designing and constructing a trickle bed reactor system that can safely carry out the above reaction under high pressure and moderate temperature. Reactor studies to evaluate the performance of these catalyst systems will thereafter be performed. The role of liquid water on catalytic activity as well as productivity and selectivity towards selective oxidation products will also be explored in this study.

3.3 Research hypothesis

It is hypothesised that the direct selective oxidation of methane can occur over platinum-based catalysts with molecular oxygen in the presence of water. This is because it is anticipated that the co-adsorption of water can help in achieving higher oxygen coverages, resulting in the selective formation of methanol through site blocking action. Furthermore, water via hydrogen

bonding and electronic modification of the platinum metal surface can generate active sites whereby reactive surface oxygen and/or hydroxyl species can react with methane to form selective oxidation products, thus improving the yield and selectivity towards C_1 oxygenates.

3.4 Key questions

In accordance with the problem statement and the findings from relevant literature, the formulated key questions for the current study are as follows:

- Can the trickle bed reactor system safely evaluate the performance of the platinum-based catalysts in the selective oxidation of methane?
- Are the platinum-based catalysts active for the selective oxidation of methane with oxygen as oxidant in the presence of water?
- Does liquid water have an influence on the methane conversion?
- Does liquid water have an influence on the selectivity of C_1 oxidation products?

3.5 Sustainable development goals

The overarching aim of this research is closely aligned with four sustainable development goals (SDGs). Methane is a highly potent greenhouse gas and a clean source of energy. This project addresses SDGs 7 and 13 by providing a means to transform it into a useful liquid fuel, thereby decreasing its concentration levels into the atmosphere and help in diminishing the effect of global warming. The direct conversion of methane into methanol is an improved alternative to the existing commercialised indirect syngas-based route which is capital-intensive and requires high thermal energy input. This research will henceforth also tackle SDGs 9 and 12 by developing an innovative DMTM process that can be potentially industrialized to promote responsible consumption and production.

4. Process design and construction of experimental set-up

4.1 Reactor system design requirements

To evaluate the performance of platinum-based catalysts in the selective oxidation of methane to methanol while co-feeding liquid water, an entirely novel experimental set-up, referred to as the trickle bed reactor (TBR) had to be designed and constructed. This is because liquid water has to be fed to the top of the catalyst bed and equally distributed over the bed. Furthermore, classical gas-phase fixed bed reactors do not have an evaporation zone, and liquid water on the expansion valves and in bends will result in pressure fluctuations during the operation (as a consequence of uneven evaporation). For the purpose of this investigation, the reactor system had to satisfy the following set of key criteria:

- Due to the high flammability of methane-oxygen mixtures, the apparatus should be designed to operate safely at high pressures with the necessary measures put in place to avoid any unforeseen circumstances
- The reactor system should be able to properly maintain and control fluid flowrates, moderate temperature, and pressure without major fluctuations
- The apparatus should allow the co-current and continuous flow of both the gases and liquid water over the packed bed so that it can operate in the trickle phase mode
- The apparatus should be designed in such a way to allow the catalytic material to be easily replaced with minimum dismantling
- The pressure drop inside the reactor should be minimal
- The product stream should be vaporised and sampled periodically via an existing gas chromatography (GC) network for accurate analysis and quantification
- To assess the practical viability of the reactor system, reliable as well as reproducible results should be obtained

In order to meet the above requirements and therefore test the research hypothesis, a trickle bed reactor system was designed and constructed. An existing stainless-steel frame (L = 800 mm, W = 700 mm, H = 1800 mm) equipped with adjustable shelf units and four wheels at its base was utilised to build the experimental set-up. The frame was already fitted with one switch box (comprising of four mains-power switch buttons) and three modular control boxes: a Brooks four-channel MFC control box and two 4-zone hot runner temperature control boxes housing Gefran temperature controllers and indicators.

Only Swagelok® high-pressure rated stainless-steel (SS 316L) tubing with outside diameters (OD) 1/8” (0.035” tube thickness) and 1/4” (0.065” tube thickness) were utilised for the lines in the reactor system. Minor components such as valves, microfilters, guard catch pots and fittings (cross and tee unions, reducers, nuts, ferrules) were also made of stainless-steel and sourced from Swagelok®. All the labelled units mentioned in this chapter refer to the final process flowsheet presented in Section 4.8.

4.2 Feedstock supply

Four gaseous components and liquid water were fed to the designed trickle bed reactor. Methane and oxygen were the main reactants, while helium was primarily used as a diluent to control the partial pressures of water, as well as methane and oxygen in the reactor (see Section 4.3.1). Argon gas fed to the reactor was utilized simultaneously for pressurization of the system and as a diluent to ensure complete and smooth vaporization of reactor effluents, and to reduce the flammability region of the effluent gas mixture (discussed in detailed in Section 4.3.2).

4.2.1 Gaseous feeds

Methane, oxygen and helium were all directly supplied from high-pressure gas cylinders (~ 200 bar) via house line connections situated above the apparatus within the walk-in laboratory fume hood. Existing pressure reducing regulators (PV-101, PV-201 and PV-301) were connected straight after the gas cylinders to maintain and deliver a constant set pressure (80-100 bar). Unlike the other gases, argon was made accessible through a centralised house gas supply line with a delivery pressure being limited to approximately 50 bar. A set of on-off valves (V-101, V-201, V-301 and V-501) were already in place in each of the house gas lines.

To prevent any particulate matter (contaminants such as fine solids, dust, dirt) that might be present in the gas cylinders or argon line from entering the system, 0.5 µm micro-filters were installed (S-101, S-201, S-301 and S-501) on the inlet lines. This was done to protect against solid impurities that may damage the sensitive components in the mass flow controllers (MFCs) such as the valves, frit or capillary and that no blockage is caused in the reactor system (S-101, S-201, S-301, S-501).

To maintain a steady total inlet pressure in the catalytic reactor, the pressure of the filtered feed gases (methane, oxygen and helium) was adjusted to the desired value using Tescom™ pressure reducing regulators (PV-102, PV-202 and PV-302). Since it is desired to control the partial pressure of the different compounds, their flowrates had to be controlled independently. This was achieved by metering each gas through their respective Brooks thermal MFC prior to entering the reactor (FV-101, FV-201 and FV-301). Check valves (V-103, V-203 and V-303) were added to the outlet lines of each MFC. These acted as a measure to prevent any material from entering the MFCs or house gas lines in case of fluid backflow. A set of on-off valves (V-102, V-202 and V-302) were installed immediately after the one-way valves.

Due to explosive nature of methane-oxygen mixtures, extra precaution had to be taken. The occurrence of flame propagation in the methane and oxygen feed lines was mitigated by using a flame arrester. This safety device functions by permitting fluid to pass through but not the flame in order to avoid a larger fire or explosion upstream. It consists of a high thermal conductivity filter element with small apertures which quenches the flame by absorbing the heat, thereby reducing its temperature below its auto-ignition point. Based on this working mechanism, a combination of sintered metal filter in series with a check valve was used as a

flame arrester for both the methane (S-102, V-104) and oxygen (S-202, V-204) feed lines [105]–[107]. Prior to being connected to the reactor top section, each feed line tubing was coiled several times (pigtail design) for ease of movement when adjusting the connection fittings during loading and unloading of catalyst, as well as reducing strain on the lines.

4.2.2 Liquid water feed

The liquid water in this system was supplied from a Schott glass bottle (T-401) containing deionised water at ambient conditions. The water was degassed by purging helium through a sparging frit to promote the displacement of dissolved carbon dioxide and air. The water was filtered using a 20 µm Teflon suction filter connected to a 1/8" Teflon hose and metered through an HPLC pump (P-401) as a means to control the flow of the liquid entering the reactor. The water feed pot was placed on an electronic mass balance to check for flow constancy during experiments. The line exiting the pump was equipped with a check valve (V-403) to protect the pump from backflow damage (when reactor is pressurized) before being connected to a three-way valve (V-402). One exit from this valve was directed to an on-off valve (V-401) then into a drain vessel downstream. This line was used to manually prime the HPLC pump to check for bubble-free flow before start-up operation. The other exit was routed via a safety pressure-relief valve (V-404 calibrated to 50 bar) prior to being connected to the reactor head. This was done as an extra precautionary measure in case of over-pressurisation in the reactor.

4.3 Trickle bed reactor design

In this section, the design and construction specifications of the catalytic packed bed reactor for the selective oxidation of methane in presence of liquid water are discussed in detail. Justifications for the choice of each reactor requirement are also provided.

4.3.1 Requirement for helium gas in the trickle bed reactor

One of the most important safety considerations that needs to be addressed when handling gas mixtures is their capability to form flammable atmospheres in air, mostly concerned with oxygen. Methane is non-toxic but is an extremely combustible gas. At the correct concentrations and in the presence of an ignition source, it can cause disastrous explosions as it was the case for the Deepwater Horizon oil spill in April 2010 [108]. For the combustion of a methane-oxygen mixture to occur, the composition of methane must lie within a certain range, known as the flammability range. The more dilute mixture is called the lower flammability limit (LFL) and at a concentration below it, the mixture lacks fuel to burn. Conversely, the more concentrated mixture is known as the upper flammability limit (UFL) and at a concentration above it, the mixture is too oxygen-deficient to burn. For a binary mixture of methane with pure oxygen at 1 bar and 25 °C, the reported LFL and UFL of methane in terms of volumetric percentages are 5% and 60%, respectively [109].

Various factors can affect the flammability limits but the most important of these are temperature, pressure and addition of a diluent [110]. Correlations developed by Zabetakis

[111] were used to investigate the influence of temperature and pressure on the flammability limits. There exists a linear relationship between temperature and the flammability limits (see Figure 4-1). Increasing the temperature results in a trivial change in both the UFL and LFL, and thus only a slight broadening of the flammability range. Thus, it can be concluded that temperature has hardly any influence on the flammability of the methane-oxygen mixture. Pressure has little influence on the lower flammability boundary as illustrated in Figure 4-2. However, a rise in pressure results in a significant increase in the upper flammability limit, which broadens the flammability envelope significantly.

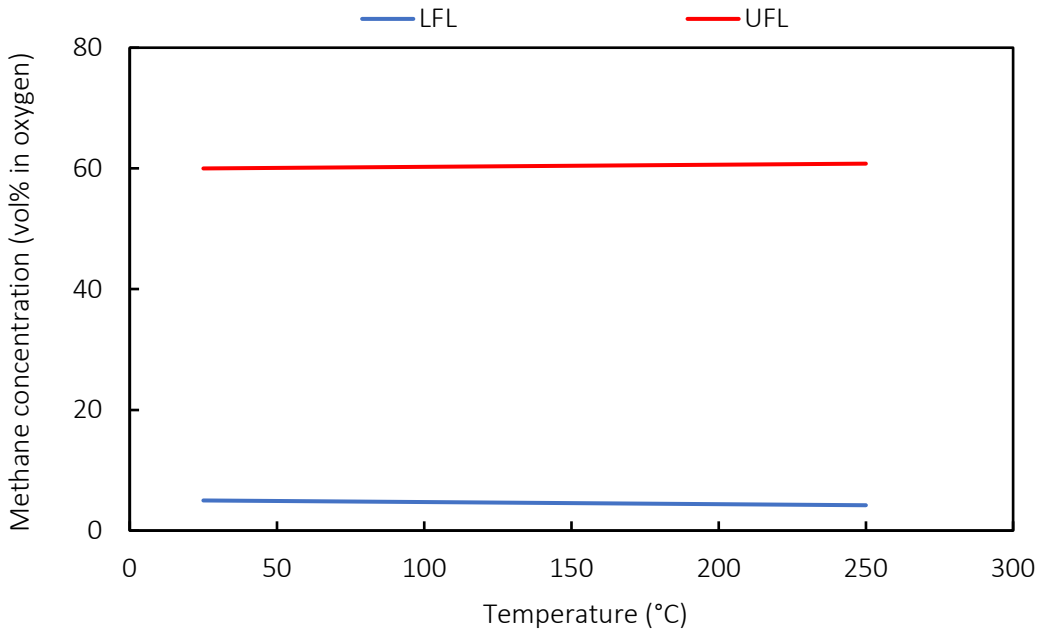

Figure 4-1: Effect of temperature on the flammability range of methane-oxygen mixtures at 1 bar

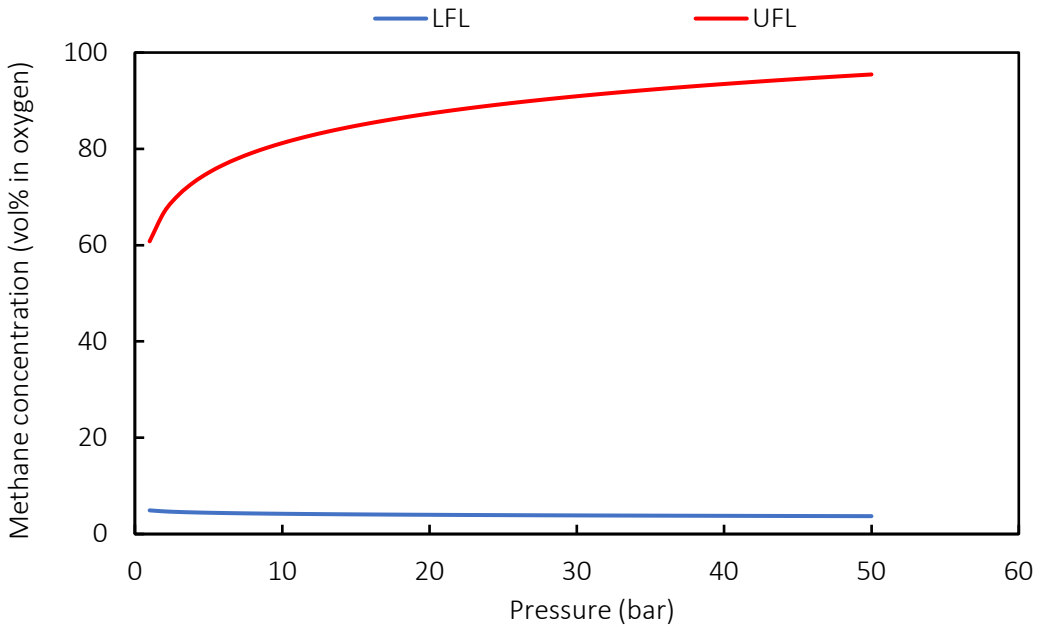

Figure 4-2: Effect of pressure on the flammability range of methane-oxygen mixtures at 25 °C

Flammability ranges are typically determined in air, which is composed of oxygen and mainly nitrogen, an inert gas. The reported LFL and UFL for a methane-air mixture at 1 bar and 25 °C are 5 vol% and 15 vol%, respectively [109]. This shows that an increase in the inert gas concentration considerably influences the UFL since at this limit, oxygen is deficient, hence any decrease in its composition results in a narrowing of the flammability. The maximum temperature that can be attained in any combustion process is thermodynamically limited to the adiabatic flame temperature (AFT). This corresponds to a temperature of 1500 K for a methane-oxygen gas mixture at the reported flammability limits mentioned above [109]. The presence of any diluent gas such as inert gases reduces the AFT by consuming a part of the energy from the exothermic combustion reaction. Consequently, introducing an inert in a combustible mixture can narrow the flammability range [112].

Figure 4-3 demonstrates the influence of different diluent gases on the flammability ranges of methane–inert–air mixtures under standard conditions. It can be observed that to reduce the flammability envelope to the point where the mixture is incombustible, argon requires a concentration two times higher than that of carbon dioxide. The observed trend in diminishing the flammability region by these diluents, CO_2 > He > N_2 > Ar, is attributed to the difference in their heat capacities. A higher heat capacity results in a smaller flammability region since the AFT is reduced to a greater extent. Despite helium and argon having a similar heat capacity, the former reduced the flammability region more, due to its much higher thermal conductivity (approximately nine times higher than that of argon) resulting in higher thermal losses [113]. Consequently, to alleviate the issue associated with the high flammability of methane-oxygen mixtures in the high-pressure trickle bed reactor, helium was chosen as the inert diluent. Helium was thus mixed with methane and oxygen via a cross union fitting just before being fed to the gas feed inlet of the reactor.

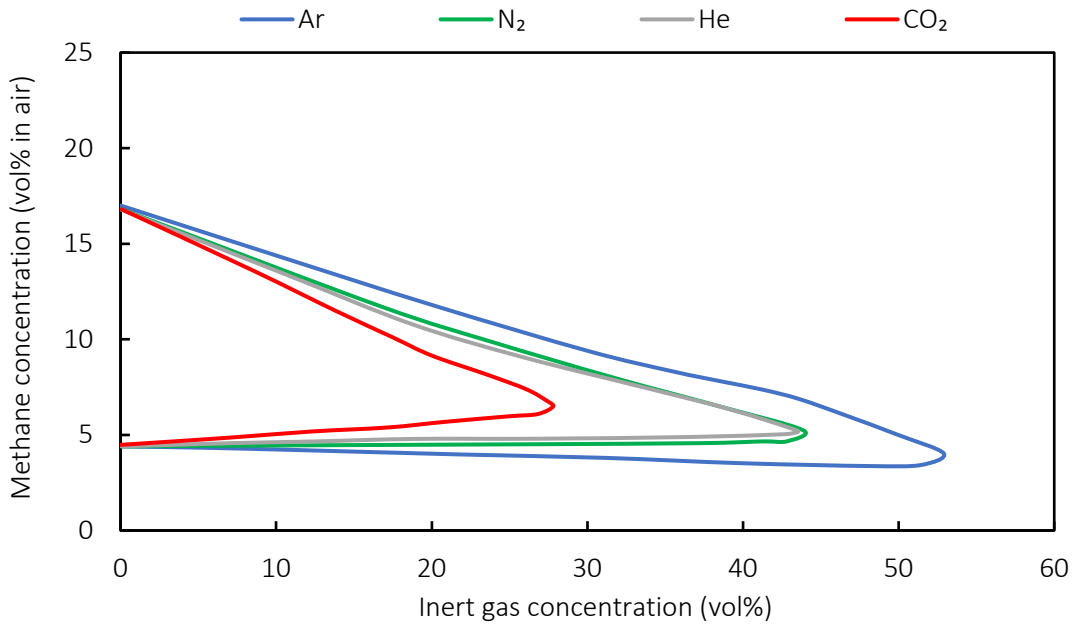

Figure 4-3: Effect of inert gases on the flammability range of methane–inert–air mixtures at 1 bar and 20 °C [113]

4.3.2 Requirement for argon gas in the trickle bed reactor

Pressure drop across catalytic bed reactors is a well-known phenomenon that can affect the performance of a reactor (lower reaction rates due to reduction in the partial pressures of reactants). Hence, it is essential to control and maintain a constant reactor pressure for stable operation and repeatable experiments. The pressure in the reactor was controlled by means of a flow-restrictive device such as the needle valve (V-602) placed directly after the reactor outlet. Pressure-controlled addition of argon gas kept the flow over this expansion valve (V-602) constant. This ensures that any variation in the flow is compensated by the make-up argon gas. Therefore, the pressure drop over the needle valve remains constant and so does the pressure in the reactor. For this pressure control gas technique to work, the flowrate of argon was not controlled; the argon MFC (FV-501) upstream was set to function as a mass flow indicator by keeping the flow setpoint to 100% (i.e., with the regulating valve fully open).

Following the argon MFC outlet, the line was also equipped with a check valve (V-503) in series with an on-off valve (V-502) prior to entering the reactor. Unlike for the other gases, a more robust pressure regulator sourced from Air Products (PV-501) was utilised for the argon line as it was later found out during experiments that it was more effective in maintaining constant pressure during operation. As mentioned previously, since the delivery pressure of the argon house line was restricted to 50 bar, this was the highest pressure that could be achieved inside the trickle bed reactor.

Most importantly, the purpose of the argon gas was to ensure complete vaporization any liquid in the reactor effluent prior to the expansion valves V-602 and V-701. The rationale for diluting the product stream with argon was to help in decreasing the partial pressures of the various compounds, especially liquid water (below its respective saturation pressure). Furthermore, in terms of safety, a high flowrate of the argon diluent would guarantee that the composition of the effluent stream in the vent line would lie outside the limits of the methane-oxygen flammability region.

4.3.3 Reactor head features

The trickle bed reactor is made from stainless-steel and comprises of two separate units: reactor head and main reactor body. The key function of the reactor head is to allow the liquid and gaseous feeds to mix properly in the initial section of the packed bed reactor. As illustrated in Figure 4-4, the reactor head has two feed inlet ports on the side (top inlet for liquid and bottom inlet for gas feed), and one inlet on top which is typically used for inserting a stationary thermocouple. However, since no such thermocouple was utilised during the experiments, a stopper was instead placed there.

The liquid feed port was designed in the form of a central 1/4" OD tube with its outlet extending a few millimetres beyond the end of the reactor head. This was done such that when the head is mounted onto the body, the liquid outlet will submerge inside the upper layer of the reactor packing, allowing the liquid to be drawn and dispersed smoothly into the void spaces between

the silicon carbide (SiC) particles. This is essential to prevent liquid droplets from forming and causing the space velocity to fluctuate due to pulsating flow. The gaseous feed was allowed to flow simultaneously in the annulus region surrounding the central liquid tube to facilitate mixing in the reactor top section as well as driving the liquid feed down the catalytic bed.

Prior to operation, the reactor head is mounted and sealed securely to the main body via Swagelok® vacuum coupling radiation (VCR) connections and a disposable metal gasket. The feed inlet ports are also connected to their respective lines via VCR seal fittings and metal gaskets. It was impractical to install a pressure relief valve directly on top of the reactor head (where thermocouples are occasionally introduced) since that would require recurring disassembly of numerous fittings during loading and unloading of catalyst. Hence, a branched line straight after the methane-oxygen-helium mixing point was installed to accommodate a pressure relief valve (V-601) and an analogue pressure indicator PI-601 (see Appendix A.1). The safety valve was calibrated to 50 bar and would solely be activated in case of uncontrollable pressure build-up under unpredictable circumstances, such as a blockage downstream (caused by solid residue). The emergency lines from both safety valves V-404 and V-601 were directed to a guard catch-pot with a dip-tube design (C-401) prior to being sent to the overhead vent in the walk-in fume hood. Any liquid collected can be periodically drained via on-off valve V-405.

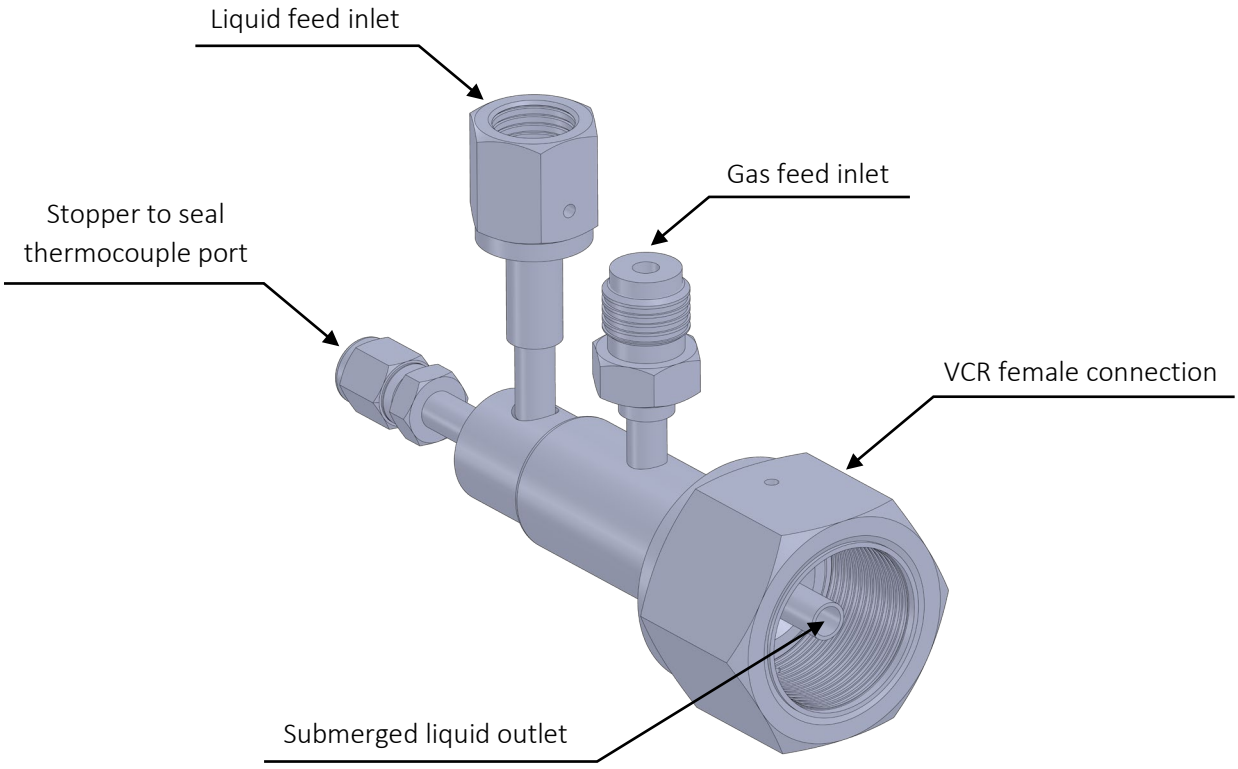

Figure 4-4: 3D illustration (not to scale) of reactor head showing gas and liquid ports, annular flow region and VCR seal connection

4.3.4 Main reactor body

4.3.4.1 Reactor body features

The standard reactor in the laboratory consisted of a stainless-steel shell, tubular in shape with an outside diameter (OD) of 19.05 mm (3/4”) and an inside diameter (ID) of 15.75 mm (wall thickness of 0.065”). A central stainless-steel thermowell (OD = 3.25 mm, ID = 1.6 mm) was incorporated in the reactor body that extended approximately 10 mm away from the upper lip of the body. The purpose of the thermowell is to house a mobile thermocouple (1 mm thick, 500 mm long, J-type) utilised to accurately measure the temperature at any point along the length of the reactor body. During catalyst testing, the tip of the thermocouple was positioned in the middle of the packed catalyst bed to measure the reaction temperature.

Since it was desired to operate at high pressures for the direct conversion of methane to methanol in the trickle bed reactor, a pressure-resistant assembly was necessary. According to previous studies, it has been demonstrated that exposing the gaseous reactants to the bare stainless steel reactor wall at elevated pressures led to reduced methanol selectivity as the formation of deep oxidation products CO_2 and CO was preferably catalysed by the metal surface [5], [74], [114]. To limit metal-surface interactions, quartz tube lined reactors have been commonly used [40], [75], [76]. Using a similar approach in this present investigation, an inner quartz tube was used to prevent the gases from reacting with the metal surface as well as withstanding high pressures. Restricted by the diameters of the reactor shell and thermowell, it was decided that the quartz liner should have an OD of 14 mm and an ID of 12 mm. The central thermowell was also sheathed with a quartz tube (OD = 6 mm, ID = 4 mm) with one dead end.

To properly seal and keep the quartz tube liner stationary in the reactor shell, an O-ring was used [40] in conjunction with a hollow cylindrical part adapted for the O-ring seal mechanism. The O-ring (OD = 19.05 mm, ID = 13.94 mm, thickness = 2.62 mm) used for this purpose was made of fluorocarbon elastomer (sourced from RS Components Ltd) as it can withstand temperatures higher than 200 °C and is resistant to oxidation and flame. The cylindrical part was also made from stainless steel (SS 316L) with an OD of 19 mm, ID of 14 mm and 20 mm in length. The interior of the reactor body was specifically modified to accommodate and provide a seat for the O-ring seal pressed by the cylindrical part (see Figure 4-7 in Section 4.3.4.2). With this type of reactor assembly, argon gas was allowed to flow pressure-controlled through the annulus between the quartz liner and stainless-steel tube instead of being fed to the reactor outlet as mentioned in Section 4.3.2 (Guo, 2018). Therefore, the reactor body was designed to include a side inlet port to feed argon gas and one exit port for the product stream as shown in Figure 4-5. It should be noted that for argon to completely evaporate the reactor effluent, the length of the quartz tube liner should not run all the way to the bottom of the reactor (discussed in detailed in the Section 4.3.4.3).

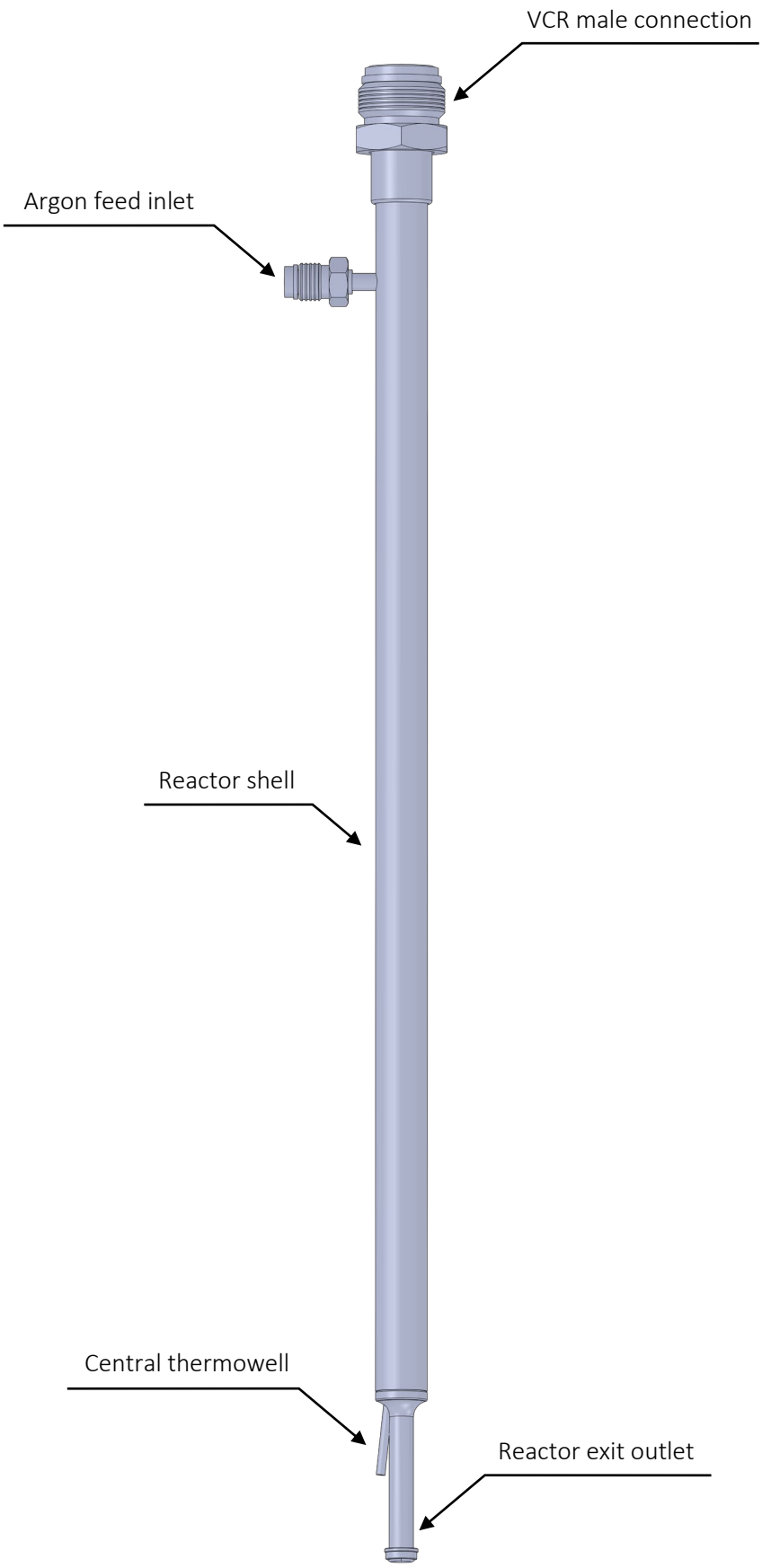

Figure 4-5: 3D illustration (not to scale) of reactor body showing argon side inlet port, reactor exit port, central thermowell and VCR seal connection

With the diameters of the reactor shell and quartz tubes already fixed, it was possible to estimate the length of the catalytic bed length required in the trickle bed reactor. Based on experimental studies in our research group performed in a 6.35 mm OD packed bed reactor for direct methane to methanol (DMTM) reaction, it was shown that a maximum space velocity of approximately 60 ml_{CH_4}/g_{cat}.min could be obtained using 10 wt% Pt_3Ag/TiO_2 catalysts. Since it was intended to introduce more catalysts in the TBR due to its higher packing volume, the space velocity was decreased by five-fold to 12 ml_{CH_4}/g_{cat}.min. With the methane MFC having a maximum flowrate of 51.4 ml_n/min and assuming a bulk catalyst bed density of 0.5 g/ml (and the annular area between the quartz liner and thermocouple quartz sheath to be 85 mm^2), the length of the catalyst bed required to meet the aforementioned space velocity was calculated to be 100 mm. As an approximate estimate, the total reactor length was calculated to be five times the length of the catalyst bed with additional space attributed to glass wool plugs at each end of the reactor packing. Consequently, the reactor body for the trickle bed reactor was designed with an overall length of 545 mm, excluding the exit outlet port (see Figure 4-6 in Section 4.3.4.2).

4.3.4.2 Detailed reactor assembly

Table 4-1 below shows the list of the various fittings and components that constitute the assembly of the packed trickle bed reactor R-601. Stainless steel tubing (Grade: 316L, OD of 1/8" and 1/4"), nuts, front and back ferrules sourced from Swagelok® were used to connect the lines to and from the trickle bed reactor. The O-ring, metal gaskets and quartz tubes were consumables and required regular replacement during the loading of a fresh batch of catalyst.

Table 4-1: List of components used for the assembly of the trickle bed reactor R-601

Components	Detailed description	Part no.	Qty	Manufacturer
High-pressure reactor shell assembly	Grade: SS 310L 15.75 mm ID, 19.05 mm OD, 545 mm L Design temp: 400 °C Max pressure: 200 bar	0500	1	Cape Catalytix (Pty) Ltd
Nickel coated thermowell	Grade: SS 316L 1.6 mm ID, 3.25 mm OD, 535 mm L			
Reactor head	Grade: SS 316L Liquid inlet port (incl. female VCR nut) Gas inlet port (incl. male VCR nut) Top inlet port (incl. 1/8" tube fitting)	1400	1	
5-zone electric furnace	Grade: SS 316L 22 mm ID, 254 mm OD, 420 mm L Design temperature: 350 ˚C	Customized	1	
Part for O-ring seal mechanism	Grade: SS 316L 14 mm ID, 19 mm OD, 20 mm L	Customized	1	

Components	Detailed description	Part no.	Qty	Manufacturer
Male VCR nut	Grade: SS 316 Size: 1/4" gasket face seal fitting	SS-4-VCR-4	1	Swagelok
Male VCR split nut	Grade: SS 316 Size: 1/4" gasket face seal fitting	SS-4-VCR-4-SN	2	
VCR tube adapter	Grade: SS 316 Size: 1/4" face seal gland	SS-4-VCR-3-4TA	4	
Female VCR nut	Grade: SS 316 Size: 1/4" gasket face seal fitting	SS-4-VCR-1	3	
Reducing union	Grade: SS 316 Size: 1/4" to 1/8” tube fitting	SS-400-6-2	4	
Reducer	Grade: SS 316 Size: 1/4" adapter to 1/8” tube fitting	SS-200-R-4	1	
Cross union	Grade: SS 316 Size: 1/8" tube fitting	SS-200-4	1	
Tee union	Grade: SS 316 Size: 1/4" tube fitting	SS-400-3	1	
Female NPT tee union	Grade: SS 316 Size: 1/4" tube fitting	SS-400-3-4TFT	1	
High pressure relief valve	Grade: SS 316 Size: 1/4" tube fitting	SS-4R3A	1	
Metal VCR gasket	Grade: SS 316L Size: 1/4", silver plated	SS-4-VCR-2	4	
Fused quartz tube sealed at one end	4 mm ID, 6 mm OD, 520 mm L	Customized	1	Technical Glass Products Inc.
Fused quartz tube	12 mm ID, 14 mm OD, 375 mm L	Customized	1	
Fluorocarbon elastomer O-Ring	13.94 mm ID, 19.05 mm OD, 2.62 mm L Temperature: -15 °C to +200 °C	129-088	1	RS Components
Analogue pressure indicator (PI-601)	1/4” male NPT thread Pressure range: 0-50 bar	-	1	Wika
Probe thermocouple	Stainless steel, J-type 1 mm OD, 500 mm L	Customized	1	Thermon
Reactor head metal VCR gasket	Grade: SS 304 14 mm ID, 29 mm OD, 1 mm L	Customized	1	Gasket & Shim Industries Ltd

Figure 4-6 illustrates an overview of the assembled trickle bed reactor enclosed by the 5-zone electric furnace with the detailed arrangement of the reactor shell, quartz tube liner, thermowell, thermowell quartz sheath and cylindrical part for the O-ring seal mechanism. The lengths of these individual components, as well as the internal packing consisting of the catalyst bed and the different packed sections of SiC are also shown.

The reactor top section is depicted in Figure 4-7 which shows the reactor head mounted on the upper end of the reactor body. The inlet ports for the feed gases and the side inlet port for argon are also shown. It can be clearly seen that the outlet of the liquid port is submerged into the upper layer of the reactor packing. The O-ring is held in place inside the reactor and pressed by the customized cylindrical part to ensure isolation of the reactant gases inside the reactor quartz liner from the argon make-up gas.

The middle section of the reactor is illustrated in Figure 4-8 which shows the detailed packing inside the trickle bed reactor including the catalyst bed, bottom and top SiC packed regions, and the evaporation zone. The outside and inside diameters of the reactor assembly are also given. The catalyst is held in place with glass wool plugs on either end. The central thermowell is quartz-sheathed and houses an internal thermocouple with the tip placed at the centre of the catalyst bed for accurate reaction temperature measurement.

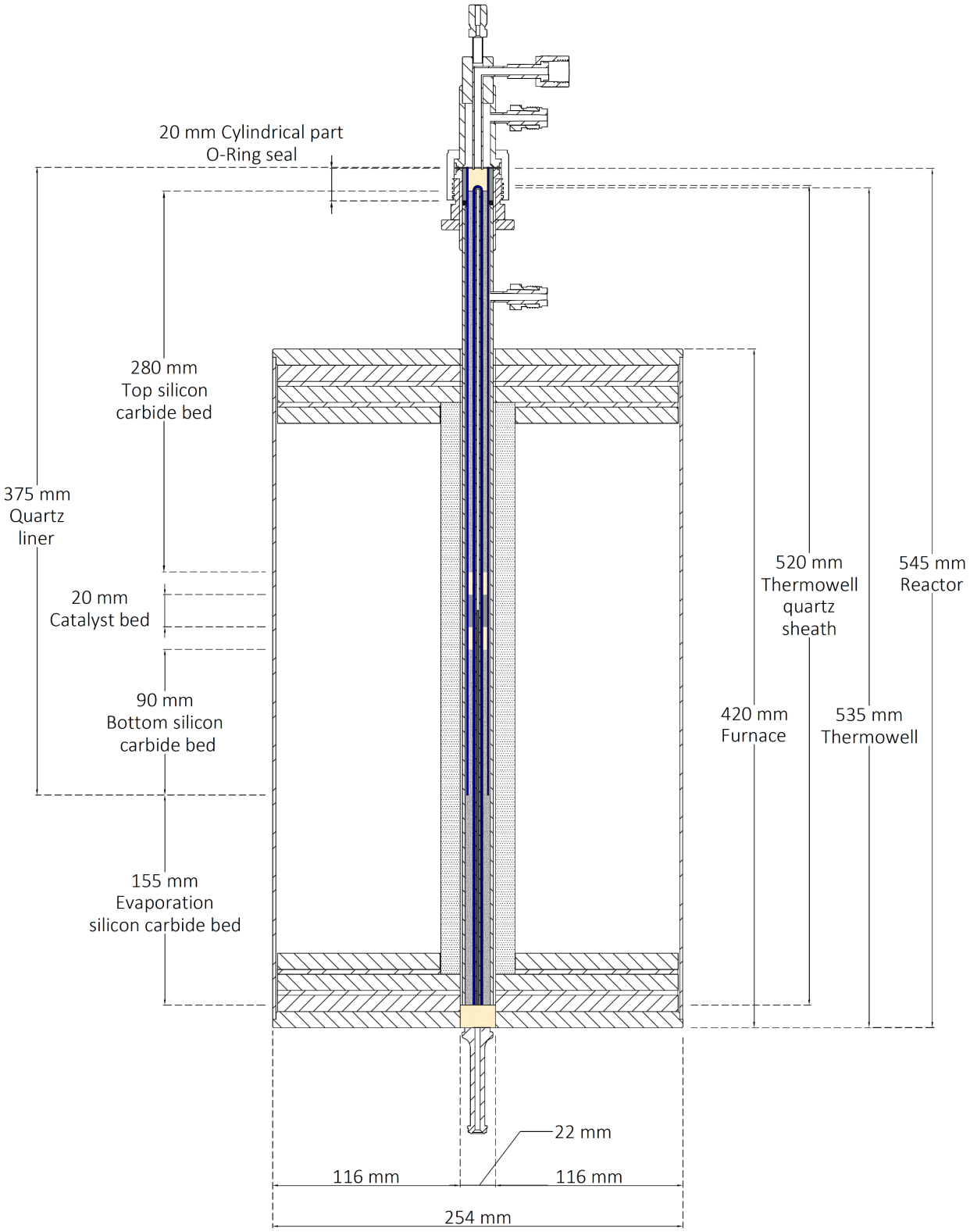

Figure 4-6: Section view of detailed internal packing and dimensions of reactor assembly consisting of reactor head and reactor body enclosed by five-zone electric furnace

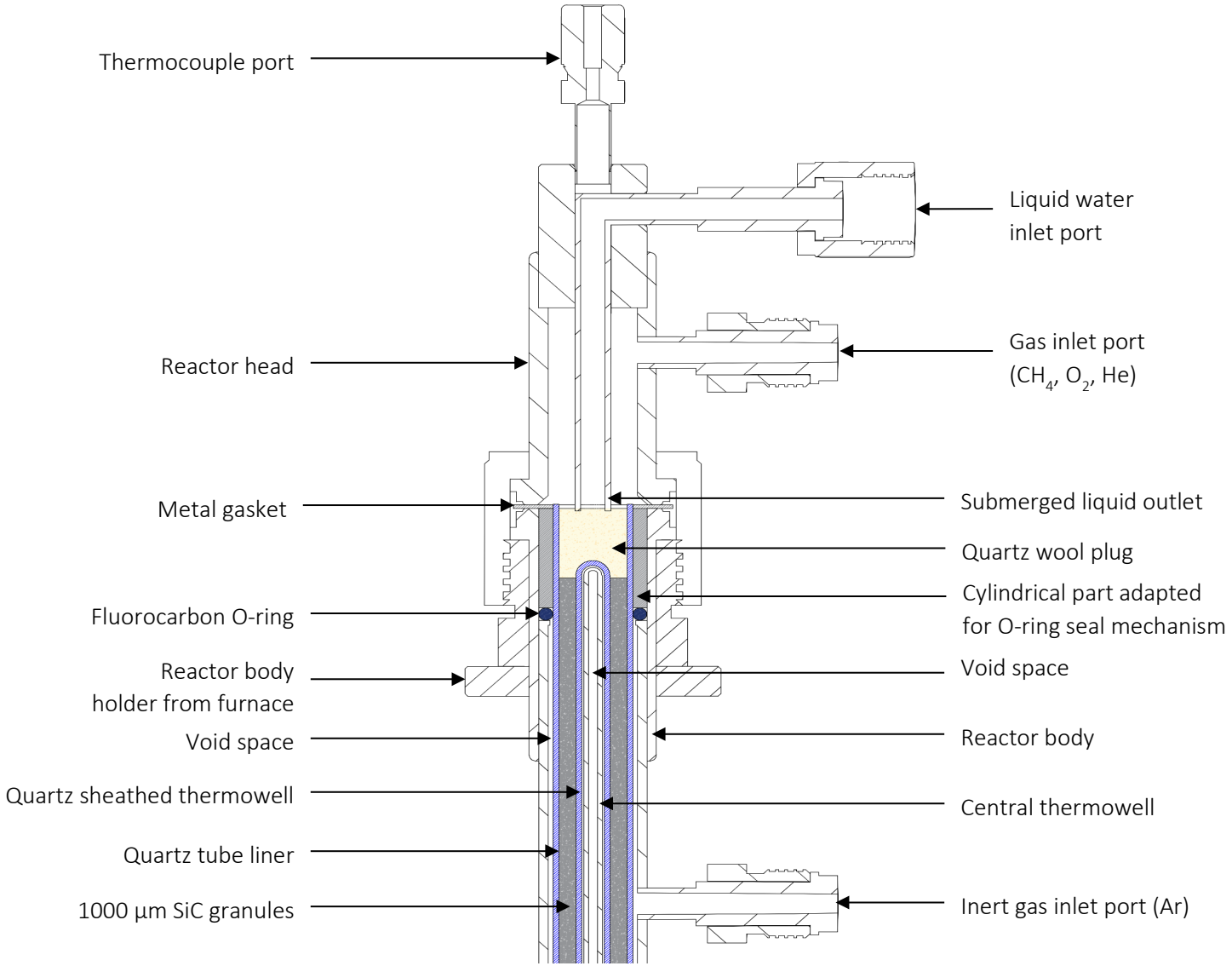

Figure 4-7: Section view of reactor top section showing reactor head, gas and liquid inlet ports and O-ring seal mechanism

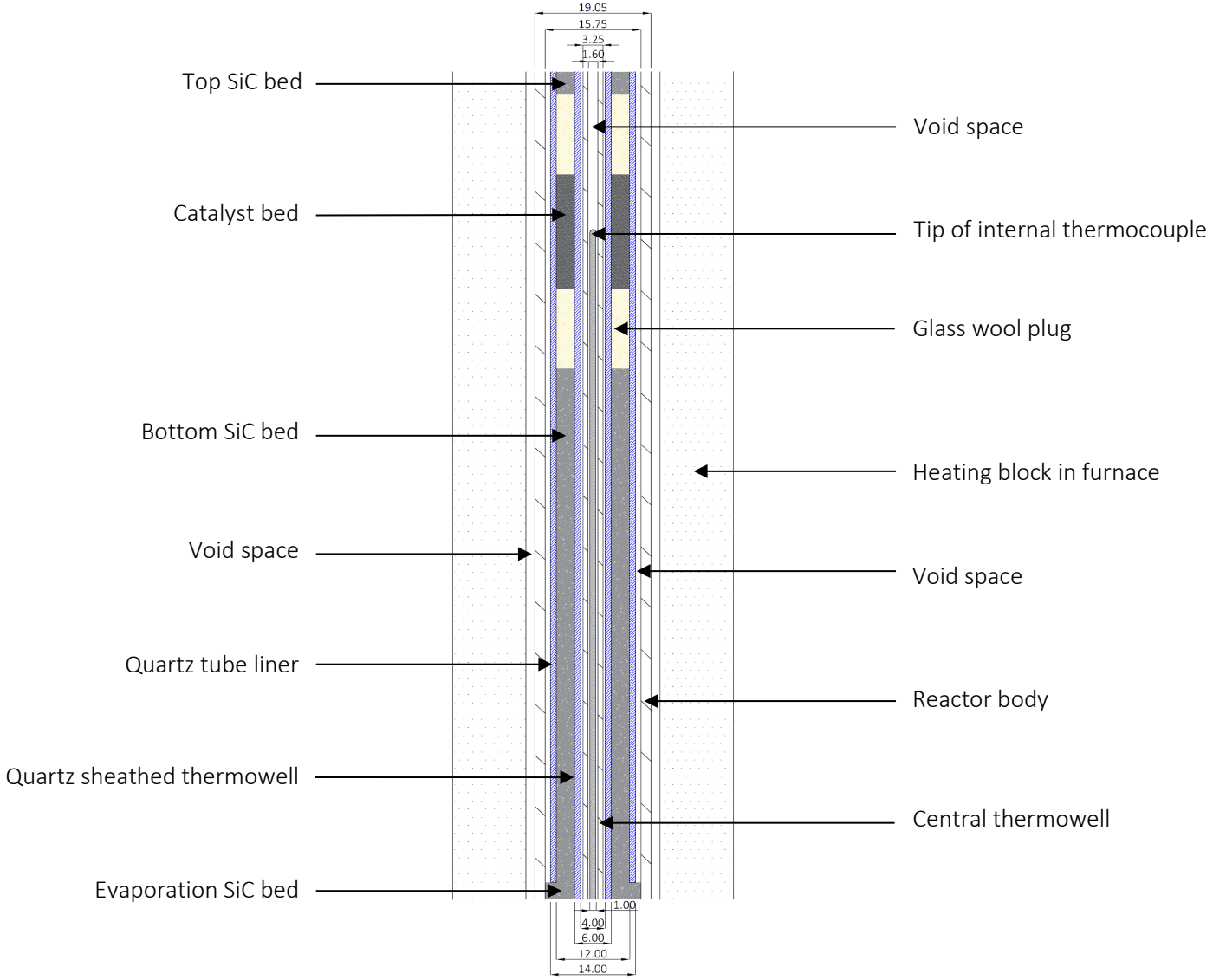

Figure 4-8: Section view of detailed packing inside the trickle bed reactor showing the catalyst bed and SiC packed regions (all units in mm)

4.3.4.3 Heating zones and catalyst location

A multi-zone electric furnace enclosing the reactor body was designed and constructed to control the temperature inside the reactor. It must be ensured that at the given operating reactor pressure, the temperature of the liquid line will be maintained below the boiling point of water, otherwise the liquid will superheat and evaporate by delayed boiling, causing fluctuations in linear gas velocity. For this reason, it was decided that the initial section (~ 130 mm) of the reactor packing should not be heated by the furnace, hence the top end of the reactor tube, including the reactor head extended out of the furnace. As illustrated in Figure 4-6, the drop tube furnace is 420 mm long with an external diameter of 254 mm and a 22 mm cylindrical slot through the centre; to closely fit the reactor body whilst also allowing its recurrent movement inside the furnace during catalyst loading and unloading. To immobilise the reactor body, a holder was installed on top of the furnace where the hexagonal male nut of the reactor body could rest as depicted in Figure 4-9.

The outer casing was made of stainless steel which housed the central heating block and five heating bands. These heating bands, each equipped with an independent J-type thermocouple, were connected to Gefran 600 temperature-controllers and supplied heat to the reactor indirectly via the central heating block. Layers of high-temperature ceramic fibre were embedded inside the casing surrounding the heating bands for thermal insulation. To support the furnace structure, it was securely mounted to the frame through a thick metal slab hinged to a bracket at the base. To facilitate the removal of the reactor, this metal slab could be leaned outwards via a tilting mechanism (to avoid obstruction by the ceiling in the reactor fume hood).

It is essential for the catalyst bed inside the trickle bed reactor to be maintained at the same reactor conditions for consistency and comparison purposes. As temperature variations will typically exist within the tubular reactor during heating (due to the ends being exposed to the surroundings), the length of the isothermal zone within which the catalyst bed should be positioned during operation had to be determined. This was achieved by setting the five heating zones of the furnace to a constant temperature and measuring the temperature at different points along the length of the reactor by means of a moveable 500 mm long thermocouple (housed in the central thermowell) which was connected to a Gefran 40 temperature-indicator. For an approximate representation of the axial temperature profile inside the trickle bed reactor during catalyst performance tests, helium was allowed to flow through a bed of SiC granules (d_p = 1000 µm) packed between the quartz liner and thermowell quartz sheath with argon flowing outside the quartz liner to maintain a total reactor pressure of 30 bar. Inert gases were used, otherwise the heat released during the exothermic reactions between the reactants CH_4 and O_2 could influence the temperature profile.

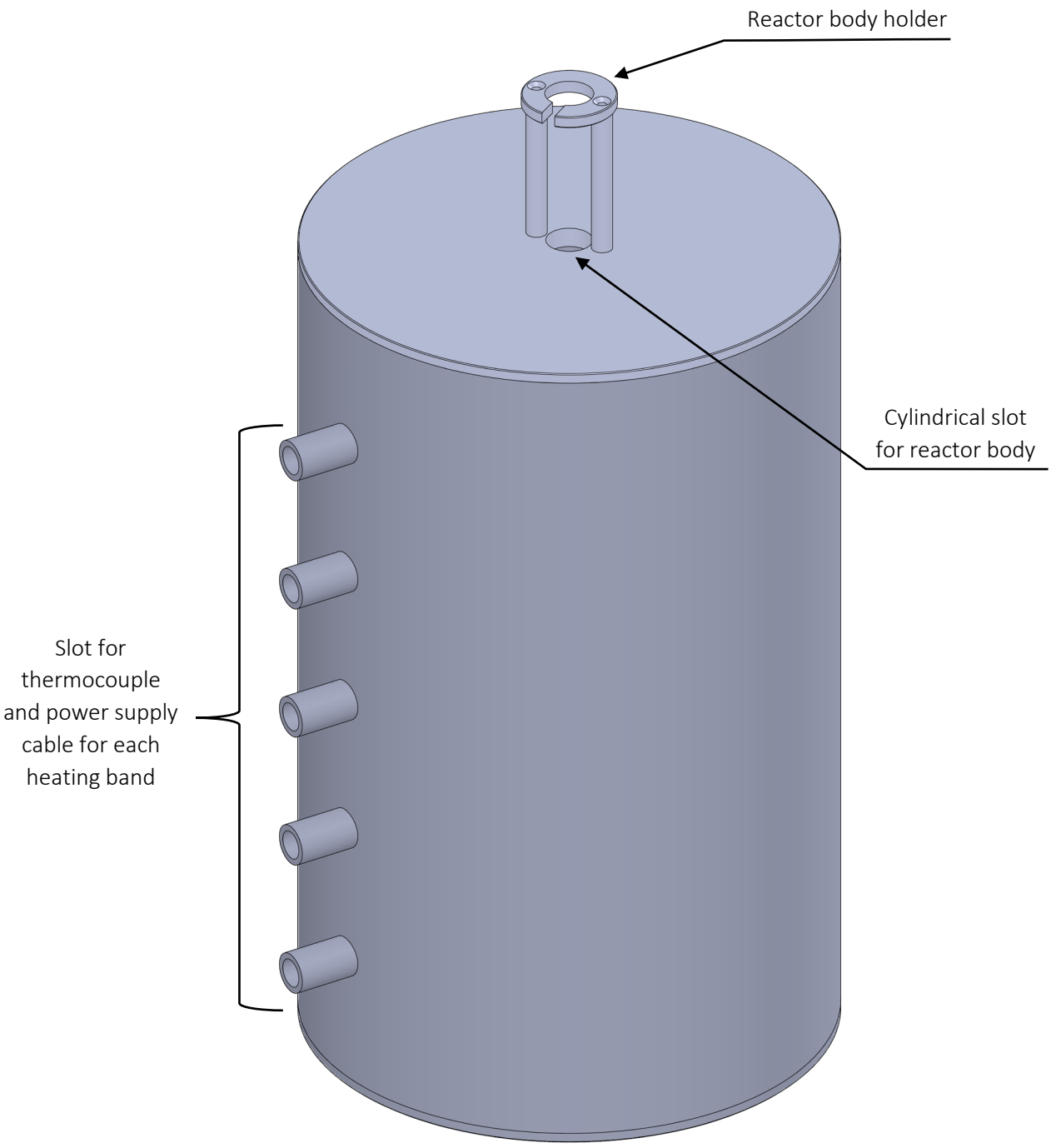

Figure 4-9: 3D illustration (not to scale) of five-zone electric stainless-steel furnace showing cylindrical slot and holder to accommodate for reactor main body

Figure 4-10 provides the axial temperature profiles generated at three distinct setpoints of the temperature which was set at the furnace. Hence, the temperatures measured by the internal thermocouple for the isothermal zone deviated by + 8-10 °C from the setpoint temperatures (see Section 4.5.3.1). The top of the reactor body was chosen as the reference point (i.e., distance = 0 mm). It can be observed that the isothermal region that must be reserved for the catalyst bed is ca. 150 mm, spreading from 220 mm to 370 mm from the top of the reactor body (indicated by the red dotted lines). To maintain isothermal conditions for the entire length of the catalytic bed, the catalyst should always be positioned within that range, hence the three central heating zones (zones 2, 3 and 4) should act as reaction zones. A SiC bed at the top of the catalyst bed (SiC bed length ~ 280 mm) extending in heating zone 1 should allow for sufficient space for the mixing and pre-heating of the liquid and gas feeds prior to entering the reaction zones. Heating zone 5 was termed as the evaporation zone since in this region, the bottom end of the quartz tube liner should rest on a bed of SiC granules (SiC bed length ~ 155 mm) to ensure that Ar gas mixes with the reactor effluents and completely vaporises any liquid products trickling out of the catalytic packed bed. To accelerate the evaporation process during operation, the temperature of heating zone 5 can be increased by 10-20 °C depending on the liquid water feed flowrate and it must be ensured that the argon gas flowrate is at least 2-3 times higher than the gas flowrate on the inside of in the quartz liner.

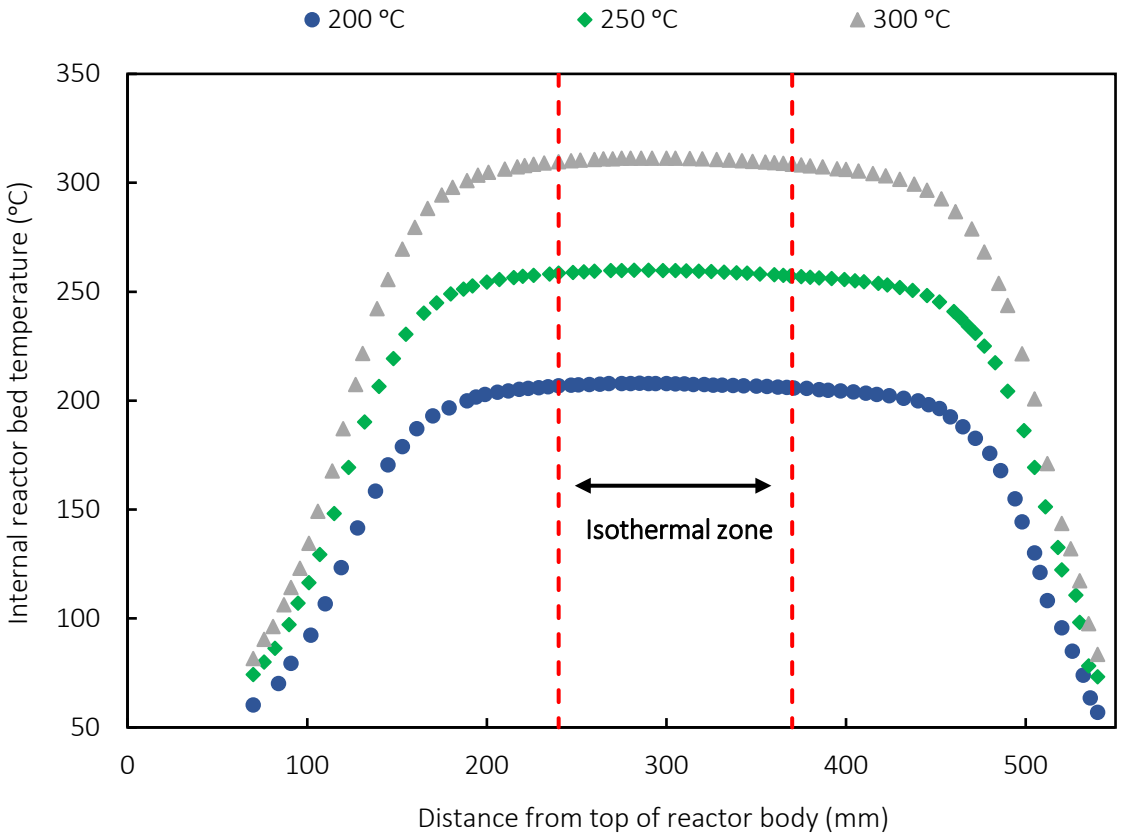

Figure 4-10: Axial temperature profile in the trickle bed reactor with furnace setpoints at 200 °C (blue), 250 °C (green) and 300 °C (grey) under 30 bar (He: 50 ml_n/min, Ar: 110 ml_n/min)

4.3.5 Pressure drop, axial dispersion and liquid hold-up

An important design parameter as defined previously is a minimum pressure drop inside the reactor here taken as a maximum pressure drop of 2 bar. This pressure drop can be rationalized as the pressure, which the quartz liner can withstand without cracking. Since only the annular space between the two quartz tubes is exposed to a pressure difference corresponding to the pressure drop inside the packed bed consisting of SiC granules and catalyst particles (due to argon make-up gas mixing at the end of the quartz tube liner), the gas phase pressure drop across this particular region was estimated. The Ergun equation combining both the laminar and turbulent components of the pressure loss through a packed bed (assuming uniform spherical particles) was used for this purpose [115]:

$$\frac{\Delta P}{L} = 150\,\frac{\mu(1-\varepsilon_B)^2 v_g}{\varepsilon_B^3 d_p^2} + 1.75\,\frac{(1-\varepsilon_B)\rho v_g^2}{\varepsilon_B^3 d_p} \qquad 4\text{-}1$$

The pressure drop (ΔP) is thus a function of the fluid properties viscosity (μ), density (ρ) and superficial gas velocity (v_g), as well as the bed characteristics such as particle diameter (d_p), bed void fraction (ε_B) and length of packed bed (L). As the worst-case scenario for this study, the maximum possible pressure drop inside the quartz tube liner was calculated based on oxygen because it is the most viscous and heaviest gas (compared to methane, helium and steam) at the operating conditions of 220 °C and 30 bar. A bed void fraction of 0.4 was assumed and a particle size of 1000 μm was used for the SiC granules. The length of the top and bottom SiC beds in the quartz tube liner were 220 mm and 50 mm, respectively and that of the catalyst bed was 100 mm. The particle size in the catalyst bed was varied between 10-200 μm.

The effect of catalyst particle diameter on pressure drop inside the packed bed was investigated for a range of total gas flowrates (laminar flow, Re < 40) that can be achieved in the packed region of the trickle bed reactor as illustrated in Figure 4-11 (assuming that the maximum flowrate of liquid water fed to the reactor is 1 ml/min, forming 1240 ml_n/min of steam). As anticipated, high flowrates lead to higher pressure drop due to increased frictional resistance caused by increased velocity gradients and viscous stresses in the fluid. At the same flowrate, the trend of the plots indicates that the pressure drop across the bed increases with decreasing catalyst particle size. This is because a reduction in particle diameter means that for the same bed void fraction, the number density of particles increases, resulting in higher contact area per unit volume between the solid catalyst and gas phase. Subsequently, there is increased resistance to fluid motion leading to an increase in pressure drop.

For the whole range of gas flowrates considered, catalysts with particle sizes between 50 μm and 200 μm in a bed length of 100 mm can be utilised in the trickle bed reactor without exceeding the limit of 2 bar pressure drop. However, particle sizes down to 10 μm can only be utilised below a flowrate of 715 ml/min to avoid a pressure drop higher than 2 bar in the reactor. It should be noted that the Ergun equation might under-predict the pressure drop

when the reactor tube-to-particle-diameter ratio $D/d_p < 10$ (in this case for particle sizes > 1200 µm) since frictional wall effects might become more pronounced [116], [117].

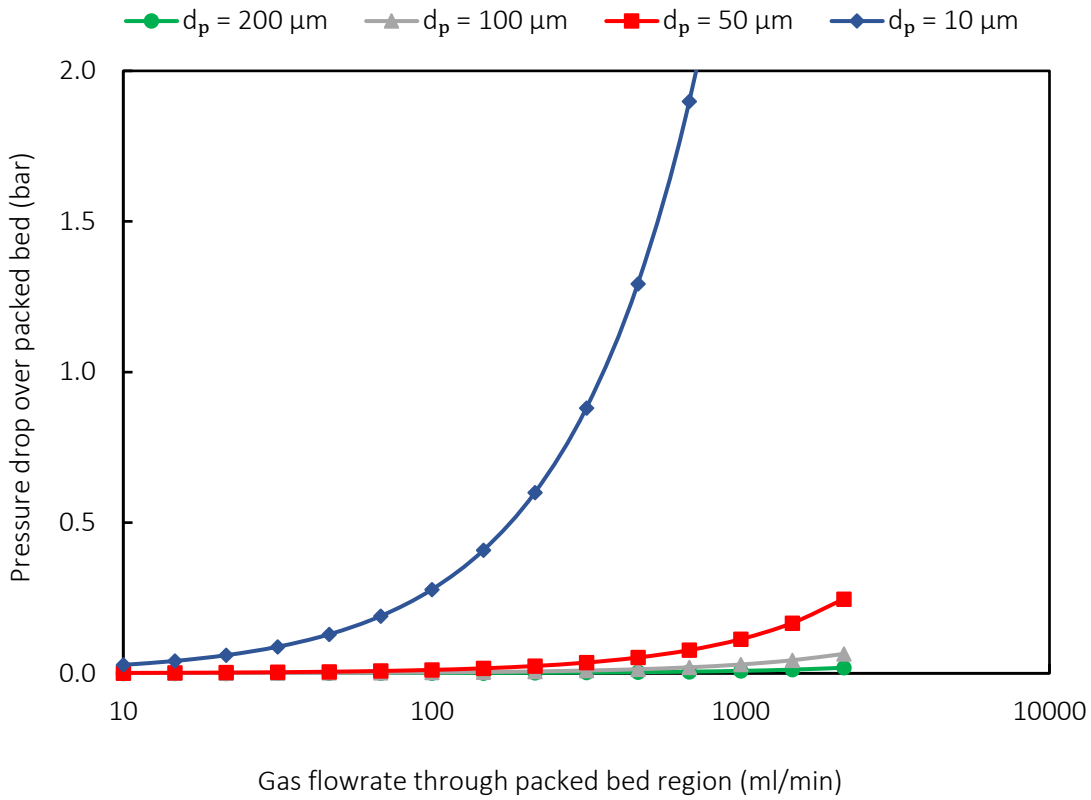

Figure 4-11: Pressure drop over packed region inside quartz tube liner as a function of gas flowrate at 220 °C and 30 bar for different spherical catalyst particle sizes (SiC d_p = 1000 µm, ε_B = 0.4, µ = 30.1 µPa·s, ρ = 23.4 kg/m^3)

It is important to estimate the extent of axial dispersion and mixing characteristics of the fluids flow in the trickle bed reactor to ensure safe design and efficient operation. The deviations from plug flow can arise from fluctuations mainly due to the combined effects of velocity profiles and molecular diffusion. It must be noted that for the trickle bed reactor system specifically designed for this study, it is a rather complex task to accurately model and experimentally investigate the effect of axial dispersion of the tri-phasic system. Therefore, the following presents only an approximate estimation of the hydrodynamics characteristics in the trickle bed reactor system.

For packed bed reactors with a bed void fraction ε_B and particle diameter d_p, the dimensionless dispersion number which is the reciprocal of the Peclet number, can be determined as follows [118], [119]:

$$\frac{D}{uL} = \frac{1}{Pe} = \frac{\text{Rate of transport by diffusion/dispersion}}{\text{Rate of transport by convection}} = \left(\frac{D\varepsilon_B}{ud_p}\right)\left(\frac{d_p}{L\varepsilon_B}\right) \qquad 4\text{-}2$$

Where the packed bed dispersion number ($D\varepsilon_B/ud_p$) is a function of the Schmidt number (Sc) and particle Reynolds number (Re_p), and ($d_p/L\varepsilon_B$) relates to the packed bed geometric factor.

As a rule of thumb, if the dispersion number is lower than 0.01, it can be assumed that there is negligible dispersion i.e., there is negligible deviation from plug flow. With this in mind, we can re-arrange the formula to determine the minimum catalyst bed length required to minimise dispersion in the reactor for different particle sizes for a range of fluid flowrates:

$$L = 100\left(\frac{D\varepsilon_B}{ud_p}\right)\left(\frac{d_p}{\varepsilon_B}\right) \qquad 4\text{-}3$$

This was achieved by using the experimental correlation [118] (see Figure 4-12), which relates Re_p to the packed bed dispersion number for fluids in packed beds. The Schmidt number was calculated at 220 °C and 30 bar for methane in oxygen (Sc = 0.7 ~ 1).

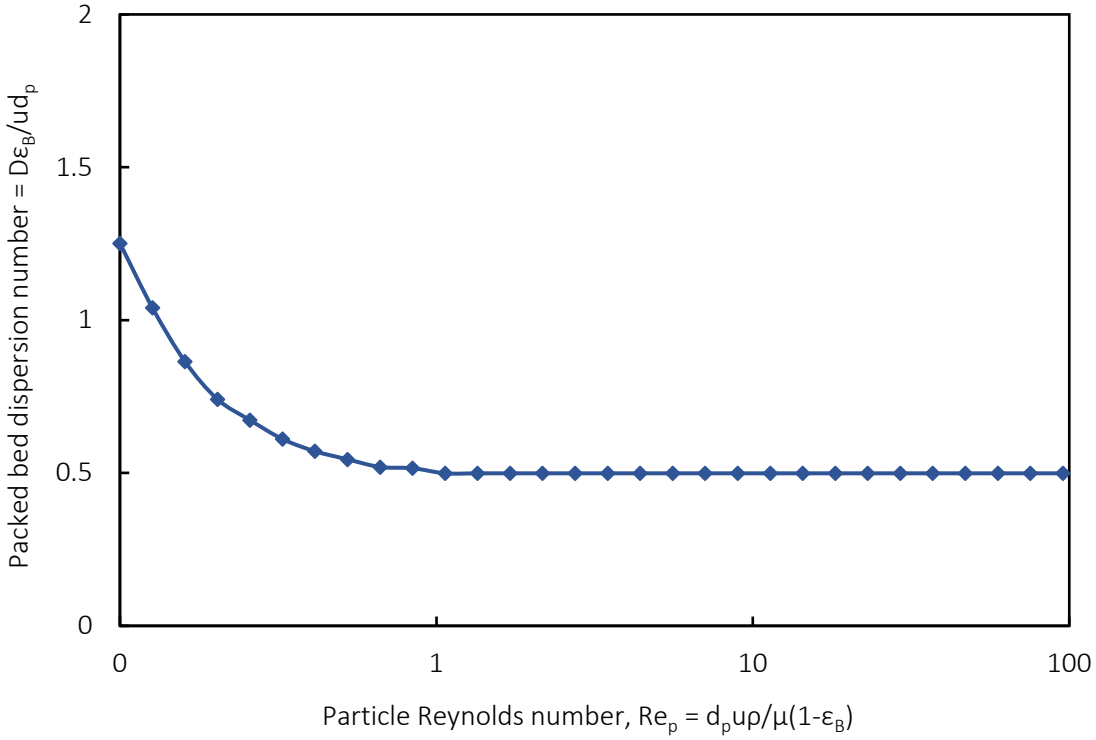

Figure 4-12: Correlations based on experimental studies on dispersion of fluids flowing through packed beds (reproduced from Levenspiel [118])

Figure 4-13 shows the minimum catalyst bed length required to limit dispersion to 0.01 for different catalyst particle sizes as a function of the gas flowrates that can be achieved in the trickle bed reactor. The effect of axial dispersion is more pronounced at low gas flowrates, a regime in which molecular diffusion dominates. With increasing gas flowrates, the contribution of the convective dispersion increases and dominates over the molecular diffusion until a plateau is reached, indicating that there is negligible deviation from plug flow. With a designed catalyst bed of 100 mm long, there should be no deviation from plug flow for catalysts with particle diameters less than 10 µm for any gas flowrate. However, for larger particle sizes the total gas flowrate should be more than 13 ml/min for 50 µm, 16 ml/min for 100 µm and 20 ml/min for 200 µm.

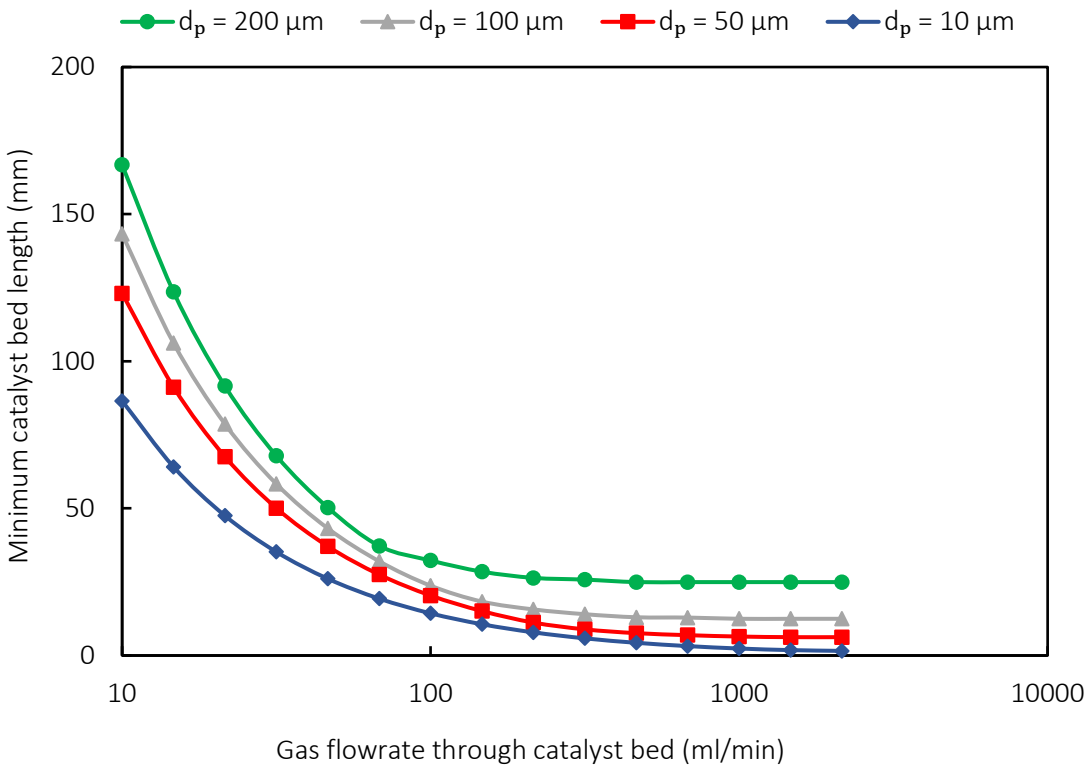

Figure 4-13: Minimum catalyst bed length as a function of oxygen flowrate at 220 °C and 30 bar (ε_B = 0.4, µ = 30.1 µPa·s, ρ = 23.4 kg/m^3, Re < 40, D_{AB} = 0.018 cm^2/s, Sc = 1)

Based on experimental hydrodynamic studies done on a variety of different liquid-gas systems, the residual liquid hold-up (β_R) through a packed column is speculated to be independent of gas and liquid flowrate, as well as reactor pressure [95], [120]. Thus, using Equation 2-11, the value of β_R for the oxygen-water system in the trickle bed reactor was estimated to be 0.05 and assumed to be constant. On the contrary, the dynamic liquid hold-up (β_D) is strongly influenced by gas and liquid flowrates at elevated pressure in the tri-phasic system. By means of inter-related empirical correlations developed by Wammes *et al*. [101], the Equations 2-15, 2-16 and 2-17 were solved simultaneously to estimate β_D and consequently the total liquid hold-up (β_T) (which is the sum of β_R and β_D) in the trickle bed reactor. These calculations were based on the assumption that the reactor is packed with only SiC granules which are non-porous and have a d_p of 1000 µm and using a bed void fraction of 0.4.

Figure 4-14 illustrates the effect of liquid flowrate at various gas flowrates on the total external liquid hold-up for the oxygen-water system in the trickle bed reactor operating at 220 °C and 30 bar. At a constant gas superficial velocity (i.e., constant gas flowrate), the total external liquid hold-up increases with increasing liquid flowrate as expected. This means that the bed void fraction decreases as liquid water tends to flow through more voids, filling up the space. As a result, the thickness of the flowing liquid film increases, as well as the wetting efficiency. Conversely, at a constant liquid flowrate, the total external liquid hold-up decreases with increasing gas flowrate. This can be explained by accounting for a higher liquid-gas shear stress since the gas phase now occupies more of the void volume between the solid particles pushing the liquid out of the packing. Consequently, the dynamic liquid hold-up is reduced, and so does the total external liquid hold-up.

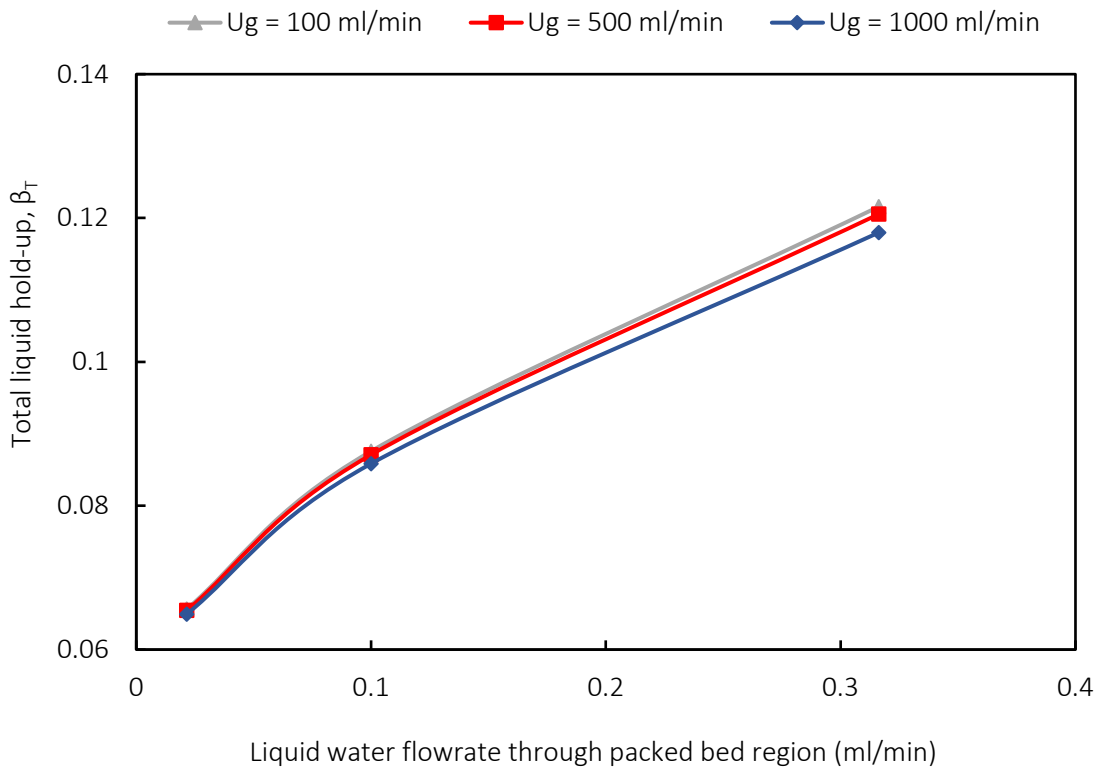

Figure 4-14: Influence of liquid water flowrate at different gas flowrates on total liquid hold-up at 220 °C and 30 bar (Ug = gas flowrate, SiC d_p = 1000 µm, ε_B = 0.4)

4.4 Post-reaction and product analysis equipment

The analysis of reaction products was to be performed by an existing online GC system [105]. The reactor effluent needs to be vaporised to be transformed into a single-phase system (vaporising the liquid in this stream) and subsequently depressurised to ambient pressure. The handling of the product stream and the instrument used for its sampling and analysis are discussed in this section.

4.4.1 Reactor effluent handling

Dilution of the reactor effluent with a high argon gas flowrate alone was not sufficient to avoid condensation in the product line. Hence, the entire length of the post-reaction line to the injection point of the GC including the numerous components in-between had to be heated. The pressurized product stream after the reactor exit was heated to a minimum temperature of 180 °C to prevent condensation whereas the lines subjected to atmospheric pressure could be heated at 100 °C. This was accomplished using high-temperature fiberglass heating cords connected to setpoint temperature controllers and insulated with a thick layer (2-3 cm) of ceramic fibre embedded in fiberglass webbing to prevent thermal loss (see Section 4.5.3.2).

In order to prevent any solid material that might dissociate from the reactor packing from exiting together with the effluent stream, a 0.5 µm micro-filter (S-601) had to be installed. Initially, it was decided to place the latter straight after the reactor exit port, however, due to its high heat capacity, condensation of water vapour would still occur even if heated at 180 °C

at the operating reactor pressure. Consequently, the regulating needle valve V-602 was placed directly under the reactor before the micro-filter, in order to reduce the pressure down close to atmospheric conditions, thereby allowing the contents leaving the heated expansion valve to be kept in the vapour phase. The main advantages of using a regulating needle valve over a back-pressure regulator (BPR) to control the pressure inside the reactor are that it is more robust, cheaper and does have less difficulties handling mixed phase fluids. Moreover, due to its lower dead volume, condensed products would be less likely to collect and, if they did the needle valve can be heated to a high enough temperature to vaporise the liquid formed. However, with a back-pressure regulator this would not be the case as it has a limited operational temperature of 200 °C mainly due to the material of the seat retainer seal (polyetheretherketone - PEEK) in the case of a spring-loaded back-pressure regulator.

The line following the micro-filter was split into two separate streams: the main one leading to the online GC system for gas samples to be analysed and the secondary one leading to a condenser (HE-801) for liquid-phase samples to be collected and analysed offline, depending on the need. Needle valves (V-701 and V-801) were installed on each stream to ensure that the pressure is reduced to atmospheric pressure, as well as to control the total effluent flowrate. Following each expansion valve, an on-off valve (V-702 and V-802) was installed since the implemented needle valve cannot be closed completely without damaging the sharp internal regulating stem. On-off valve V-702 was especially important for shutting off the reactor outlet to build up pressure inside the trickle bed reactor during start-up. The heated effluent stream proceeding the splitting point was routed to the online GC where it was injected over a pneumatically operated internal Vici® 6-way valve, also heated at 180 °C during operation. The secondary effluent stream was directed to a coiled line within the Teflon condenser HE-801 (operating at ambient pressure) around which a coolant at 10 °C would circulate when required. A 1:1 volume ratio of ethylene glycol/water coolant mixture would be utilised whereby it would be cooled and pumped by a chiller (Lauda Microcool MC 250). The resultant cooled stream would be fed to a liquid/gas separator (T-801) to collect the liquid condensate while the incondensable vapours would be directed to the overhead vent through a bubble flowmeter (FM-801) in the walk-in fume hood. This flowmeter was used during commissioning of the TBR system to independently calibrate the four MFCs.

4.4.2 Sampling and gas chromatography system

The reactor effluent from the trickle bed reactor was continuously sampled by means of the actuating 6-port injection valve prior to being analyzed by an existing online gas chromatography system. The switching mechanism of the 6-way injection valve consisted of two positions as illustrated in Figure 4-15. In the first position (Figure 4-15a), the reactor effluent is loaded in the 1 ml sample loop (made of 1/16” 316 SS tubing) and thereafter routed to the overhead vent while hydrogen carrier gas is diverted to the GC column port. To introduce the reactor effluent into the GC column (at the start of a GC run), the valve is automatically switched to the second position (Figure 4-15b), whereby the hydrogen carrier

gas is now able to flush the effluent out of the sample loop into the GC column; meanwhile the reactor effluent is directly transferred to the overhead vent. Approximately 60 seconds after the run has started, the 6-way injection valve is switched back to the sample loop filling position in preparation for the next analysis. To ensure a completely vaporous feed to the GC column during operation, the 6-way valve including the sample loop were enclosed in an existing aluminium block which was heated at 180 °C using heating cartridges. The 1/8" line transporting the contents from the sample loop to the GC injection point also required heating at 180 °C and insulation.

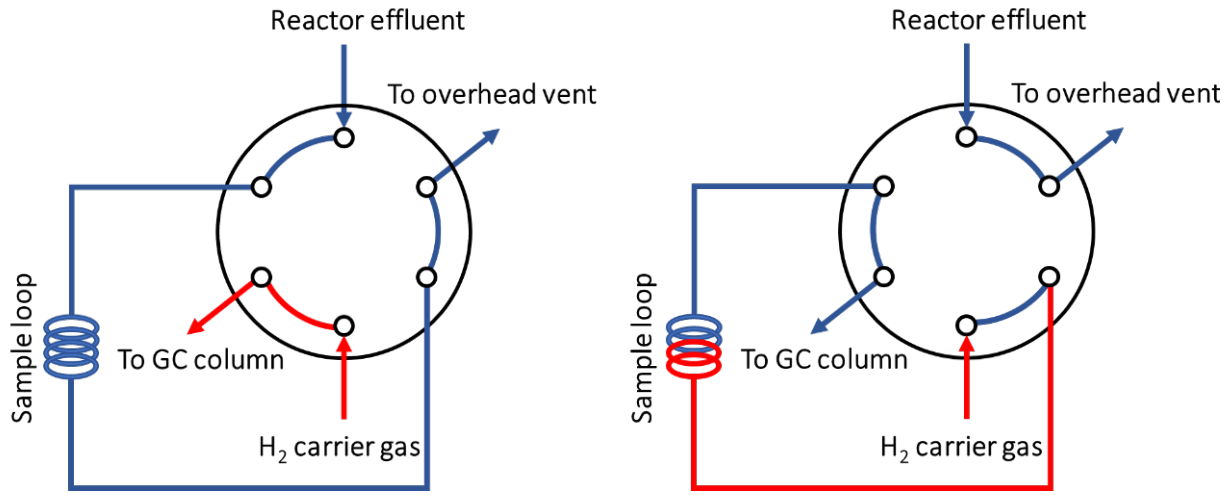

(a) Sample loop filling with reactor effluent (b) Sample loop injection using H_2 carrier gas

Figure 4-15: Schematic of switching mechanism for heated 6-way injection valve

To allow for the separation and detection of the various products anticipated for the selective oxidation of methane to methanol using platinum catalysts in presence of water, an Agilent 6890N GC was utilized. The latter was equipped with a flame ionization detector (FID) and retrofitted with a dual catalytic combustion-reduction reactor (Polyarc™ microreactor sourced from Activated Research Company) positioned between the outlet of the GC column and the inlet to the FID (henceforth referred to as the GC-Polyarc™-FID). The reaction products were separated using an Agilent HP-PLOT Q PT capillary column with polystyrene-divinylbenzene as the stationary phase (OD = 0.32 mm, L = 30 m, 20 µm stationary phase film thickness). The function of the Polyarc™ microreactor was to first oxidize any organic analytes eluting out of the column with air to produce CO_2, then to hydrogenate the CO_2 to CH_4 before being fed to the FID. By completely converting the compounds to methane, the GC-Polyarc™-FID system allowed for a uniform carbon response in the FID as it enabled the detection of all carbon-containing compounds with equal sensitivity to CH_4 within experimental error [105], [121], [122]. Thus, this system reduces the need to perform time-consuming individual calibrations and provides a uniform response to carbonaceous species such as CO and CO_2 which are otherwise undetectable using a standard FID detector. Furthermore, it also allows for the increased sensitivity of low-level FID detection for compounds such as formic acid, formaldehyde and formamide [123].

In the FID, hydrogen gas and air (oxidant) were used to fuel the flame, with inert nitrogen fed as a make-up gas to provide additional flow. The effluent from the 6-port injection valve is passed through a condenser (C-701) operating at ambient conditions prior to being sent to the overhead vent in the walk-in fume hood. Any liquid formed is drained via on-off valve V-703; frequent draining of the condensate is vital especially when operating at high liquid water flowrates. A bubble flowmeter (FM-701) was installed on the vent line to monitor the total flow exiting the TBR system during operation. To control the GC as well as capturing and processing data, the GC network was connected to a desktop computer in the laboratory whereby the software Agilent Chemstation™ was installed for these purposes.

4.5 Trickle bed reactor instrumentation and control strategies

This section highlights the instrumentation and control strategies put in place to safely maintain the process at the operating conditions and set points, as well as to transition from one condition to another. The measurable variables that need to be controlled and monitored in the trickle bed reactor set-up mainly include the feed flowrates, pressure and temperature inside the designed reactor and for the reactor effluents.

4.5.1 Pressure control

To control the feed pressure of methane, oxygen and inert helium inside the trickle bed reactor, miniature BB-1 series Tescom^{TM} pressure reducing regulators were installed upstream (prior to the MFCs), respectively labelled as PV-102, PV-202 and PV-302. Wika analogue pressure gauges were connected at the inlet and outlet gauge ports of these piston-sensed control valves to act as pressure indicators (see Appendix A.1). To adjust the delivery pressure the control hand-knob is manually turned either clockwise to increase pressure or anticlockwise to decrease pressure until the desired setpoint is observed on the pressure indicator downstream. During operation these regulators were set at a pressure higher than the reactor pressure (< 10 bar) as any tubing with elbows, fittings, control valves or frit and capillary in the MFCs can create flow resistance in the line, hence it is important to allow a pressure difference between the regulator and MFC outlet.

The pressure inside the reactor was controlled using the pressure-controlled addition of argon using a pressure reducing regulator PV-501 in conjunction with needle valve V-602 downstream the reactor body. A different type of pressure regulator sourced from Air Products was utilized for this purpose since due to its piston-sensed design, the Tescom^{TM} one could not effectively maintain stable output pressure. A diaphragm-sensed pressure regulator providing better sensitivity and accurate regulation for the outlet pressure was thus selected. This is because the diaphragm sensing element provides a higher sensing area and lower friction as compared to the piston type design. PV-501 is a single-stage regulator which is cheaper and shows little droop (decrease in outlet pressure caused by an increase in flowrate) compared to a dual-stage pressure regulator. One main drawback however is that if the argon supply pressure decays over time, the delivery pressure will increase since there is less pressure

exerted on the valve stem. Therefore, frequent control hand-knob adjustment might be required to maintain constant output pressure. To measure the reactor pressure, a pressure indicator PI-601 (Wika analogue gauge) was placed on the branched line connecting the pressure relief valve V-601 to the reactor head. The same pressure reading should be observed on this pressure indicator and the outlet pressure gauge of PV-501 during operation (see Appendix A.1).

4.5.2 Feed and inert gas flowrate control

The gas flowrates of reactants methane and oxygen, and inert helium and were separately metered by their individual Brooks thermal mass flow controllers (FV-101, FV-201 and FV-301) linked to a four-channel Brooks MFC control module (see Appendix A.2). The MFC control box was retrieved from an old reactor set-up present in our laboratory. Argon gas flowrate was not controlled but its MFC FV-501 functioned more as a mass flow indicator (by setting the flow to 100% during operation) and was also connected to the MFC control unit.

The flows for each channel are represented as percentages and are projected on the display read-out. During commissioning, each MFC was calibrated specifically for its intended gas by measuring its flowrate through the TBR system using the bubble flow meter FM-801 for different setpoints between 0 and 100% with at least ten measurements performed for a particular setpoint. Only MFCs with model number 5850S/BC1BA1BA0CA1B1 were compatible with the existing MFC control read-out box. Table 4-2 shows the specifications of the different MFCs used in the trickle bed reactor set-up and their calibration curves for their intended gas can be found in Appendix A.2.

Table 4-2: Brooks mass flow controller specifications

Intended gas	MFC calibrated for (ml_n/min)		Max. measured flow (ml_n/min)	Serial No.
Oxygen	N_2	0-200	238	T77002/001
Methane	CO_2	0-50	57	T45285/010
Helium	N_2	0-200	319	T86298/002
Argon	N_2	0-1000	1620	T88450/002

The liquid water flowrate was controlled using the Lab Alliance Series I HPLC pump (P-401) with a stainless-steel (SS 316) pump head assembly. The single-piston reciprocating pump can continuously deliver flowrate in the range: 0.01-10 ml/min allowing increments of 0.01 ml/min and a maximum pressure of 340 bar. A diaphragm-type pulse damper is internally located within the pump housing which allows for the smooth and constant liquid flow out of the pump during operation. The pump flowrate is shown on the digital display of the control panel and can be adjusted using the up and down arrow keypads (see Appendix A.2).

4.5.3 Temperature control

Based on the different temperature requirements, the heating strategy implemented for the trickle bed reactor set-up was split into two distinct regions. These include the heating of the tubular trickle bed reactor body and the reactor effluent lines. The existing two temperature control modules (4-zone hot runner control system sourced from Unitemp), which housed six Gefran 600 temperature-controllers and two Gefran 40 temperature-indicators were utilised for this purpose, as well as another 2-zone hot runner control box housing two Gefran 600 temperature-controllers (see Appendix A.3).

4.5.3.1 Heating of reactor via drop tube furnace

The temperature of the trickle bed reactor body was controlled using the 5-zone electric furnace as discussed previously. Each heating band surrounding the central heating block of the furnace incorporated a steel jacketed J-type (iron/constantan) thermocouple which was connected to a Gefran 600 single-point controller. The Gefran 600 controllers can only be used for ballistic heating to a single setpoint but not for step-by-step temperature ramping programmes. Hence, before start-up the desired temperature for zones 1-5 should be adjusted manually by increasing the temperature in increments of 50 °C for safety and practical reasons.

The J-type thermocouple inside the central thermowell used to measure the reaction zone temperature during operation was connected to a Gefran 40 temperature-indicator. As mentioned earlier, it was observed that the actual temperature reading from the Gefran 40 differed by + 8-10 °C from the setpoint temperature maintained by the Gefran 600 controller for that specific zone. This deviation is believed to be possibly due to the position of the tip of the controlling thermocouple on the heating band which might not be in full contact with the external surface of the central heating block, creating a small insulation gap and allowing thermal loss. Thus, to achieve the desired reactor temperature reflected by the Gefran 40 indicator, it was ensured that prior to operation the temperature setpoints on the Gefran 600 controllers should always be adjusted by 10 °C lower than the desired temperature.

4.5.3.2 Heating of reactor effluent lines

The temperature control strategy employed for heating the product stream exiting the reactor was achieved through the utilisation of high-temperature fiberglass heating cords. The post-reactor heating loop was subdivided into two regions. The first loop was reserved for heating the pressurized effluent passing through the needle valve V-602, up to the in-line micro-filter S-601. The J-type controlling thermocouple responsible for this loop, which was connected to a Gefran 600 temperature controller, was placed directly on a 1/4” nut fitting prior to the needle valve (due to its high heat capacity and relative thickness to V-602). Furthermore, to avoid tendency toward runaway heat, the tip of thermocouple was secured with adhesive aluminium tape on the fitting. The bare line, needle valve, filter and fittings were all wrapped in 2-3 layers of heavy-duty aluminium foil with the fiberglass heating trace spiralled around.

Thereafter, they were insulated with multiple layers of ceramic fibre embedded in fiberglass webbing to prevent thermal loss to the surroundings.

Another J-type thermocouple linked to a Gefran 40 temperature-indicator was positioned on the heated expansion valve V-602 to measure and monitor its temperature during operation (see Appendix A.1). It was especially crucial when operating under trickle flow regime as the measured temperature on the valve could be used as an indicator for the presence of liquid on the valve; this may cause pulsating flow, but adjustment of the needle valve position could then rectify this problem. During gas phase reactions the first heating loop was usually heated to 180 °C. However, for trickle phase reactions, the temperature setpoint would be increased up to 220 °C depending on the liquid water feed flowrate.

The function of the second heating loop was to heat the contents leaving the in-line micro-filter leading up to the actuating 6-port injection valve and the subsequent line proceeding to the GC column injection point. Whilst also being highly diluted in argon, the contents in this heating loop were already at ambient pressure, thus the line was maintained at a lower temperature than in the first heating loop, usually between 150-180 °C. The second heating loop consisted of multiple heating cords, all set to the same setpoint temperature and controlled by Gefran 600 temperature controllers as the trickle bed reactor was positioned ca. 3-4 m away from the GC-Polyarc™-FID. All the various sections in the second heating loop were heated and insulated in a similar manner to the first heating loop as described above.

4.6 Trickle bed reactor safety considerations and precautions

4.6.1 Explosive methane-oxygen mixtures inside the reactor

In the design section of the trickle bed reactor, the safety measures put in place to mitigate the risks and hazards involved in using flammable methane-oxygen mixtures in the reactor have already been discussed. These include: the dilution of oxygen and methane with helium prior to being mixed and fed to the reactor, the installation of flame arresters and pressure relief valves, and the dilution of the reactor effluent with argon before being sent to the overhead vent system. Furthermore, the utilization of thick quartz tubes combined with the high-pressure and corrosion-resistant stainless-steel reactor shell body will facilitate total containment of any explosive material. In the highly unlikely instance that these preventive measures fail, methane and smoke detectors present in the walk-in fume hood will be triggered and alarm systems in the laboratory will alert of possible hazards.

4.6.2 Leakages and effluent disposal

It was of uttermost importance for the entire TBR system to be leak-free in order to avert flammable methane-oxygen mixtures from potentially getting into contact with an ignition source causing fires and explosion hazards. Extensive leak testing was performed after construction of the whole reactor set-up, as well as each time after having replaced a component. Leak test experiments were conducted by pressurizing parts of the trickle bed

reactor set-up with inert helium gas at 40 bar (10 bar higher than the desired operating pressure). Helium has a lower viscosity than mixtures of the gas under consideration in this study, and thus for a given pressure difference will result in a higher leak rate. By spraying Swagelok Snoop™ liquid leak detector on every pressurized fitting and visually spotting the formation of bubbles, leakages in the system were detected. A GL Sciences gas leak detector was also used in some instances to identify the presence of smaller leaks. Once identified, these fittings were tightened further (after the system was de-pressurized) and re-tested. In the case that they fail the leak test again, they were simply replaced with new Swagelok fittings and tubing. The procedure was once again repeated to ensure no leakages.

The gaseous reactor effluent and gaseous mixtures coming from the trickle bed reactor set-up were safely disposed of through extraction via the centralised overhead vent system in the walk-in fume hood. With the reactor effluent consisting of methane-oxygen mixtures highly diluted in argon at ambient pressure, it would be very unlikely that this poses a risk of explosion in the vent lines. Prior to being sent to the overhead vent system, the effluents were passed through pressure-resistant cylinders (SS 316L) acting as condensers or guard catch pots, with each having an on-off valve installed at the exit port. Consequently, any liquid formed via condensation would be collected and trapped at the bottom of the vessel. These were periodically drained and discarded in the appropriate waste disposal drums available in the laboratory. Flexible leak-resistant silicone hoses were used to connect these vessels to the overhead vent lines.

4.6.3 Pressure build-up and blockages

Preventive and safety measures were implemented to mitigate the risks associated with over-pressurization as it was a major concern in the TBR system. Pressure build-up may be caused by blocked outlets, malfunction, or operational error. Two pressure relief valves, each calibrated to 50 bar (20 bar above operating reactor pressure) were thus installed such that if triggered, any fluid released would be safely trapped in the guard catch pot C-401 and any gas would be directed to the vent line. Pressure relief valve V-601 was installed on the mixed gas feed line (in close proximity to the reactor head) in case of uncontrollable pressure build-up, for instance caused by a blockage at the reactor exit. Another pressure relief valve V-404 was installed on the water feed line exiting the pump as a secondary measure, especially in case P-401 would start to malfunction and deliver excessive pressures > 300 bar (see Appendix A.2).

It was very unlikely for excessive pressure to cause rupture of the Swagelok seamless tubing (SS 316L) as they were specifically designed to withstand extremely high pressures, even at elevated temperatures. As shown in Figure 4-16, the pressure rating calculated for the tubing utilised in the trickle bed reactor set-up decreases with increasing temperature. For instance, at 25 °C the allowable working pressure for the 1/8” OD tubing was 751 bar while at 537 °C, it was reduced by a factor of 0.76 to 571 bar [124]. However, this is still high enough compared to the maximum pressure of 340 bar that can be delivered by the HPLC pump P-401.

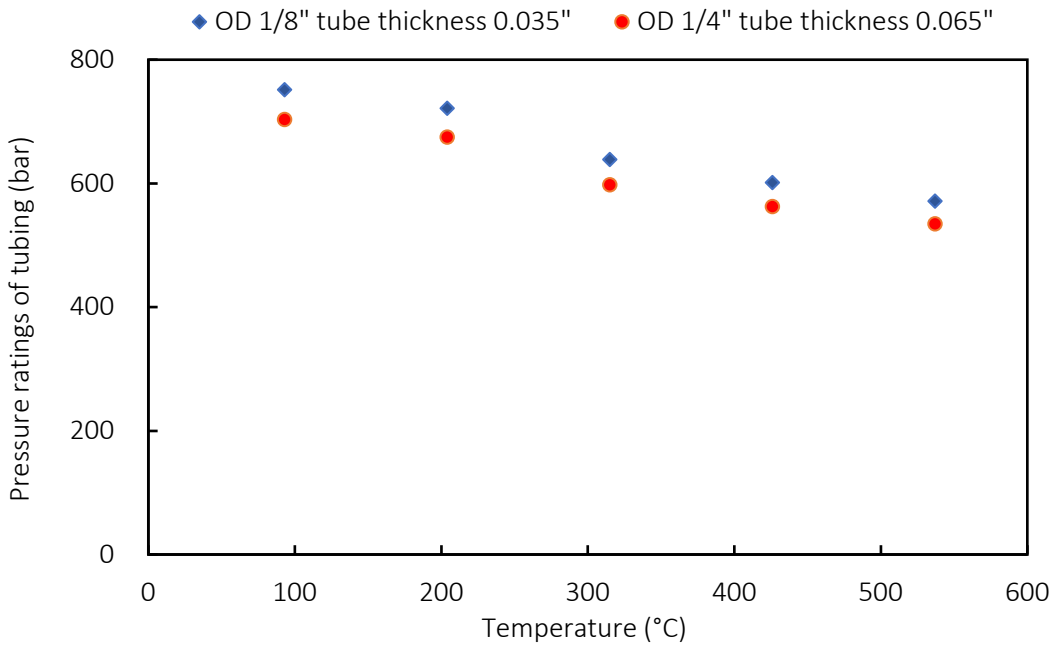

Figure 4-16: Pressure ratings of stainless steel seamless (SS 316L) tubing utilised in the TBR system at different temperatures [124]

The catch-pots C-401 and C701 had a capacity of 500 ml and 300 ml, respectively. In the event that they would be filled completely due to a blockage downstream, as an extra precautionary measure check-valves were installed on the lines proceeding every MFC. That way, in case of fluid backflow these sensitive devices would be protected, and most importantly to prevent the house gas manifold from getting contaminated. Build-up of a solid residue (polymeric deposits) in the reactor exit line was a recurring event during catalyst testing in the TBR. Therefore, it was common practice to regularly replace the line following immediately the reactor outlet port (which was connected to the expansion valve V-602) after each experiment, and sometimes also replace the GC transfer line.

4.7 Description of components utilized in the trickle bed reactor set-up

The detailed description of the major units utilized to construct the novel trickle bed reactor system for the selective oxidation of methane to methanol is shown in Table 4-3 below. Their functions have already been discussed in the previous sections. Tubing with 1/4” OD having the highest wall thickness available (0.065”) were used for the supply gas lines prior to the mixing point (represented by the cross union in the process flowsheet). The main reason for this is that compared to 1/8” OD tubing, they were less malleable and stronger, thus could hold in place the heavy components that needed to fit on the metal plates within the existing frame. The connections to the pressure relief valves and catch pots also required 1/4” OD tubing. In other parts of the system, such as the feed lines prior to the reactor and the exit lines all the way to the GC-Polyarc™-FID were made of 1/8” OD tubing with wall thickness of 0.035”. Numerous trivial components and fittings such as ferrules, nuts, reducers, bolts, heating cords, fibreglass webbing, silicone tubing, electrical wiring, etc. were also required but these were readily available in our laboratory, thus they were not included in Table 4-3.

Table 4-3: Lists of minor components in trickle bed reactor system

Unit	Symbol	Detailed description	Manufacturer
Water stream	T-401	Schott glass bottle, 1000 ml	Duran Schott
	P-401	Series I HPLC pump (liquid flow range: 0.01-10 ml/min)	Lab Alliance
	V-401	Stainless steel 1/8" two-way ball valve, nylon handle, SS-41GS2	Swagelok
	V-402	Stainless steel 1/8" three-way ball valve, nylon handle, SS-41GXS2	
	V-403	Stainless steel 1/8" check valve, ⅓ psi cracking pressure, SS-2C-1/3	
	V-404	Stainless steel high pressure 1/4" proportional pressure relief valve, SS-4R3A	
	V-405	Stainless steel 1/4" two-way ball valve, nylon handle, SS-43GS4	
	C-401	Stainless steel 500 ml double-ended vessel, 316L-50DF4-500	
Methane stream	CH_4 cylinder	50 L Methane 3.5 gas cylinder, initially at 190 bar	Air Products
	PV-101	Diaphragm pressure control valve (max inlet pressure 6000 psi, max outlet pressure 1800 psi)	Tescom
		Pressure gauges (inlet: 0-250 bar, outlet: 0-100 bar)	Wika
	PV-102	Pressure reducing regulator, non-venting (max inlet pressure 6000 psi, max outlet pressure 1800 psi)	Tescom
		Pressure gauges (inlet: 0-250 bar, outlet: 0-100 bar)	Wika
	FV-101	Mass flow controller, 5850S (max flow: 50 ml_n/min CO_2)	Brooks
	S-101	Stainless steel 1/4 " tee-type sintered metal filter, 0.5 µm pore size, SS-4TF-05	Swagelok
	S-102	Stainless steel 1/4 " tee-type sintered metal filter, 0.5 µm pore size, SS-4TF-05	
	V-101	Stainless steel 1/8" two-way ball valve, nylon handle, SS-41GS2	
	V-102	Stainless steel 1/4" two-way ball valve, nylon handle, SS-43GS4	
	V-103	Stainless steel 1/4" check valve, ⅓ psi cracking pressure, SS-4C-1/3	
	V-104	Stainless steel 1/4" check valve, ⅓ psi cracking pressure, SS-4C-1/3	

Unit	Symbol	Detailed description	Manufacturer
Oxygen stream	O_2 cylinder	50 L Oxygen gas cylinder, initially at 200 bar	Air Products
	PV-201	Diaphragm pressure control valve (max inlet pressure 6000 psi, max outlet pressure 1000 psi)	Tescom
		Pressure gauges (inlet: 0-250 bar, outlet: 0-100 bar)	Wika
	PV-202	Pressure reducing regulator, non-venting (max inlet pressure 6000 psi, max outlet pressure 1800 psi)	Tescom
		Pressure gauges (inlet: 0-250 bar, outlet: 0-100 bar)	Wika
	FV-201	Mass flow controller, 5850S (max flow: 200 $ml_n/min\ N_2$)	Brooks
	S-201	Stainless steel 1/4 " tee-type sintered metal filter, 0.5 µm pore size, SS-4TF-05	Swagelok
	S-202	Stainless steel 1/4 " tee-type sintered metal filter, 0.5 µm pore size, SS-4TF-05	
	V-201	Stainless steel 1/8" two-way ball valve, nylon handle, SS-41GS2	
	V-202	Stainless steel 1/4" two-way ball valve, nylon handle, SS-43GS4	
	V-203	Stainless steel 1/4" check valve, ⅓ psi cracking pressure, SS-4C-1/3	
	V-204	Stainless steel 1/4" check valve, ⅓ psi cracking pressure, SS-4C-1/3	
Helium stream	He cylinder	50 L Helium gas cylinder, initially at 200 bar	Air Products
	PV-301	Diaphragm pressure control valve (max inlet pressure 6000 psi, max outlet pressure 1000 psi)	Tescom
		Pressure gauges (inlet: 0-250 bar, outlet: 0-100 bar)	Wika
	PV-302	Pressure reducing regulator, non-venting (max inlet pressure 6000 psi, max outlet pressure 1800 psi)	Tescom
		Pressure gauges (inlet: 0-250 bar, outlet: 0-100 bar)	Wika
	FV-301	Mass flow controller, 5850S (max flow: 200 $ml_n/min\ N_2$)	Brooks
	S-301	Stainless steel 1/4 " tee-type sintered metal filter, 0.5 µm pore size, SS-4TF-05	Swagelok
	V-301	Stainless steel 1/8" two-way ball valve, nylon handle, SS-41GS2	
	V-302	Stainless steel 1/4" two-way ball valve, nylon handle, SS-43GS4	
	V-303	Stainless steel 1/4" check valve, ⅓ psi cracking pressure, SS-4C-1/3	

Unit	Symbol	Detailed description	Manufacturer
Purge stream	V-304	Stainless steel 1/8" bonnet needle valve	Swagelok
Argon stream	PV-501	Single stage non-corrosive cylinder regulator, brass with SS trim (inlet: 415 bar, outlet: 5-70 bar)	Air Products
		Pressure gauges (inlet: 0-100 bar, outlet: 0-60 bar)	Wika
	S-501	Stainless steel 1/4 " tee-type sintered metal filter, 0.5 µm pore size, SS-4TF-05	Swagelok
	V-501	Stainless steel 1/8" two-way ball valve, nylon handle, SS-41GS2	
	V-502	Stainless steel 1/4" two-way ball valve, nylon handle, SS-43GS4	
	V-503	Stainless steel 1/4" check valve, ⅓ psi cracking pressure, SS-4C-1/3	
	FV-501	Mass flow controller, 5850S (max flow: 1000 ml_n/min N_2)	Brooks
Post-reactor	V-601	Stainless steel high pressure 1/4" proportional pressure relief valve, SS-4R3A	Swagelok
	S-601	1/8 " tee-type sintered metal filter, 0.5 µm pore size, SS-2TF-05	
	V-602	1/8" needle valve, stainless-steel bar metal handle, SS-ORS2-SH	
	V-701	1/8" needle valve, stainless-steel bar metal handle, SS-ORS2-SH	
	V-702	Stainless steel 1/8" two-way ball valve, nylon handle, SS-41GS2	
	V-703	Stainless steel 1/4" two-way ball valve, nylon handle, SS-43GS4	
	C-701	Stainless steel 300 ml double-ended vessel, 316L-50DF4-300	
	V-801	1/8" needle valve, stainless-steel bar metal handle, SS-ORS2-SH	
	V-802	Stainless steel 1/8" two-way ball valve, nylon handle, SS-41GS2	
	T-801	Schott glass bottle, 1000 ml	Duran Schott
	FM-701	50 ml burette (bubble flow meter)	Hirschman
	FM-801	50 ml burette (bubble flow meter)	
	HE-801	Teflon cylindrical condenser	Cape Catalytix (Pty) Ltd

4.8 Process flow diagram

The final process flowsheet of the novel trickle bed reactor system designed and constructed for the direct conversion of methane to selective oxidation products using molecular oxygen as oxidant in the presence of water is presented in Figure 4-17. This experimental set-up was used in our investigation to evaluate the performance of platinum-based catalysts.

The Gefran 600 temperature-controllers used to control the temperature of the 5-zone electric furnace are labelled as TIC-601, TIC-602, TIC-603, TIC-604, and TIC-605 in the flowsheet while TIC-606 and TIC-701 represent those utilised to heat the first and second heating loops of the reactor effluent line, respectively. The Gefran 40 temperature-indicator for the moveable thermocouple located inside the central thermowell for catalyst bed temperature measurements in reactor R-601 is denoted as TI-601 and the other one for the thermocouple positioned on the heated needle valve V-602 is labelled as TI-602 (see Appendix A.3).

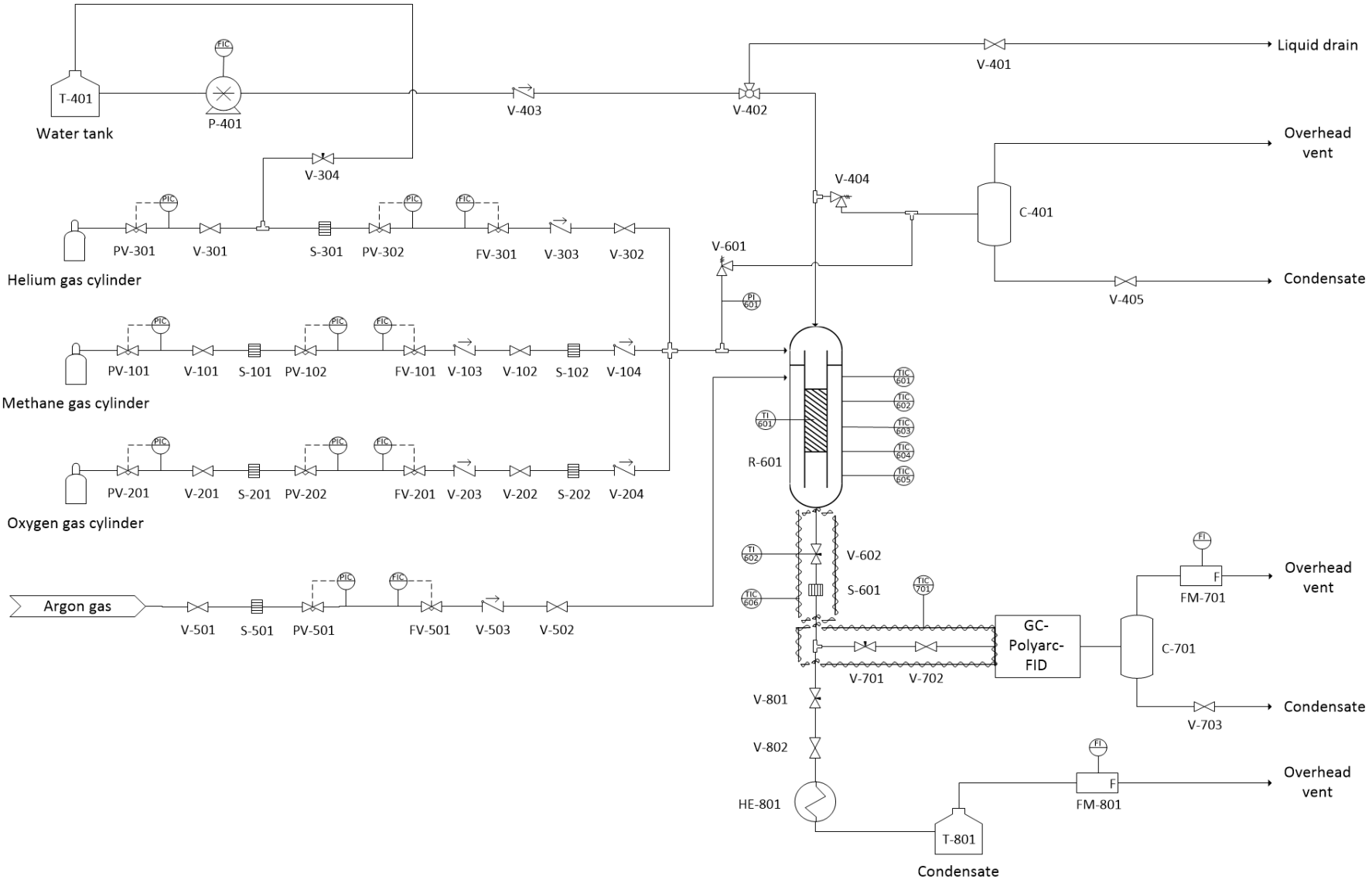

Figure 4-17: Trickle bed reactor system flowsheet for the selective oxidation of methane

5. Experimental conditions and procedures

5.1 Experimental conditions

To commission the newly designed and constructed trickle bed reactor set-up successfully and safely for catalytic testing in the selective conversion of methane with prime focus the influence of water, a set of operating conditions had to be selected. More information on the platinum catalysts investigated in this study is also provided in this section.

5.1.1 Reaction conditions

A wide range of temperatures from 50-600 °C has been utilised by researchers in the field of DMTM as summarised in Table 2-4. With that into consideration, in our heterogeneous catalytic system using oxygen as oxidant, it is desired to operate at temperatures above 150 °C for heat recovery and enhanced kinetic rate of reaction, but also not too high such that the formation of CO or CO_2 is favoured [40], [43]. Furthermore, to achieve a feasible water vapour saturation pressure in the TBR, the reaction temperature had to be less than 260 °C. This is mainly because the saturation pressure of pure water increases exponentially with temperature as illustrated in Figure 5-1. Therefore, a reaction temperature of 220 °C was selected to conduct the experiments in this study.

As postulated previously, it is of interest to investigate the effect of high oxygen and water partial pressures for the selective oxidation of methane. At the chosen reactor temperature of 220 °C, the saturated vapour pressure of pure water is 23.1 bar (depicted by dotted red line in Figure 5-1 below). At this particular value, steam is in thermodynamic equilibrium with its saturated water. Since a pressure of 23.1 bar is necessary for obtaining water in the liquid state and that the maximum pressure achievable in the reactor is capped at 50 bar (due to the high-pressure argon supply line), it was decided that the trickle bed reactor would operate at a total pressure of 30 bar.

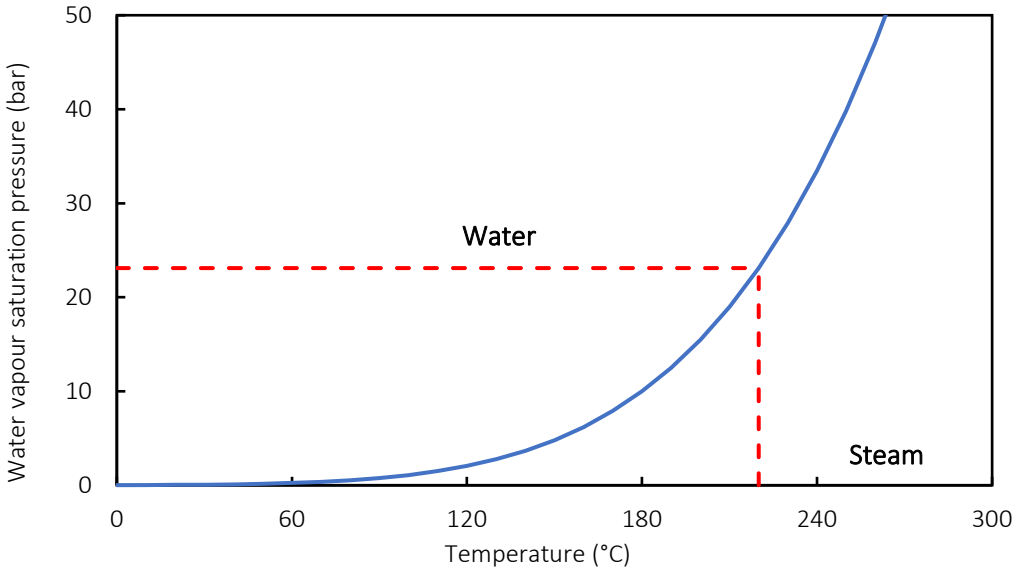

Figure 5-1: Water vapour saturation pressure as a function of temperature

To evaluate the influence of co-feeding water on the catalytic activity and selectivity of oxidation products, a range of flowrates for liquid water was investigated. To achieve a water partial pressure of at least 23.1 bar in the reactor, the corresponding volumetric flowrate at which the pump has to feed liquid water is approximately 0.08 ml/min (provided that the gas flowrates for CH_4 and O_2 are kept constant at 2 ml_n/min and 6 ml_n/min, respectively). Assuming a constant reactor temperature of 220 °C, this means that at any liquid water flowrates lower than 0.08 ml/min, water in the packed bed reactor will be present in the gaseous phase. Conversely, at liquid throughputs higher than 0.08 ml/min, water will exist in the trickle flow regime (flooding region) whereby liquid water flows in the form of films or rivulets over the packed particles while the gases pass through the remaining void space. The operating range for the feed water flowrate delivered by the pump (P-401) was thus varied from 0-0.3 ml/min.

Table 5-1 provides the set of experimental conditions used in this study, comprising of inlet feed flowrates and the associated partial pressures for each component. For comparison's sake, only the liquid water feed flowrate was allowed to vary while keeping the inlet partial pressures of CH_4 (P_{CH_4}) and O_2 (P_{O_2}) constant at 0.5 bar and 1.5 bar, respectively. In this study, a liquid feed flowrate of 0.02 ml/min (P_{H_2O} = 6.9 bar) was defined as the baseline condition as the reactor system was the most stable at this liquid flowrate and could be run unsupervised. Moreover, as it was decided to increase the water flowrate gradually over a long period of time, it was deemed essential to intermittently revert back to the baseline condition to evaluate the extent of catalyst deactivation. To maintain the reactor pressure at 30 bar whenever more water was introduced, less helium was allowed to flow through the reactor until the transition to the flooding region was reached (P_{H_2O} = 23.1 bar). At times, before transitioning from gas phase into the flooding region, it was necessary to pump water at high throughputs (1.5-2.5 ml/min) for several minutes (~ 10 min) to ensure that liquid water reaches the evaporation zone at the bottom of the reactor. As such, the time delay response in the TBR system could be avoided, especially when transitioning immediately from baseline condition to trickle flow.

Table 5-1: Set of experimental reactor conditions used for the selective oxidation of methane

	Flowrate (ml/min)	Flowrate (ml_n/min)			Partial pressure (bar)			
Inlet feed	H_2O	CH_4	O_2	He	H_2O	CH_4	O_2	He
Gaseous phase	0	2	6	111	0	0.5	1.5	28
	0.02	2	6	83.6	6.9	0.5	1.5	21.1
	0.04	2	6	56.5	13.7	0.5	1.5	14.3
	0.06	2	6	29.5	20.6	0.5	1.5	7.4
Trickle flow	0.08	2	6	19.4	23.1	0.5	1.5	4.9
	0.1	2	6	19.4	23.1	0.5	1.5	4.9
	0.2	2	6	19.4	23.1	0.5	1.5	4.9
	0.3	2	6	19.4	23.1	0.5	1.5	4.9

In the trickle flow regime, as increasing amounts of liquid water will be present in the reactor, more argon will have to be fed to fully vaporise the reactor effluent in the evaporation zone. Figure 5-2 illustrates the theoretical minimum amount of argon that is necessary to achieve effluent vaporisation at a constant reactor pressure of 30 bar and temperature of 220 °C for various liquid water feed flowrates.

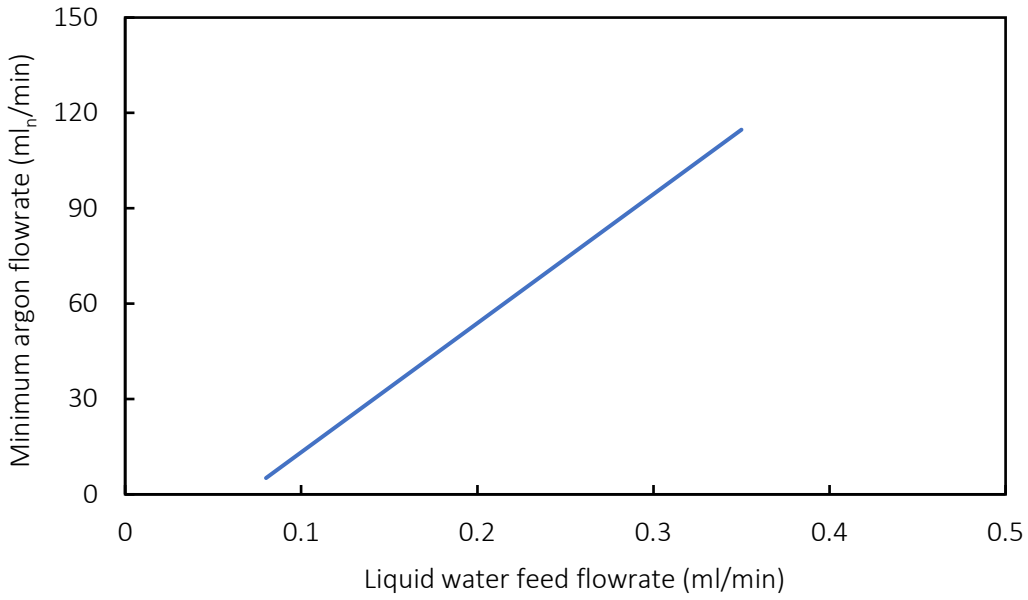

Figure 5-2: Minimum argon flowrate required for complete vaporization of effluent for various water feed flowrates at 200 °C and 30 bar (inlet partial pressures P_{CH_4} = 0.5 bar, P_{O_2} = 1.5 bar)

5.1.2 Platinum catalysts to be tested in the trickle bed reactor

In-house prepared platinum catalysts supported over titania (TiO_2), as rutile (Sigma Aldrich) and P25 (Evonik) were investigated in the TBR for the selective oxidation of methane to methanol. P25 is made up of a 75/25-mixture of the anatase and rutile form of TiO_2. The catalysts were synthesized via incipient wetness impregnation whereby the TiO_2 support was saturated with a known amount of metal precursor solution platinic acid (H_2PtCl_6, Sigma Aldrich) in deionized water to obtain a metal loading of 10 wt.% on the support. The resulting solid formed was dried, calcined in air at 400 °C, and finally reduced in hydrogen for 5 hours at 400 °C to attain metallic state. The catalyst particles were thereafter compressed under 3 tons of force using a hydraulic press to form pellets before being cautiously crushed and sieved into the desired size fractions. To minimise the effects of pressure drop across the trickle bed reactor, the catalysts were pelletised to obtain particle sizes in the range of 150-250 µm.

5.2 Operating procedures

The standard operating procedures for the steady-state functioning of the TBR system commissioned for the selective methane oxidation process are outlined in this section. There are six main components in this section, including the detailed procedures for catalyst packing, pressure testing, catalyst pre-treatment, start-up, shutdown and catalyst removal (refer to flowsheet presented in Figure 4-17 where applicable).

5.2.1 Catalyst loading procedure

The step-by-step procedure for packing the reactor with catalyst is presented below:

1. Ensure that both the reactor head and reactor body are clean and empty
2. Securely clamp down the reactor body in an upright position ensuring it is always fixed during loading of the catalyst
3. Insert a small plug of glass wool around the central thermowell and push it to the bottom of the reactor in order to cover the exit port
4. Shield the central thermowell with the 6 mm OD quartz tube sealed at one end
5. Add SiC granules (d_p = 1000 µm) gradually to a height of 370 mm from the top of the reactor body and tap gently to help settle the bed
6. Place the fluorocarbon O-ring (ID = 13.94 mm, OD = 19.05 mm) around the 14 mm OD quartz tube liner
7. Place the customized part for the O-ring sealing mechanism around the 14 mm OD quartz tube ensuring that it sits on the O-ring
8. Gently insert the 14 mm OD quartz tube over the thermowell quartz sheath ensuring that approximately 1.5 mm of the tube is above the upper lip of the reactor body
9. Fill the annular region between the outside of the thermowell quartz sheath and the interior of the 14 mm OD quartz tube with SiC to a length of approximately 90 mm
10. Insert a small plug of glass wool on top of the SiC bed
11. Measure the appropriate amount of pelletized catalyst required and using a pipette tip as a funnel, pour it into the reactor while gently tapping to settle the bed evenly
12. Insert a small plug of glass wool on top of the catalyst bed
13. Fill the remaining gap with SiC to approximately 1.5 mm from the upper lip of the reactor and tap gently to facilitate settling of the bed
14. Insert a small plug of glass wool on top of the SiC bed
15. Place a clean new 3/4” gasket on the reactor lip
16. Loosely tighten the reactor head and secure it by tightening the VCR fitting with a shifting spanner ensuring that no excess pressure is exerted otherwise this might cause breakage of the quartz liner
17. Release the reactor from the clamp and gently place it into the furnace housing
18. Use clean new 1/4” VCR gaskets to connect the inlet and exit ports to the reactor and tighten the fittings
19. Insert a 1 mm thick (500 mm long) thermocouple in the central thermowell, ensuring that the tip of the thermocouple is located approximately 280 mm away from the upper lip of the reactor body, i.e. at the centre of the catalyst bed
20. Wrap the reactor exit line with 2-3 layers of heavy-duty aluminium foil and spiral around fiberglass heating trace
21. Insulate the reactor exit line with ceramic fiber embedded in fiberglass webbing and secure with adhesive aluminium tape

5.2.2 Pressure test

Prior to pre-treating the catalyst, pressure testing of the reactor was conducted as follows:

1. Open the valve of the helium (V-301) house gas line
2. Check inlet pressure and ensure that the outlet pressure of the helium pressure regulator (PV-302) is set to 40 bar
3. Close all the exit valves, including the post-reactor needle valve V-602 as well as the on-off valves V-702 and V-802
4. Ensure that the feed valves (V-102, V-202, V-402 and V-502) are also closed so as to isolate the pressurized section of the reactor
5. Begin to pressurize the reactor by setting the helium flow on its respective MFC (FV-301) to 100% (319 ml/min) and open the feed valve V-302
6. Once the pressure from the pressure indicator PI-601 located on top right of the reactor head reads 40 bar, close the helium feed valve V-302
7. Monitor the pressure inside the reactor over a 4-hour period and measure rate of pressure drop over that period, if any
8. If there is no pressure decrease, the reactor system passed the pressure test and is deemed leak-tight, and the system can be depressurized by opening the exit valves
9. If the measured leak rate is high, either the GL Sciences gas leak detector or Snoop™ liquid is used to locate the leaks. It is ensured that the system is depressurized before tightening and replacing any connection fittings. Steps 1-7 are then repeated until the system passes the pressure test.

5.2.3 Catalyst pre-treatment

Once the catalyst is loaded and that the TBR system indicates no source of leakage, pre-treatment of the catalyst is performed in a helium-oxygen atmosphere to remove any pre-adsorbed species as described below:

1. Open the valves of the oxygen (V-201) and helium (V-301) house gas lines
2. Check inlet pressure and ensure that the outlet pressure of the pressure regulators for both oxygen (PV-202) and helium (PV-302) are set to 40 bar
3. Ensure that the valves V-602, V-701 and V-702 are open to route the reactor effluent to the GC system
4. Ensure that all drain valves as well as valves V-801 and V-802 are closed
5. Set the oxygen flowrate on its respective MFC (FV-201) to 6 ml/min (1.8%)
6. Set the helium flowrate on its respective MFC (FV-301) to 50 ml/min (15.2%)
7. Open the feed valves V-202 and V-302 to allow the gases to flow through the reactor
8. Set the temperature of all reactor zones 1-5 to 210 °C and effluent lines to 180 °C
9. Check that the desired total gas flowrate is achieved on the flowmeter (FM-701) located after the GC system
10. Allow system to run overnight (maximum of 24 hours) before start-up

5.2.4 Start-up procedure

The start-up procedure for conducting a catalytic experiment in the TBR is detailed as follows:

1. Open the valves of all the four house gas lines (V-101, V-201, V-301 and V-501)
2. Check inlet pressure and ensure that the outlet pressure of the pressure regulators for methane (PV-102), oxygen (PV-202) and helium (PV-302) are set to 40 bar
3. Set the operating pressure of the reactor on the argon pressure regulator (PV-501) to 30 bar
4. Ensure that all drain valves and valves V-801 and V-802 are closed
5. Close the post-reactor needle valve V-602 fully as well as valve V-702 on the reactor effluent lines
6. Begin to pressurize the reactor by setting the helium flow on its respective MFC (FV-301) to 100% (319 ml/min) and open the feed valve V-302
7. Once the desired reaction pressure is achieved (by reading off from the pressure indicator PI-601 located on top right of the reactor head), enter the desired flow setpoint for helium on the MFC control module
8. Set the argon flow on its respective MFC (FV-501) to 100% so that it functions as a mass flow indicator since argon is used as a pressure control gas
9. Open the argon feed valve and slightly adjust (ca. 5° of a turn) needle valve (V-602) until pressure on reactor gauge stays constant at 30 bar and ensure that the argon setpoint on the MFC control module is constant within a range of 5% for 15 minutes
10. Enter the desired flowrate setpoints on the MFC control module for oxygen (FV-201) and methane (FV-101), respectively. Record time at which methane gas is introduced
11. Open the feed valves V-102 and V-202 to allow the reactants to flow through the packed bed reactor
12. Ensure that the valves V-701 and V-702 are open to route the reactor effluent to the GC system
13. Set the temperature of reactor zones 1-4 to 210 °C, zone 5 to 220 °C and effluent lines to 180 °C (increase temperatures accordingly as water flowrate is increased) ensuring that the internal thermocouple is reading 220 °C at the centre of the catalyst bed.
14. Switch on the balance and HPLC pump P-401 and ensure that fresh liquid water is filled in the feed tank T-401
15. Slightly adjust (ca. 5° of a turn) bonnet valve V-304 to degas water by purging helium
16. Prime the pump for 2 minutes and switch three-way valve V-402 to direct the liquid via the drain valve V-401
17. Adjust the water flowrate to the desired setpoint on the pump, press the run button and switch three-way valve V-402 to route the water to the reactor inlet port. Record mass of water before starting experiment
18. Carefully adjust post-reactor needle valve V-602 if argon flow setpoint on MFC control module fluctuates dramatically (flow range should be between 20% and 60%)

19. Ensure that the argon flowrate is always high enough compared to the combined flowrates of methane and oxygen so that reactor effluent being released via the vents is dilute and not flammable
20. Check that the desired total gas flowrate is achieved on the flowmeter (FM-701)
21. Allow the system to stabilize and reach steady-state operation before sampling
22. Ensure that reactor effluent lines leading to the GC are all heated to 180-200 °C
23. Generate a new sequence on the GC software (Agilent Chemstation™) and instruct GC to carry out on-line sampling for 100 runs (ca. 41 hours)
24. Record the times and masses of water fed whenever there is a change of condition such as a change in the liquid flowrate
25. Periodically empty the vent catch pot C-701 when running at high liquid flowrates (water flowrate in the range of 0.1-0.3 ml/min)

5.2.5 Shutdown procedure

Upon completion of a catalytic experiment, the steps below must be followed for the safe shutdown of the TBR:

1. Record the time at which the experiment is done, as well as the mass of water on the balance before switching off the water pump
2. Close the methane and argon feed valves (V-102 and V-502)
3. Set the helium flowrate on its respective MFC (FV-301) to 50 ml/min (15.2%)
4. Open post-reactor needle valve (V-602) to depressurize the system
5. Allow helium and oxygen to flow in the system overnight to dry the liquid water out of the reactor packing as it is easier to unload spent catalyst
6. Switch off any heating to the reactor including the furnace and reactor exit lines
7. Close the oxygen and helium feed valves (V-102 and V-302)
8. Close the valves of all the four house gas lines (V-101, V-201, V-301 and V-501)
9. Allow the system to cool before disconnecting heating lines (by checking temperature readings of the thermocouples)
10. Switch off the power to the reactor system comprising of the MFC and temperature control modules, pump and balance
11. Open drain valves and empty the vent catch pots if necessary
12. Remove the insulation and heating cables around the reactor exit port to facilitate removal of the reactor body from the furnace housing
13. Untighten the VCR fittings of the inlet and outlet ports to disconnect the reactor and gently remove it from the furnace housing

In case of emergency shutdown, this two-step procedure must be followed:

1. Shut off electrical power to the entire system by switching off blue plug (1PH Plug 5) located on top of the test unit A7 in walk-in fume hood
2. Close the valves V-101, V201, V301 and V-501 of house gas lines above test unit (A7)

5.2.6 Catalyst unloading procedure

The procedure below is followed for the removal of the spent catalyst and reactor packing:

1. Securely clamp down the reactor body in an upright position ensuring it is always fixed during unloading of the catalyst
2. Untighten the reactor head using a shifting spanner to detach if from the reactor body
3. Remove the used 3/4" gasket
4. Use a tweezer to remove the plug of glass wool
5. Unclamp the reactor body and gently tap to empty the spent SiC granules
6. Use a thin wire curled at the end to remove the plug of glass wool immobolised between the SiC and catalyst bed (if stuck, poke holes in the glass wool to disintegrate it into pieces to facilitate its removal)
7. Retrieve the spent catalyst in a container with caution (sieve before post-reaction analysis)
8. Remove any glass wool and remaining SiC granules as mentioned previously
9. Clamp down the reactor body, grip the exposed part of the reactor quartz liner and gently move it upwards (if stuck, hold the reactor body in an upside-down position and insert a thin wire at the exit port to carefully move the quartz liner from the inside)
10. Retrieve the customized part for the O-ring sealing mechanism and dispose of the used O-ring
11. Use a silicon tubing to grip the thermowell quartz liner and gently move it upwards
12. Use compressed air to force out the plug of glass wool located at the bottom of the reactor body (if stuck, poke holes in the glass wool to disintegrate it into pieces to facilitate its removal)
13. Carefully clean the reactor head and body as well as the customized component with soap and rinse with acetone
14. In case of rusting or white deposits at the exit port, allow reactor parts to soak in dilute oxalic acid overnight and rinse with water
15. Allow the reactor and its components to dry

5.3 Gas chromatography analysis procedure

As stated earlier, the 6890N GC-Polyarc™-FID system was utilized for the continuous on-line sampling of reactor effluents. In this section, an existing GC method for accurately identifying the different peaks in a chromatogram is presented, as well as how to interpret the chromatographic data generated by the GC software to quantify each compound.

5.3.1 Gas chromatography method and peak retention times

Since each compound elutes at a specific time in the GC column, a method to detect all the carbon-containing species had to be established. In this study, the method developed by Guo [105] was followed to identify the various reaction products as outlined in Table 5-2.

Table 5-2: GC method summary employed for analysis of reaction products [105]

Column	HP-PLOT Q PT
Stationary phase	Polystyrene-divinylbenzene
Diameter	0.32 mm
Length	30 mm
Film thickness	20 µm
Carrier gas	H_2
Flowrate	3.5 ml_n/min
Gas sampling	
Loop volume	1 ml
Load time	1 min
Injection time	0.11 min
Valve temperature	150 °C
Injector	Split mode
Temperature	150 °C
Split ratio	10:1
Oven	
Initial temperature	40 °C
Initial time	2 min
Ramp rate	20 °C/min
Ramp time	7 min
Final temperature	180 °C
Final time	6 min
Run time	15 min
Methanator	Polyarc^{TM} reactor
Heater temperature	293 °C
H_2 flowrate	35 ml_n/min
Air flowrate	2.5 ml_n/min
Detector	FID
Temperature	250 °C
H_2 flowrate	1.5 ml_n/min
Air flowrate	350 ml_n/min
N_2 make-up gas flowrate	20 ml_n/min

To determine the individual retention times of each carbon-containing product in this study, their corresponding pure compounds had to be injected into the GC-Polyarc®-FID system. This process was previously achieved using the GC method above which resulted in an error margin of less than 5% when compared to calibrated mixtures comprising of carbon monoxide, methane, carbon dioxide, ethane and methanol [105]. The respective retention times of all carbon-containing species found in this study are tabulated in Table 5-3.

Table 5-3: Approximate retention times of all carbon-containing compounds detected in the selective oxidation of methane during this investigation

Retention time (min)	Peak identity	Chemical formula	Comments
2.1	Carbon monoxide	CO	
2.2	Methane	CH_4	
2.6	Carbon dioxide	CO_2	
2.9	Unidentified	-	Possibly ethene
3.2	Ethane	C_2H_6	
5.3-6.3	Formaldehyde	CH_2O	Broad peak with a tail
7.2	Methanol	CH_3OH	
7.7	Methyl formate	CH_3OCHO	
9.3	Unidentified	-	Possibly methyl bicarbonate
9.5	Methoxy methanol	$CH_3OCH_2(OH)$	
10.1	Dimethoxymethane	$CH_3OCH_2OCH_3$	
10.9	Formic acid	HCOOH	
11.7	Dimethyl carbonate	$(CH_3)_2CO_3$	
12.9	1,3,5-Trioxane	$C_3H_6O_3$	
13.3	Methyl hydroperoxide	CH_3OOH	
14.9	Paraformaldehyde	$HO(CH_2O)_nH$	n = 8-100

5.3.2 Evaluation of experimental data from gas chromatograms

Using customized integration parameters on the Agilent Chemstation™ GC software, the generated chromatograms were integrated correctly to compute the peak areas of the different compounds. From these data, it was possible to estimate important performance indicators such as conversion of the methane feed, product yields and selectivities.

Assuming that a carbon mass balance is achieved over the trickle bed reactor system (i.e., no accumulation or loss of carbon) and that the GC-Polyarc®-FID system demonstrates equal sensitivity to all carbon-containing species, the methane conversion can be calculated:

$$X_{CH_4} = \left(1 - \frac{\text{Peak area of } CH_4}{\text{Total peak area}}\right) \times 100\ (C - \%) \qquad 5\text{-}1$$

The yield of any carbon-containing product, denoted by i, can be calculated:

$$Y_i(C - \%) = \frac{\text{Peak area of i}}{\text{Total peak area}} \times 100\ (C - \%) \qquad 5\text{-}2$$

Alternatively, the summation of the yields of all products can be used to determine methane conversion as it is the only carbon-containing being fed into the TBR system:

$$X_{CH_4} = \sum Y_i(C - \%) \qquad 5\text{-}3$$

The selectivity of any carbon-containing product, i, over other products can be calculated from the yield of that particular product divided by the methane conversion as follows:

$$S_i(C - \%) = \frac{Y_i}{X_{CH_4}} \times 100\ (C - \%) \qquad 5\text{-}4$$

The turnover frequency (TOF) is typically used to quantify the catalytic activity, which is a measure of kinetic reactivity, i.e., how fast one or more reactions proceed in the presence of a catalyst. Assuming that the variation in reactant concentrations is small along the length of the TBR and that the dispersion of Pt is approximately 14.5% [125] on the surface of the catalyst, the TOF can be calculated as follows:

$$\text{TOF}\ (h^{-1}) = \frac{\text{Number of } CH_4 \text{ molecules converted per unit time}}{\text{Number of active centers}}$$

$$= \frac{\text{Molecular weight of Pt}\ \left(\frac{g}{mol}\right) \times\ X_{CH_4}(\%) \times \text{Inlet flow of } CH_4\ \left(\frac{mol}{h}\right)}{0.145\ \times \text{Metal Pt loading}\ (\%) \times \text{Mass of catalyst}\ (g)} \qquad 5\text{-}5$$

6. Results and discussion

6.1 Commissioning of trickle bed reactor set-up

The novel trickle bed reactor system specifically designed and constructed for the selective oxidation of methane was commissioned by conducting two sets of catalytic experiments. These experiments were run continuously for a long period of time (1.5-3.5 weeks) over platinum impregnated on TiO_2(P25) and TiO_2(rutile) at 30 bar and 220 °C with water co-feeding in order to test the hypothesis developed in Section 3.3. The inlet liquid water flowrate was increased in increments of 0.02 ml/min from 0-0.3 ml/min with intermediate return to the baseline condition to monitor catalyst activity. The set of experimental conditions (refer to Table 5-1 and Figure 5-2) and the operating procedures outlined in the previous chapter were followed to safely conduct the experiments in the TBR system, as well as the GC method to identify the compounds. The equations presented in Section 5.3.2 were used in this chapter to compute for each run the methane conversion, yield and selectivity of the various compounds formed during this investigation.

6.2 Selective oxidation of methane over Pt/TiO_2(P25) catalyst

The first platinum catalyst tested in the TBR system was an in-house 10 wt.% Pt/TiO_2(P25). Approximately 1.58 g of this catalyst (catalyst bed length ~ 20 mm) was loaded in the quartz lined reactor. This experiment was conducted for a duration of 270 hours on stream.

6.2.1 Methane conversion

Figure 6-1 shows the methane conversion as a function of time-on-stream for the Pt/TiO_2(P25) catalyst at 220 °C and 30 bar at different liquid water feed flowrates. The measured conversion obtained over the Pt/TiO_2(P25) catalyst was initially rather high (see Appendix B.1; not shown in Figure 6-1 because of the scale). As water was introduced in the reactor at a flowrate of 0.02 ml/min, the conversion of methane decreased sharply to 0.40 ± 0.04% within the initial 14 hours. This is possibly an indication of the time delay for the water in the gas phase to reach the catalyst bed and the generation of surface hydroxyl species completely saturating the bare metal surface to inhibit CH_4 activation on the metal surface by blocking its active sites [81], [89]. The gap between times 860-1500 minutes was a consequence of a power outage whereby the experiment had to be temporarily stopped. The methane conversion appeared to decrease further to ca. 0.24% (around ~ 2200 min). The catalyst has been slowly deactivating over the initial 5000 minutes before reaching quasi-steady state. From this point forward when the system was returned back to the baseline condition, the CH_4 conversion seemed to stabilise at 0.08 ± 0.02%.

With further increase in the feed rate of liquid water, methane conversion slightly picked up. The second gap between times 6100-7200 minutes was again due to a power outage in the laboratory. As the system entered the flooding region (inlet liquid water flowrate > 0.08 ml/min, P_{sat,H_2O} = 23.1 bar) with water now being present in the reactor as a liquid, higher

methane conversions were obtained with increasing water flowrates. This is clearly shown in Figure 6-1 between times 9800-10500 minutes with a maximum CH_4 conversion of 2.6% at an inlet water flowrate of 0.3 ml/min. It must be noted that runs that involved feeding water at flowrates above 0.02 ml/min required constant supervision of the system to ensure stable operation. This was done by monitoring the argon flowrate on MFC FV-501 (ensuring it did not drop drastically during operation) and manually adjusting the needle valve V-602 when necessary to avoid pressure build-up. Between the times 11000-14700 minutes on stream, the reactor was operating at baseline condition and no data was collected during this period. The experiment was then resumed by feeding high liquid flowrates into the reactor, whereby an average methane conversion of 0.69 ± 0.37% was obtained. However, the runs had to be terminated as it became more difficult to achieve stable operation of the system due to polymeric deposition in the exit line, as well as the catalyst slowly deactivating.

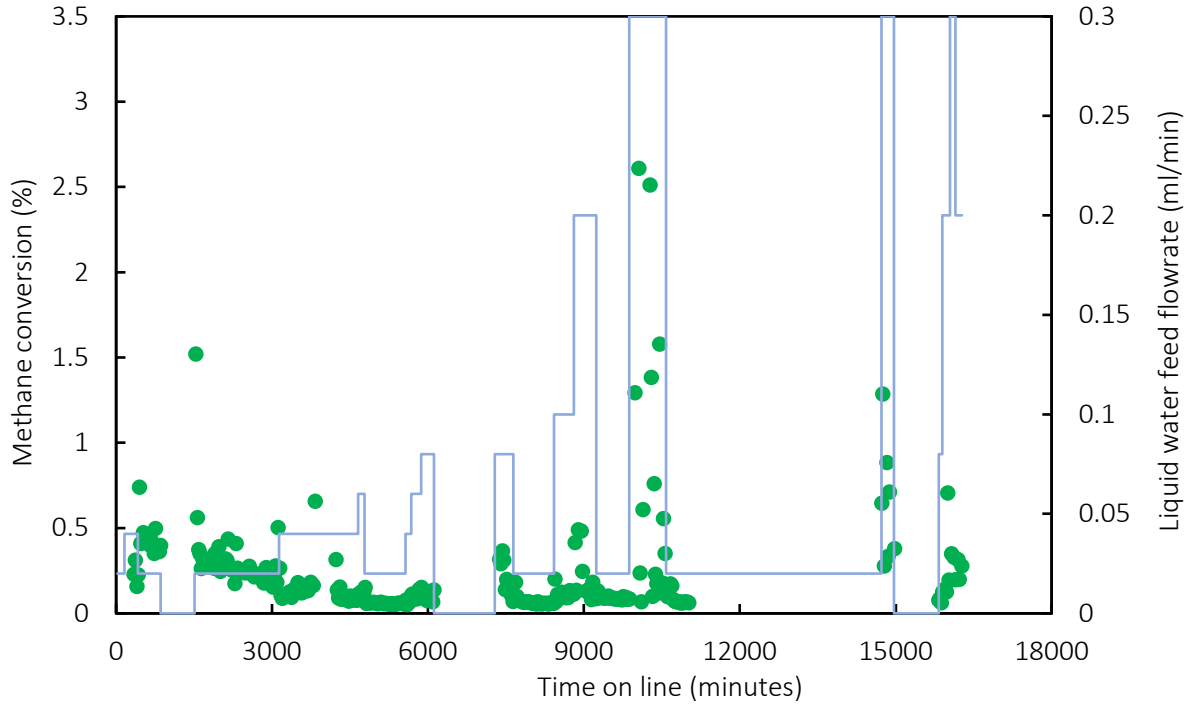

Figure 6-1: Conversion of methane as a function of time on line over 10 wt.% Pt/TiO_2(P25) catalyst in presence of water at 220 °C and 30 bar (inlet partial pressures P_{CH_4} = 0.5 bar, P_{O_2} = 1.5 bar, P_{sat,H_2O} = 23.1 bar, $F_{CH_4,o}/W$ = 3.1 mmol/g_{cat}.h; blue line indicating liquid water feed rate)

Figure 6-2 illustrates the average methane conversion as a function of liquid water feed rate for the Pt/TiO_2(P25) catalyst at 220 °C and 30 bar. Each data point at a given liquid flowrate represents the average conversion obtained for at least five consistent and reliable samples collected at a specific time period. The error bars for each point represent the standard deviation of the average data point. Upon co-feeding more water into the trickle bed reactor set-up while still being in the gaseous phase, water had only a minor influence on the catalytic activity until the transition to the trickle flow regime (i.e., up to the saturation point). Beyond the flooding region, methane conversion started to increase gradually with increasing liquid water feed flowrate. For instance, increasing the molar composition of the liquid water in the

feed from 83 mol% to 91 mol% resulted in a two-fold increase in the average conversion from 0.13% to 0.24%, respectively. An even higher conversion of 0.59 ± 0.22% was obtained at feed flowrate of 0.3 ml/min, representing a reaction rate of 18.5 µmol/g_{cat}.h. However, stabilisation of the trickle bed reactor system was a major issue when operating under trickle flow conditions; adjusting of the heated expansion valve V-602 became more frequent, as well as draining the catch-pot C-701. This is well represented in Figure 6-2 with larger error bars obtained for higher liquid throughputs.

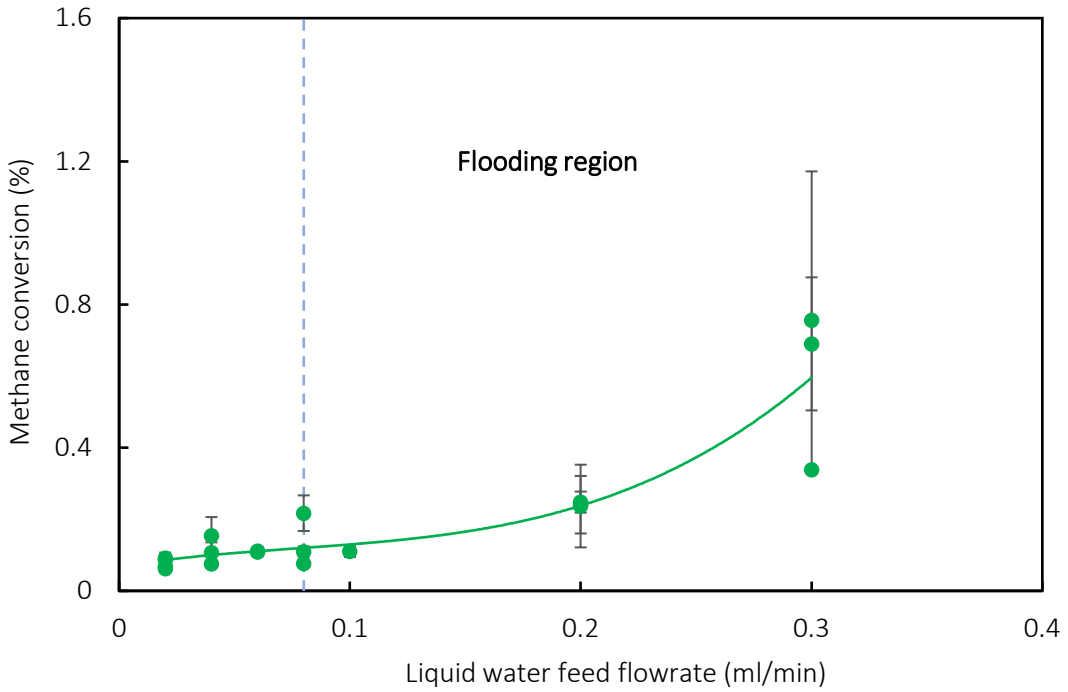

Figure 6-2: Average conversion of methane as a function of liquid water feed flowrate over 10 wt.% Pt/TiO_2(P25) catalyst at 220 °C and 30 bar (inlet partial pressures P_{CH_4} = 0.5 bar, P_{O_2} = 1.5 bar, P_{sat,H_2O} = 23.1 bar, $F_{CH_4,o}/W$ = 3.1 mmol/g_{cat}.h)

Around 3950 minutes on stream with an inlet water flowrate of 0.04 ml/min, a sharp increase in the conversion was observed, reaching up to ca. 29% (see Appendix B.1; not shown in Figure 6-1 because of the scale). This unexpected rise in conversion was attributed to a pressure build-up occurring overnight, possibly caused by a combination of blockage due to solid deposition in the exit line (later identified as polyoxymethylene) and the piston-sensed Tescom™ argon pressure regulator not being able to maintain constant output pressure. This resulted in the automatic shut-off of the feed gases by their respective MFCs and in the steady accumulation of liquid water in the reactor. Interestingly, this environment promoted the formation of methanol, methoxy methanol (see Section 6.2.2), dimethyl carbonate and an unidentified product (possibly methyl bicarbonate) with a retention time of 9.3 minutes in the GC trace.

6.2.2 Selectivity for C_1 oxygenates

The selectivity for C_1 oxidation products as a function of time-on-stream for the Pt/TiO_2(P25) catalyst at 220 °C and 30 bar is shown in Figure 6-3 while the average selectivity obtained for consistent runs with respect to water feed flowrate is illustrated in Figure 6-4. Minor products

methanol and methoxy methanol were the main selective oxidation compounds formed over this catalyst (see chromatogram in Figure 6-5). In the initial 50 hours at the baseline condition, trace amounts of formaldehyde were detected with a selectivity of ca. 1.3%. As the water flowrate was increased to 0.04 ml/min, methanol with low selectivity (ca. 1.9%) could be observed whilst the formation of formaldehyde was totally supressed. During the pressure build-up episode (~ 3650 min), small quantities of methoxy methanol could be detected with a selectivity of 1.3 ± 0.4%. This compound was seen occasionally after every 16 hours (see Figure 6-3) upon increasing the water content in the feed whereas the selectivity of methanol seemed to increase rather slightly whilst remaining in the gaseous phase.

Beyond the flooding point, both the selectivity of methanol and methoxy methanol improved moderately with increasing liquid water flowrate up to 0.2 ml/min. At this test run condition, the highest oxidation product selectivity was achieved at ca. 10% for the Pt/TiO_2(P25) catalyst. It is speculated that the increase in selective oxidation products might be ascribed to the co-adsorption of water which hydrolyses the methoxy intermediate and/or adsorbed methanol, facilitating the desorption process. A further increase in the water flowrate in the trickle flow regime is observed to induce a decline in methanol selectivity whereas the methoxy methanol selectivity is rather constant. The selectivity towards the formation of C_1 oxygenates was still quite low and CO_2 was observed as the major product over the Pt/TiO_2(P25) catalyst. This is possibly attributed to the inability of the methanol and methoxy methanol species to desorb from the catalyst surface, instead undergoing further over-oxidation to CO_2.

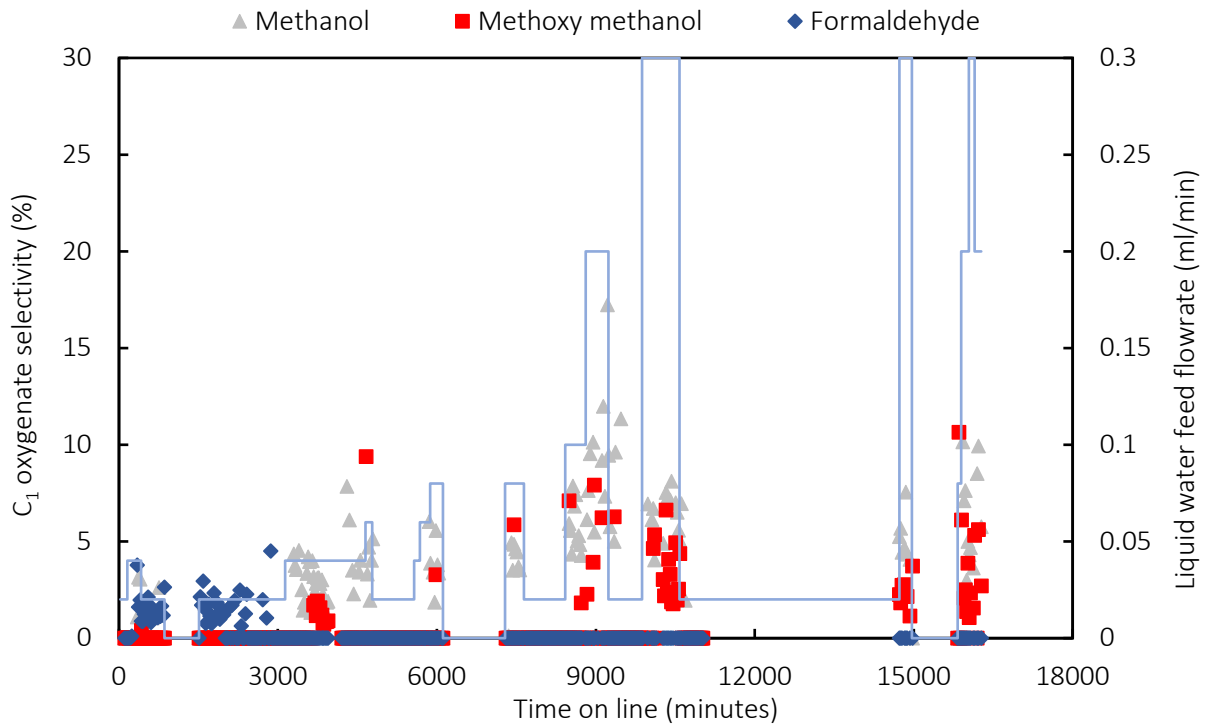

Figure 6-3: Selectivity for the selective oxidation of C_1 oxygenates of methane as a function of time on line over 10 wt.% Pt/TiO_2(P25) catalyst in presence of water at 220 °C and 30 bar (inlet partial pressures P_{CH_4} = 0.5 bar, P_{O_2} = 1.5 bar, P_{sat,H_2O} = 23.1 bar, $F_{CH_4,o}/W$ = 3.1 mmol/g_{cat}.h; blue line indicating liquid water feed rate)

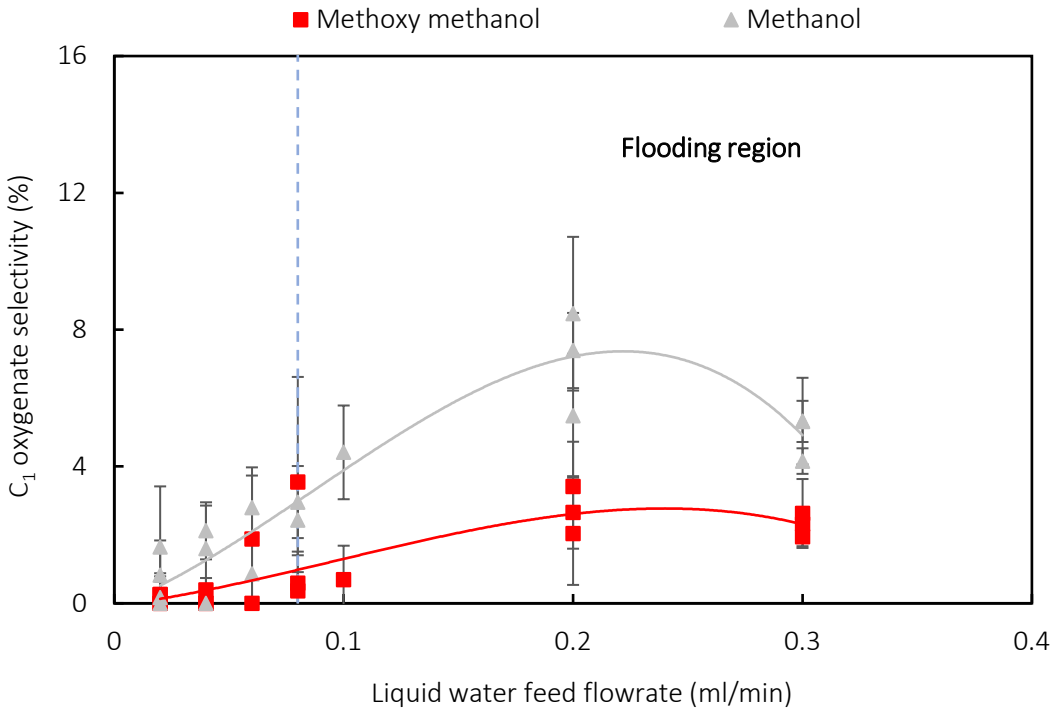

Figure 6-4: Average selectivity for the formation of C_1 oxygenates as a function of liquid water feed flowrate over 10 wt.% Pt/TiO_2(P25) catalyst at 220 °C and 30 bar (inlet partial pressures P_{CH_4} = 0.5 bar, P_{O_2} = 1.5 bar, P_{sat,H_2O} = 23.1 bar, $F_{CH_4,o}/W$ = 3.1 mmol/g_{cat}.h)

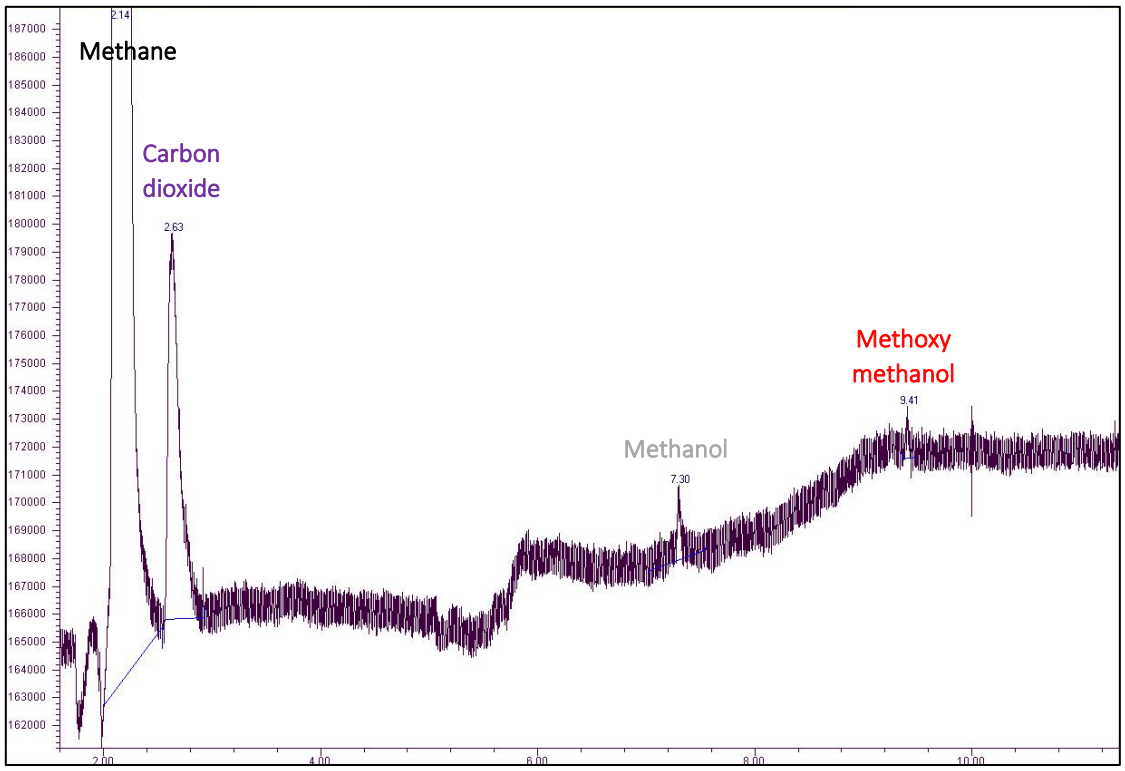

Figure 6-5: Gas chromatogram of products formed from the selective oxidation of methane over 10 wt.% Pt/TiO_2(P25) catalyst at 220 °C and 30 bar (inlet partial pressures P_{CH_4} = 0.5 bar, P_{O_2} = 1.5 bar, P_{sat,H_2O} = 23.1 bar, $F_{CH_4,o}/W$ = 3.1 mmol/g_{cat}.h, liquid water feed rate = 0.3 ml/min)

6.2.3 Selectivity for deep oxidation products

Figure 6-6 illustrates the time on stream behaviour with respect to selectivity for CO_2, the only deep oxidation product formed over the Pt/TiO_2(P25) catalyst at 220 °C and 30 bar. The average CO_2 selectivity obtained for steady runs as a function of liquid water feed flowrate is also presented in Figure 6-7. CO_2 was the dominant product obtained in the direct oxidation of methane over this catalyst with a selectivity above 80%. No carbon monoxide was detected, indicating that methane was preferably combusted completely to CO_2.

Selectivity for CO_2 at the baseline condition was 99.2 ± 0.8% and with increasing water flowrate to the reactor this selectivity decreased by 2.5% at the transition of the flooding region. Upon co-feeding more water whilst in the trickle flow regime, a lower yield of CO_2 was obtained as more of the minor products methanol and methoxy methanol were being formed. For example, CO_2 selectivity was reduced from 96.7 ± 0.4% to 90.2 ± 1.5% with an increase in the inlet molar composition of water from 83 mol% to 91 mol%, respectively.

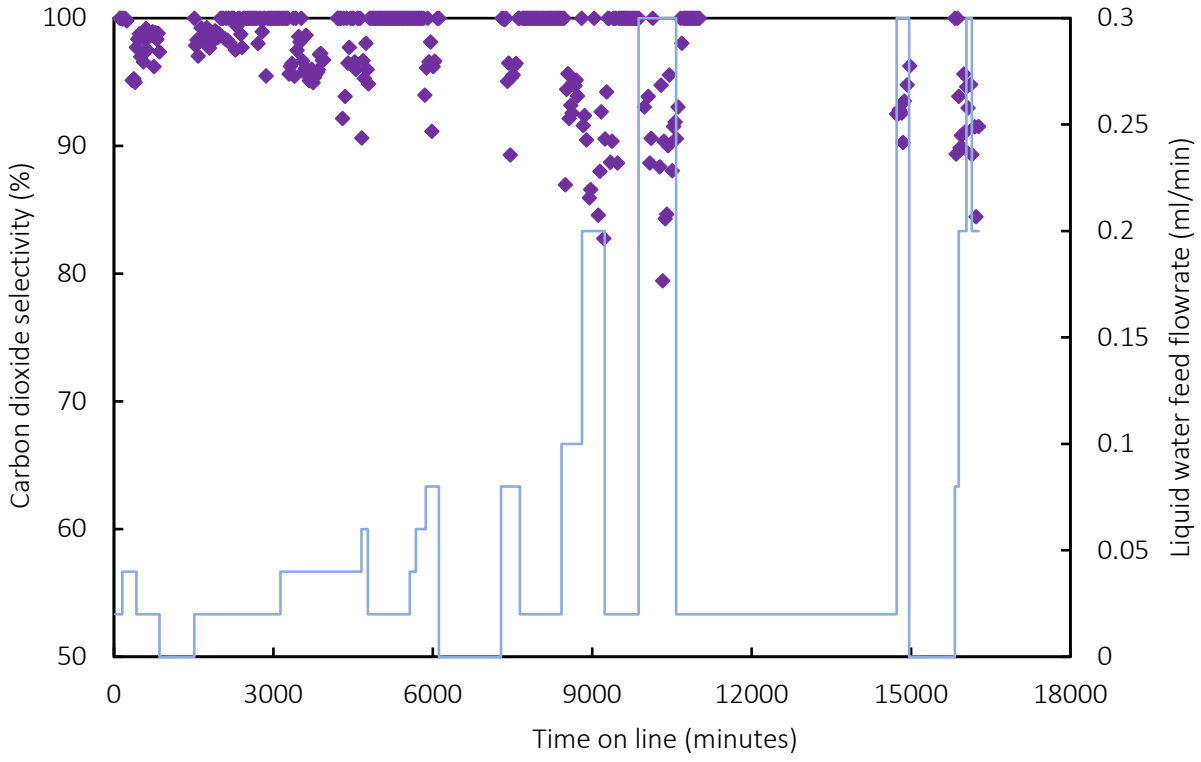

Figure 6-6: Selectivity for the formation of CO_2 as a function of time on line over 10 wt.% Pt/TiO_2(P25) catalyst in presence of water at 220 °C and 30 bar (inlet partial pressures P_{CH_4} = 0.5 bar, P_{O_2} = 1.5 bar, P_{sat,H_2O} = 23.1 bar, $F_{CH_4,o}/W$ = 3.1 mmol/g_{cat}.h; blue line indicating liquid water feed rate)

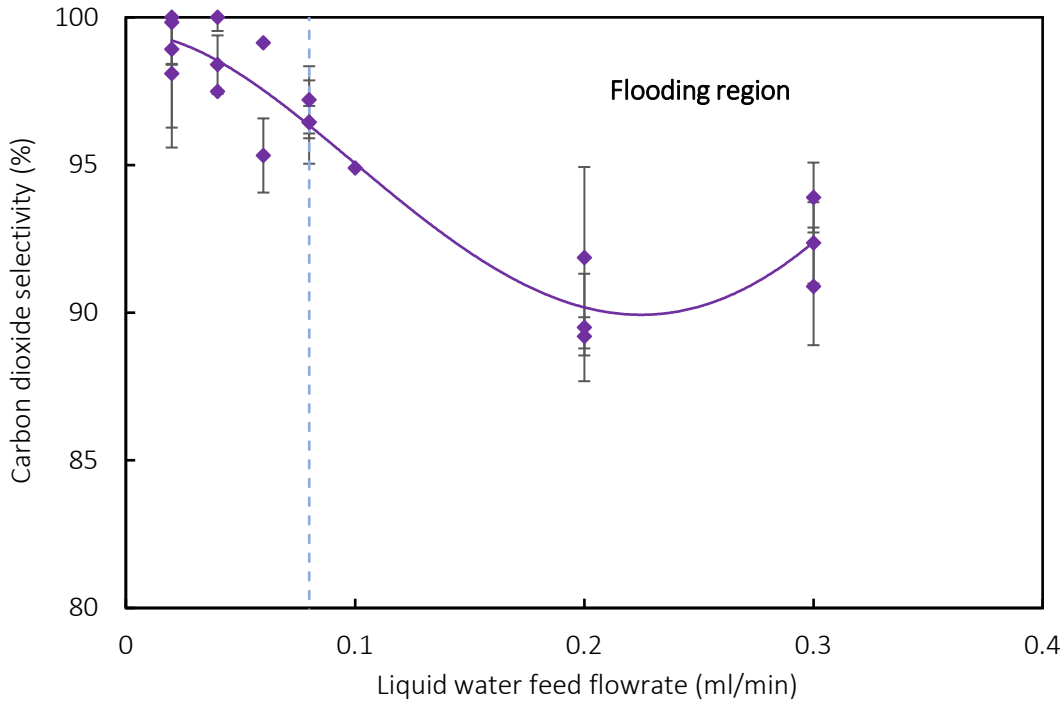

Figure 6-7: Average selectivity for the formation of CO_2 as a function of liquid water feed flowrate over 10 wt.% Pt/TiO_2(P25) catalyst at 220 °C and 30 bar (inlet partial pressures P_{CH_4} = 0.5 bar, P_{O_2} = 1.5 bar, P_{sat,H_2O} = 23.1 bar, $F_{CH_4,o}/W$ = 3.1 mmol/g_{cat}.h)

6.3 Selective oxidation of methane over Pt/TiO_2(rutile) catalyst

The next in-house platinum catalyst tested for the direct conversion of methane in the trickle bed reactor system was 10 wt.% Pt/TiO_2(rutile). This catalyst was loaded in the quartz lined reactor with an approximate measured mass of 1.52 g (catalyst bed length ~ 20 mm).

This time, the argon pressure regulator was replaced by a more robust diaphragm-sensed pressure regulator, sourced from Air Products to enable for a more stable steady-state operation. Furthermore, this experiment was run for a longer time period compared to the first one, with a time on stream of 600 hours.

6.3.1 Methane conversion

The plot of the methane conversion against time-on-stream for the Pt/TiO_2(rutile) catalyst at 220 °C and 30 bar for different inlet liquid water flowrates is displayed in Figure 6-8. In this experiment, no water was added to the reactor in the initial 1000 minutes. The conversion of methane during this time period was approximately 3.4%. However, upon introducing water at a flowrate of 0.02 ml/min, it dropped sharply to ca. 0.05%. This sudden decline in activity was also observed over the Pt/TiO_2(P25) catalyst, which is attributed to the possible inhibition effect of the hydroxyl species completely covering the metal surface sites, otherwise available for CH_4 activation.

There was a brief period of pressure build-up around 3700-4000 minutes on-line whereby water was allowed to flow in at an inlet flowrate of 0.04 ml/min overnight. This was mainly due

to the needle valve V-701 not being open wide enough during operation, which caused the pressure build-up and the accumulation of liquid water at the bottom of the reactor. The rise in reaction pressure with the presence of water in the liquid phase facilitated the temporary formation of methanol species (as was previously seen with the Pt/TiO_2(P25) catalyst). The reactor was operating at baseline condition between times 4600-9900 minutes on-line with no data being collected during this period.

Increasing the inlet partial pressure of water in the regime up to the saturation point resulted in a four-fold increase in CH_4 conversion from 0.05% to 0.20% as observed in Figure 6-9. With intermediate return to the baseline condition (whilst still in the gas phase region at ~ 10400 min), the catalytic performance seemed to have declined, as evidenced by a reduction in methane conversion to 0.03 ± 0.01%.

Upon entering the trickle flow regime by flowing in high throughputs of liquid water in the reactor, the catalytic activity was observed to increase steadily with increasing water flowrate. However, by comparing the CH_4 conversion at baseline condition, the associated rate of deactivation progressed rapidly as the conversion dropped to ca. 0.01% (at times 200-300 hours on-line). Beyond the flooding point, at an inlet water flowrate of 0.3 ml/min, a conversion of methane of ca. 1.0% was achieved over the Pt/TiO_2(rutile), corresponding a methane consumption rate of 33.3 µmol/g_{cat}.h. The major product formed at that particular condition was formaldehyde.

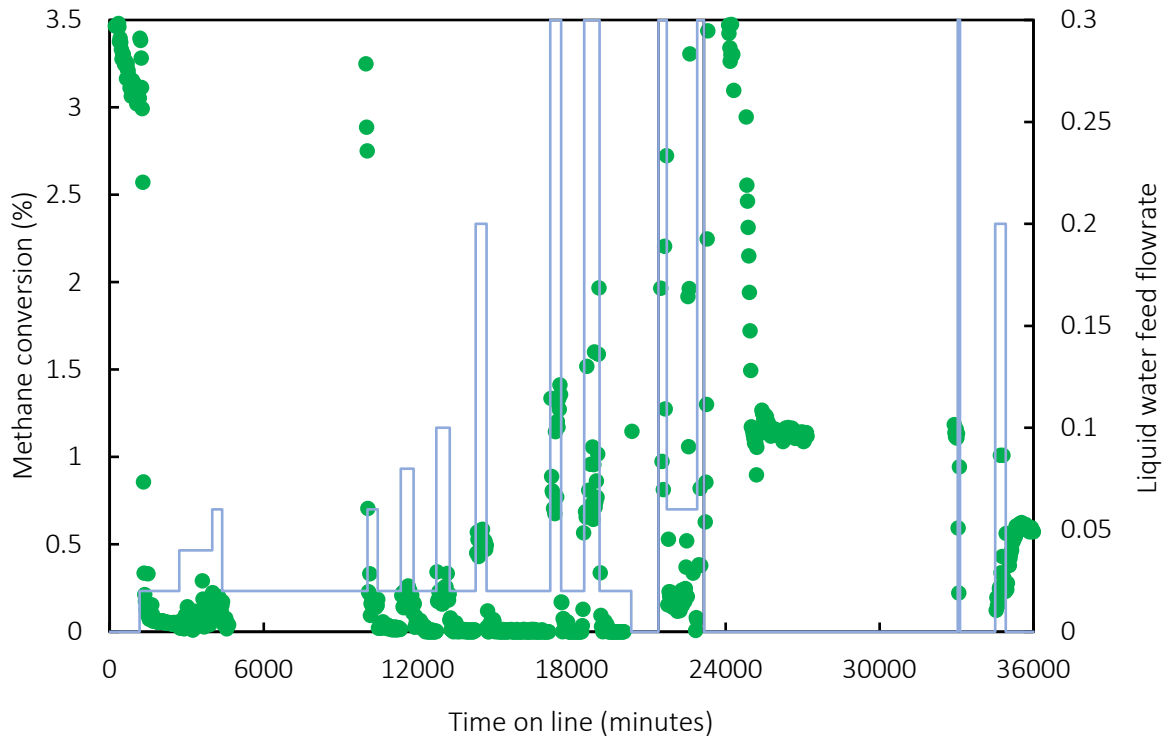

Figure 6-8: Conversion of methane as a function of time on line over 10 wt.% Pt/TiO_2(rutile) catalyst in presence of liquid water at 220 °C and 30 bar (inlet partial pressures P_{CH_4} = 0.5 bar, P_{O_2} = 1.5 bar, P_{sat,H_2O} = 23.1 bar, $F_{CH_4,o}/W$ = 3.2 mmol/gcat.h; blue line indicating liquid water feed rate)

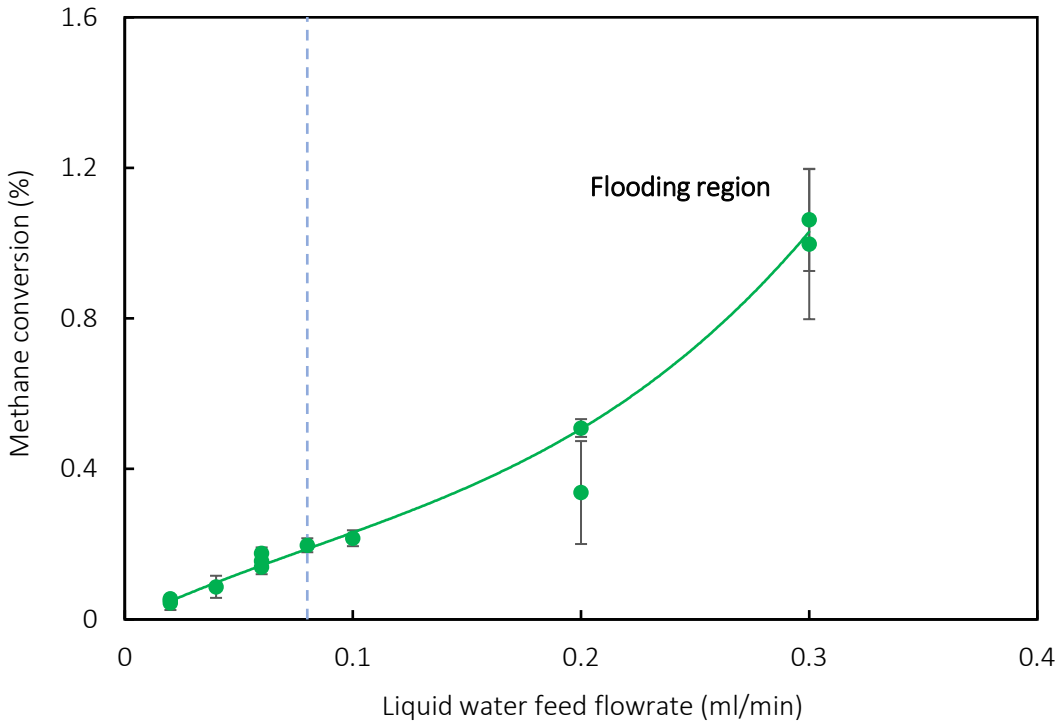

Figure 6-9: Average conversion of methane as a function of liquid water feed flowrate over 10 wt.% Pt/TiO_2(rutile) catalyst at 220 °C and 30 bar (inlet partial pressures P_{CH_4} = 0.5 bar, P_{O_2} = 1.5 bar, P_{sat,H_2O} = 23.1 bar, $F_{CH_4,o}/W$ = 3.2 mmol/g_{cat}.h)

Water co-feeding was temporarily halted at around 20300 minutes on stream. A sudden spike in CH_4 conversion was then observed which decreased gradually with time (see Appendix B.2). It is speculated that the reason for this was probably caused by the slow formation of polymeric deposit in the GC transfer line, which later resulted in a pressure build-up in the reactor (~ 22700 min). After having replaced the GC transfer line and returning back to no water co-feeding, the CH_4 conversion stabilised at 1.14 ± 0.05%. Before termination of the experiment, upon reverting back to the same conditions, the conversion decreased even further to 0.58 ± 0.05%, indicating that the catalyst has permanently deactivated.

6.3.2 Selectivity for C_1 oxygenates

The selectivity for C_1 oxygenates with respect to time-on-stream for the Pt/TiO_2(rutile) catalyst at 220 °C and 30 bar is shown in Figure 6-10. The major selective oxidation product formed over this catalyst was formaldehyde and only trace amounts of methanol were occasionally observed throughout the experiment. During the initial 19 hours without water being introduced in the TBR, no C_1 oxygenate was produced. Once water was co-fed at a flowrate of 0.02 ml/min, minute amounts of formaldehyde were briefly detected.

As the partial pressure of water was increased from baseline condition (6.9 bar) to 13.7 bar, the selectivity towards formaldehyde started to pick up to an average value of ca. 47.4%. The selectivity towards formaldehyde improved sharply upon increasing water flowrate up to the transition point. This is well illustrated in Figure 6-11 which shows the average selectivity obtained for consistent runs as a function of liquid water feed flowrate. For instance, increasing

the water partial pressure from 13.7 bar to 23.1 bar in the trickle bed reactor led to an increase in formaldehyde selectivity to 81.6 ± 2.6%.

Upon entering the trickle bed regime, the methane oxidation became highly selective towards formaldehyde, reaching a maximum selectivity of almost 90%. This occurred at a liquid water feed flowrate of 0.3 ml/min as illustrated by the broad formaldehyde peak with its characteristic long tail in the chromatogram in Figure 6-12. However, it must be noted that the presence of liquid water beyond the flooding point did not have a considerable effect on the formaldehyde selectivity as it appeared to increase gradually until it reached a plateau (see Figure 6-11). It is speculated that this occurs as the selectivity is possibly only affected by the surface composition which is fixed at a given partial pressure of H_2O and O_2, however the rate of reaction may further increase due to the presence of liquid water.

Interestingly, during both pressure build-up scenarios occurring at 3700 and 22700 minutes on stream, the selectivity towards formaldehyde declined while detectable amounts of methanol could be momentarily observed in the product spectrum. This probably hints at the positive effect of increased reaction pressure towards the formation of methanol in the tri-phasic system when flooding the catalyst bed.

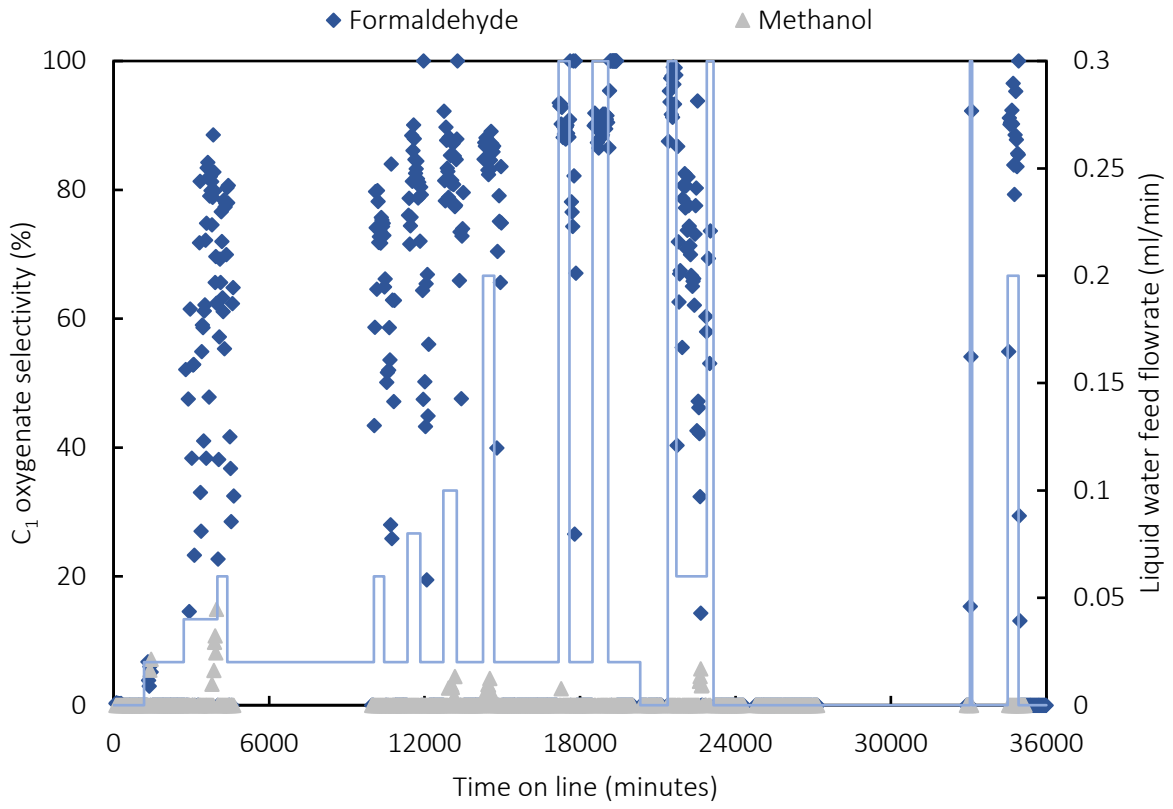

Figure 6-10: Selectivity for the formation of C_1 oxygenate (formaldehyde) as a function of time on line over 10 wt.% Pt/TiO_2(rutile) catalyst in presence of water at 220 °C and 30 bar (inlet partial pressures P_{CH_4} = 0.5 bar, P_{O_2} = 1.5 bar, P_{sat,H_2O} = 23.1 bar, $F_{CH_4,o}/W$ = 3.2 mmol/g_{cat}.h; blue line indicating liquid water feed flowrate)

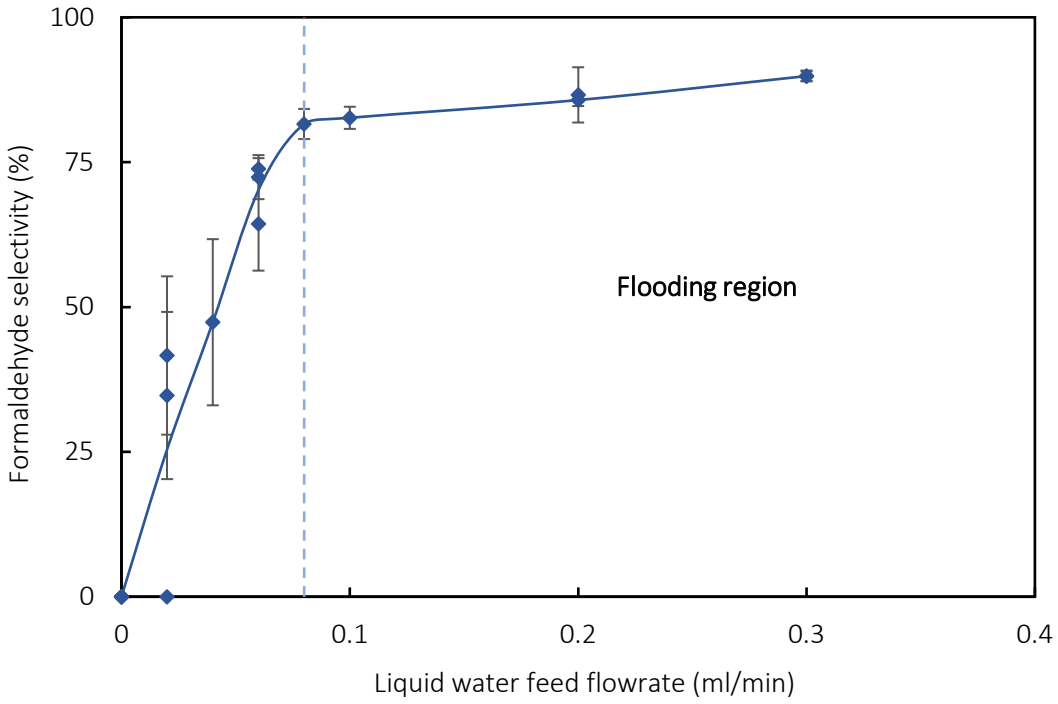

Figure 6-11: Average selectivity for the formation of formaldehyde as a function of liquid water feed flowrate over 10 wt.% Pt/TiO_2(rutile) catalyst at 220 °C and 30 bar (inlet partial pressures P_{CH_4} = 0.5 bar, P_{O_2} = 1.5 bar, P_{sat,H_2O} = 23.1 bar, $F_{CH_4,o}/W$ = 3.2 mmol/g_{cat}.h)

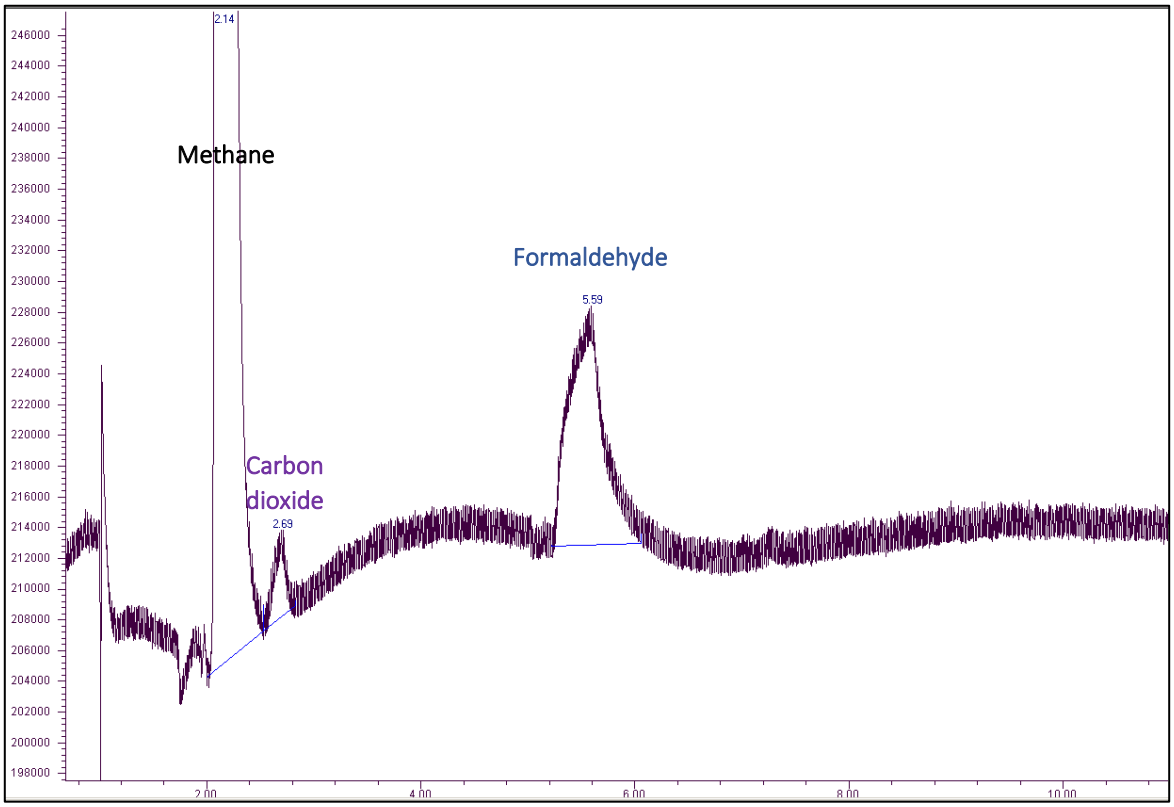

Figure 6-12: Gas chromatogram of products formed from the selective oxidation of methane over 10 wt.% Pt/TiO_2(rutile) catalyst at 220 °C and 30 bar (inlet partial pressures P_{CH_4} = 0.5 bar, P_{O_2} = 1.5 bar, P_{sat,H_2O} = 23.1 bar, $F_{CH_4,o}/W$ = 3.2 mmol/g_{cat}.h, liquid water feed rate = 0.3 ml/min)

6.3.3 Selectivity for deep oxidation products

The time on stream behaviour with respect to the deep oxidation products CO_2 and CO, formed over the Pt/TiO_2(rutile) catalyst at 220 °C and 30 bar is shown in Figure 6-13. In the absence of water in the trickle bed reactor during the initial 19 hours on-line, the only product obtained was CO_2. Introducing water at a flowrate of 0.02 ml/min resulted in a decline in CO_2 formation as more formaldehyde and CO were being formed. A high yield of CO with a maximum selectivity of approximately 40% was obtained at this test condition. This is well illustrated in Figure 6-14 showing the respective average selectivity for CO_2 and CO obtained for consistent runs as a function of inlet liquid water flowrate.

With further increase in the partial pressure of water in the reactor up to the saturation point, the selectivity towards CO_2 decreased even more to 11.4 ± 3.0%; the same trend was observed for CO with a selectivity of 7.0 ± 3.5%. However, the decrease in CO production progressed at a relatively higher rate compared to that of CO_2 with increasing water co-feeding. In the flooding region as the main compound formed was formaldehyde, lower yields of CO and CO_2 were obtained. At an inlet liquid water flowrate of 0.3 ml/min, the average selectivity towards CO_2 was approximately 9.8% whereas only trace amounts of CO were detected.

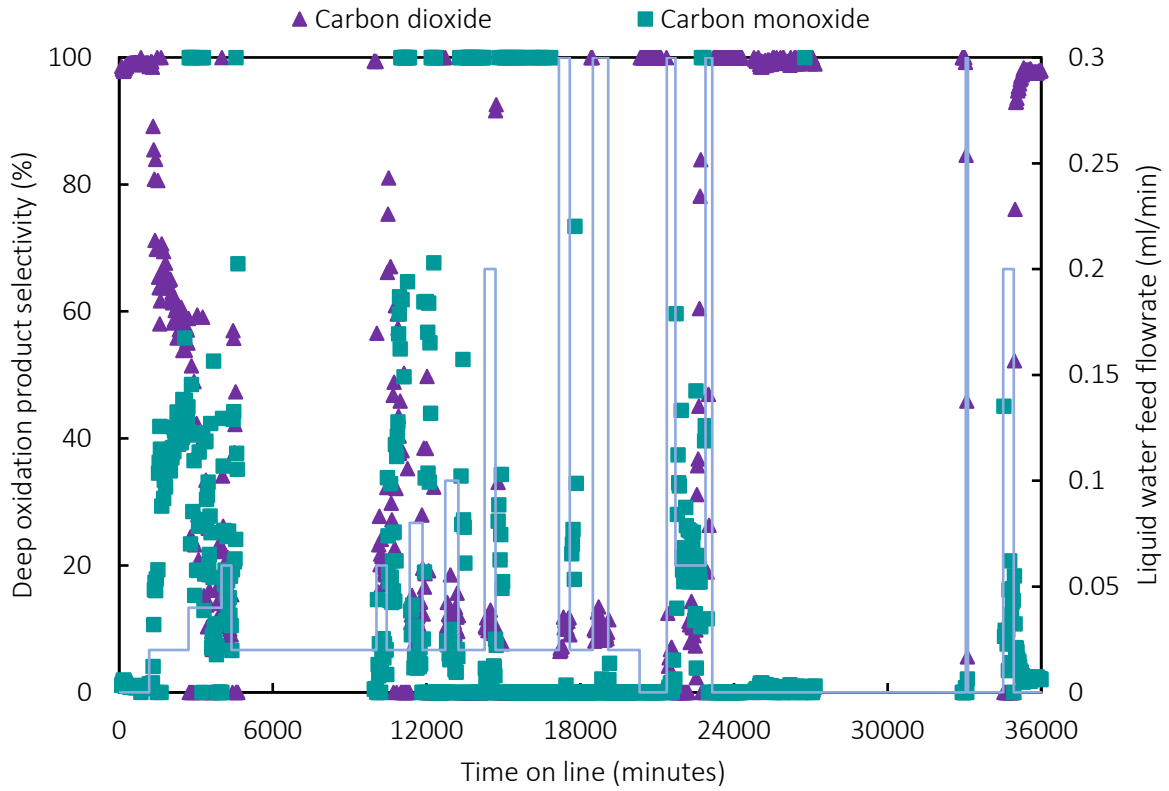

Figure 6-13: Selectivity for the formation of deep oxidation products as a function of time on line over 10 wt.% Pt/TiO_2(rutile) catalyst in presence of water at 220 °C and 30 bar (inlet partial pressures P_{CH_4} = 0.5 bar, P_{O_2} = 1.5 bar, P_{sat,H_2O} = 23.1 bar, $F_{CH_4,o}/W$ = 3.2 mmol/g_{cat}.h; blue line indicating liquid water feed rate)

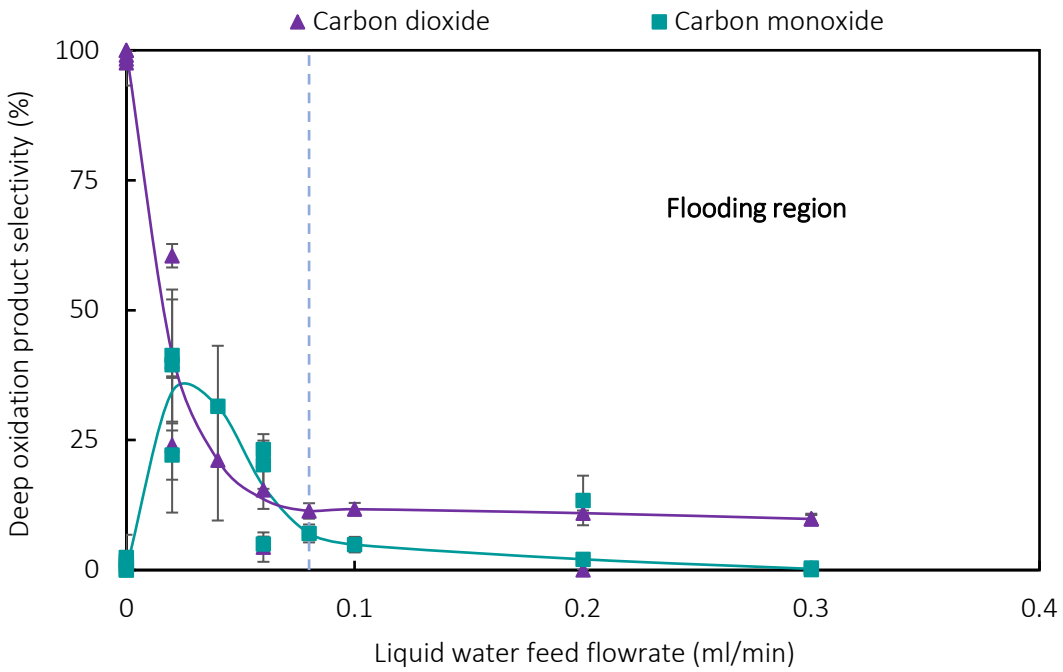

Figure 6-14: Average selectivity for the formation of deep oxidation products as a function of liquid water feed flowrate over 10 wt.% Pt/TiO_2(rutile) catalyst at 220 °C and 30 bar (inlet partial pressures P_{CH_4} = 0.5 bar, P_{O_2} = 1.5 bar, P_{sat,H_2O} = 23.1 bar, $F_{CH_4,o}/W$ = 3.2 mmol/g_{cat}.h)

6.4 Stability of reactor operation

The steady state operation in the trickle bed reactor set-up can be evaluated by monitoring the total peak area of the experiments as a function of time on stream as presented in Figure 6-15 and Figure 6-16 for Pt/TiO_2(P25) and Pt/TiO_2(rutile), respectively. There is some scattering in the total peak area after each condition change with respect to inlet water flowrate. This has to do with the helium flowrate being adjusted to keep the inlet partial pressures of CH_4 and O_2 constant, and the occasional adjustment of the argon flowrate through the expansion valve V-602. A high degree of scattering in the total peak area for both catalysts is observed when operating in the trickle flow regime. This may be caused by changes in the argon dilution ratio (when manually adjusting the expansion valve), the erratic flow patterns caused by steam condensing out inside the needle valve (non-uniform heating due to its high thermal mass) or fluctuations caused by the actuating 6-port injection valve. Compared to Pt/TiO_2(rutile), this effect is more pronounced for Pt/TiO_2(P25), especially at a feed water flowrate of 0.3 ml/min between 9900-10600 minutes (see Figure 6-15). It is because a more robust argon pressure regulator was used over Pt/TiO_2(rutile), which was more effective in maintaining constant pressure during operation. Therefore, the stability of reactor operation was much smoother over Pt/TiO_2(rutile).

Based on a student's t-test with a confidence level of 95%, there is a significant relationship between the total peak area and the time on stream for both catalysts. The slope of the regression line between the total peak area and time on stream is negative (i.e., it is decreasing gradually with time on stream). It does not necessarily mean that the carbon molar flowrate exiting the reactor is not constant but may indicate that the concentration of carbon in the

sample loop is decreasing. This can be explained by the increase in argon flowrate when operating in the trickle flow regime (higher dilution ratio, thus lower carbon concentration), lower gas volume present in the sample loop caused by liquid condensation or lower pressure and/or higher temperature in the injection sample volume.

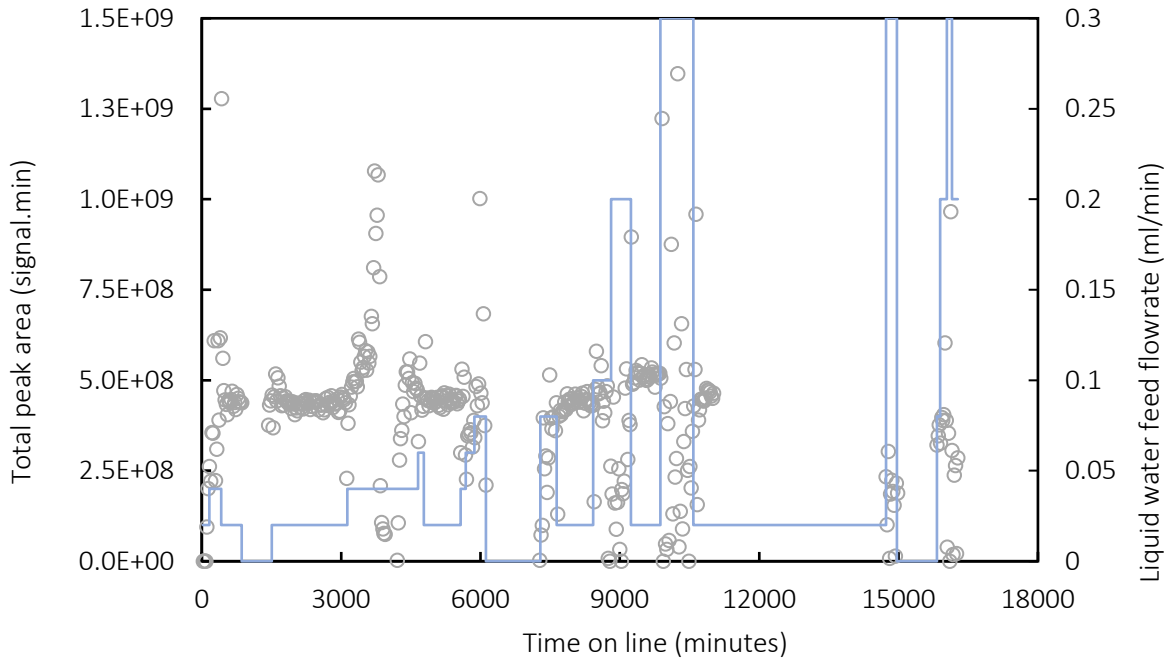

Figure 6-15: Total peak area as a function of time on line over 10 wt.% Pt/TiO_2(P25) catalyst in presence of water at 220 °C and 30 bar (inlet partial pressures P_{CH_4} = 0.5 bar, P_{O_2} = 1.5 bar, P_{sat,H_2O} = 23.1 bar, $F_{CH_4,o}/W$ = 3.1 mmol/g_{cat}.h; blue line indicating liquid water feed rate)

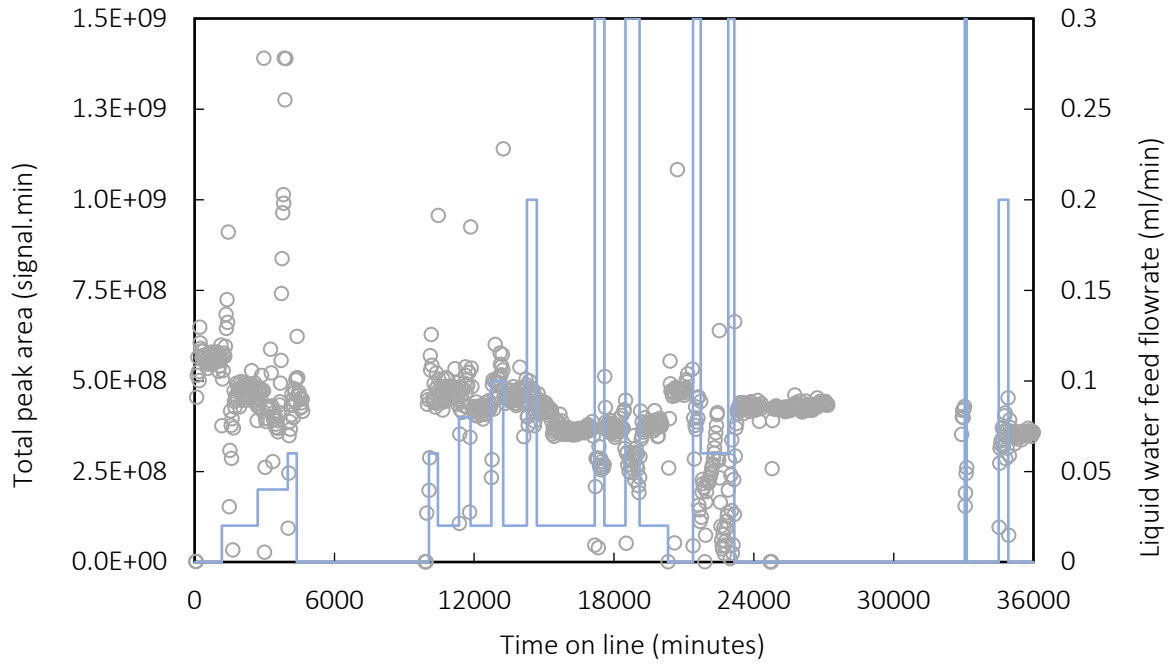

Figure 6-16: Total peak area as a function of time on line over 10 wt.% Pt/TiO_2(rutile) catalyst in presence of water at 220 °C and 30 bar (inlet partial pressures P_{CH_4} = 0.5 bar, P_{O_2} = 1.5 bar, P_{sat,H_2O} = 23.1 bar, $F_{CH_4,o}/W$ = 3.2 mmol/g_{cat}.h; blue line indicating liquid water feed rate)

6.5 Comparison between Pt/TiO_2(P25) and Pt/TiO_2(rutile) catalysts

Both catalytic experiments were performed under similar reactor conditions with the catalysts having the same platinum loading of 10 wt%, same metal dispersion of 14.5% and exhibited similar metal surface area [125]. Nevertheless, their performances differed greatly in terms of activity and product spectrum.

6.5.1 Catalyst activity

In the initial hours of operation for both experiments (without water co-feeding), a high turnover frequency of ca. 12 h^{-1} was obtained over Pt/TiO_2(P25) compared to Pt/TiO_2(rutile) which was ten-fold lower at 1.5 h^{-1}, indicating that the former catalyst was much more active in the absence of water. The extent of catalyst deactivation was monitored in both experiments by repeatedly returning to the baseline condition (i.e., inlet water flowrate of 0.02 ml/min). The initial catalyst deactivation (instigated by water) over Pt/TiO_2(P25) occurred at a lower rate compared to Pt/TiO_2(rutile) as it took 5000 minutes for the methane conversion to stabilize, while for the latter it reached steady state after approximately 2000 minutes on stream. Both catalysts seem to have lost some activity in the long term, with the most obvious decline occurring after flooding the reactor with liquid water at a flowrate of 0.3 ml/min.

Figure 6-17 compares the catalytic performance of the catalysts as a function of inlet water flowrate. In the gaseous phase region, the turnover frequencies of both Pt/TiO_2(P25) and Pt/TiO_2(rutile) catalysts lie on top of each other. A very modest increase in the activity is observed up to the saturation point, which may be attributed to the increase in the chemical potential of water. However, when moving into the trickle flow regime, the respective activity for both Pt/TiO_2(rutile) and Pt/TiO_2(P25) becomes more pronounced despite the chemical potential of water remaining constant in the flooding region. As the wetting efficiency of the catalyst surface increases with increasing inlet liquid water flowrate, it is thought that this improvement in activity may be ascribed to the high concentration of liquid water near the active sites. This may imply that water or water-derived species in the bulk fluid phase may be actively participating in the rate determining step of methane oxidation. The TOFs of both catalysts are highest at the water feed flowrate of 0.3 ml/min with Pt/TiO_2(rutile) clearly outperforming Pt/TiO_2(P25). The corresponding average TOF for Pt/TiO_2(P25) is 0.25 h^{-1}, whereas for Pt/TiO_2(rutile) the catalytic activity has substantially doubled with an estimated average TOF of 0.43 h^{-1}. The reported turnover frequencies in this study are comparable to those obtained for the oxidation of methane with H_2O_2 over 5 wt% $AuPd/TiO_2$ catalysts [56] and are higher than those obtained over Cu-MOR catalysts [52] with molecular oxygen as oxidant. However, they are quite low compared to the TOFs of 31-2110 h^{-1} obtained by Hammond *et al.* [59] using iron- and copper-containing zeolites in an aqueous medium of H_2O_2 (see Table 2-4).

The difference in catalyst activity obtained under the same conditions at a water feed flowrate of 0.3 ml/min for the two Pt/TiO_2 catalysts may be ascribed to the difference in the support titania and its interactions with water molecules (i.e., the wettability of the support). The

wetting properties on the TiO_2 surface, dictated by a combination of surface roughness, phase crystallinity and surface chemistry differ for the pure rutile phase and P25, a mixture of mainly anatase and rutile, with the former believed to have a more hydrophobic surface [126]–[128]. However, the conditions in the trickle bed reactor system are different (particularly at high pressure and moderate temperature), hence the wettability of the support may not necessarily follow the same behaviour. Assuming the pure rutile phase to be more hydrophobic, it could mean that in the flooding regime, the water molecules interact less with the support and are preferentially attracted and/or exposed to the metal active sites resulting in an increase in the frequency of interactions, thus increased catalytic activity. Whereas under similar conditions for the P25 mixed phase, the catalytic activity is lower due to fewer interactions of the water molecules with the active platinum catalyst.

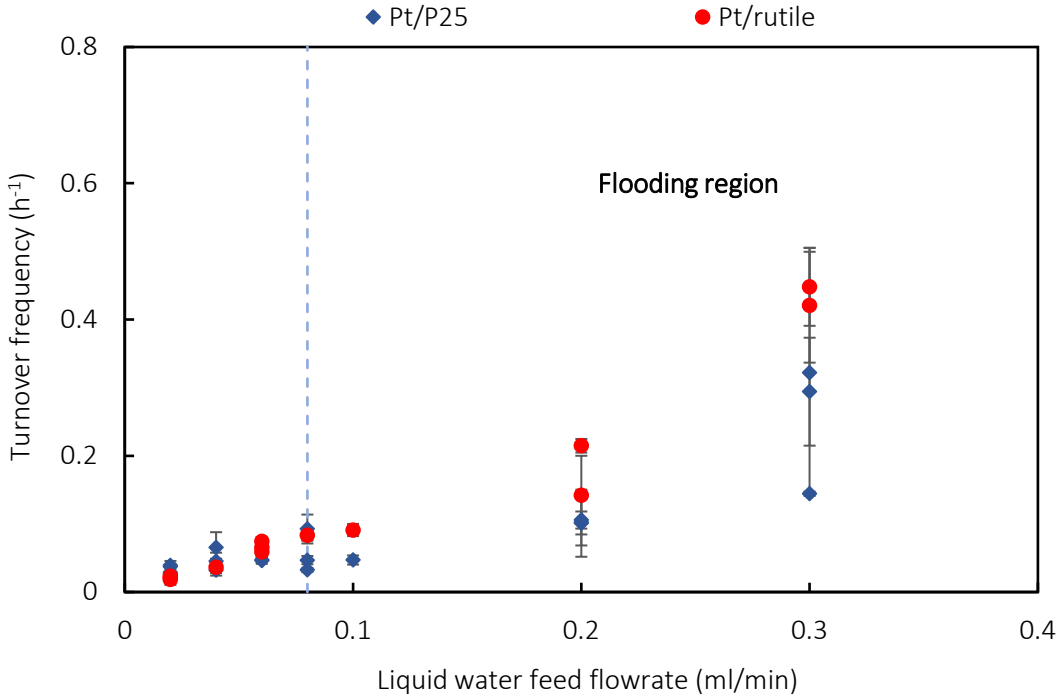

Figure 6-17: Average turnover frequency as a function of liquid water feed flowrate over 10 wt.% Pt/P25($F_{CH_4,o}$/W = 3.1 mmol/g_{cat}.h) and Pt/rutile($F_{CH_4,o}$/W = 3.2 mmol/g_{cat}.h) catalysts at 220 °C and 30 bar (inlet partial pressures P_{CH_4} = 0.5 bar, P_{O_2} = 1.5 bar, P_{sat,H_2O} = 23.1 bar)

6.5.2 Effect of water on the selectivity towards C_1 oxygenates

Water has demonstrated to be an essential ingredient towards the formation of C_1 oxygenates in the selective oxidation of methane in the trickle bed reactor. This may have been facilitated through its site blocking action hampering the formation of deep oxidation products, as well as its role in improving the desorption of selective oxidation products. Although full coverage of the metal surface is achieved via water co-feeding, the methane molecule may still be activated (via surface oxygen or surface hydroxyl species) to produce surface methoxy and other surface species (e.g., hydroxy-methoxy species) [129]. It is possible that these species interact with water in the bulk liquid phase to form methanediol, which can further dehydrate yielding formaldehyde [130].

Over Pt/TiO_2(rutile) formaldehyde was exclusively formed with a remarkable selectivity of 90%. Conversely, methanol and methoxy methanol were obtained over Pt/TiO_2(P25) with a maximum combined selectivity of only ca. 10%. This highlights another difference between the two catalysts, which may be ascribed to the role of the support in the presence of water on product formation in the selective methane oxidation. The intermediate product formed over Pt/TiO_2(P25) may bond too strongly to the support which results in the overoxidation of the methanol and methoxy methanol species into CO_2, thus reducing the selectivity towards C_1 oxygenates. Another reason could be due to the acidity and basicity of the supports. Under basic conditions, the primarily formed formaldehyde may be converted via a Cannizzaro type of reaction into methanol and formic acid, with the latter immediately overoxidized to CO_2. In contrast, under acidic conditions formaldehyde can be decomposed directly to CO [131].

7. Conclusions

The prime focus of this research study was to investigate the role of liquid water in the selective oxidation of methane over platinum-based catalysts with molecular oxygen as oxidant. This was achieved by designing and constructing a continuously operating trickle bed reactor (TBR) system capable of evaluating the performance of these catalysts safely at 30 bar and 220 °C while co-feeding water. Safety measures were implemented to mitigate the risks associated with the flammability of methane-oxygen mixtures, such as flame arresters, pressure relief valves, dilution of methane and oxygen feeds with helium and dilution of the reactor effluent with argon. The reactor system was commissioned by conducting two long-run (1.5-3.5 weeks) catalytic experiments over Pt/TiO_2(P25) and Pt/TiO_2(rutile) while keeping the inlet partial pressures of CH_4 and O_2 constant at 0.5 bar and 1.5 bar, respectively and varying the liquid water feed flowrate. It was able to operate at steady state conditions, as well as providing reliable and repeatable results in terms of measurements for the methane conversion, product yield and selectivity. Thus, it can be concluded that the novel trickle bed reactor system has successfully met its design requirements for the selective oxidation of methane with liquid water co-feeding at high pressure (< 50 bar) and moderate temperature (< 400 °C).

This study has shown that co-feeding liquid water has a major influence on the activity of platinum-based catalysts in the selective oxidation of methane. Under similar flooding conditions, a general trend was observed for both catalysts, whereby the conversion of methane increased with increasing inlet water flowrate. The maximum conversion was achieved for a feed containing 93 mol% of water, i.e., when operating in the trickle flow regime at a feed flowrate of 0.3 ml/min. This corresponded to a conversion of 0.6% over Pt/TiO_2(P25) with a methane consumption of 18.5 $\mu mol/g_{cat}.h$, and 1% over Pt/TiO_2(rutile) with a methane consumption of 33.3 $\mu mol/g_{cat}.h$ (corresponding to an estimated turnover frequency of 0.25 h^{-1} and 0.43 h^{-1}, respectively). These turnover frequencies are comparable in magnitude to those obtained over 5 wt% $AuPd/TiO_2$ catalysts for the oxidation of methane to methanol with H_2O_2 [56]. Although for noble metal-based catalysts to be cost-effective, the turnover frequency has to be much higher at ca. 3600 h^{-1} for practical uses [16], [25]. It is thought that this increase in activity is not related to the chemical potential of water, instead it may be attributed to the presence of liquid water close to the catalytically active sites or other factors which have not yet been established in this research.

It was also shown that the presence of liquid water in the reactor was essential for driving the selectivity towards C_1 oxygenates. In other words, the selectivity for the formation of C_1 oxygenates increased with increasing feed water flowrate, especially in the flooding region (P_{H_2O} > 23.1 bar). Under this test condition, methanol and methoxy methanol were formed over the Pt/TiO_2(P25) catalyst with a modest combined selectivity of ca. 10% while CO_2 was the major product. In contrast, formaldehyde was the only exclusive selective oxidation product obtained over the Pt/TiO_2(rutile) catalyst with a high selectivity of 90% (with the balance CO and CO_2). The increase in the selectivity of C_1 oxygenated products may be ascribed to the site

blocking action of water, restricting the over-oxidation to CO and CO_2. Furthermore, water from the bulk fluid phase is believed to be essential in enforcing the desorption of selective oxidation products. The reported difference in catalyst activity and product selectivity obtained over the two platinum catalysts is speculated to be due to the interactions of the metal support with water molecules (in relation to hydrophobic sites and basic/acidic sites on the pure and mixed TiO_2 phases), although it is not evident yet.

Despite not achieving a methanol selectivity of 80% at a single-pass methane conversion of at least 10% (the benchmark in DMTM to compete with the commercialized syngas route [5], [12]), a very high selectivity of 90% for formaldehyde was obtained in the continuous single-step conversion of methane in this study. It should be noted that formaldehyde is industrially produced from natural gas via three main processes with methanol as intermediate product [130]. Thus, it is believed that the findings obtained in this study can prove to be valuable towards the development of highly selective catalysts for the formation of C_1 oxygenated products such as formaldehyde and methanol in the direct conversion of methane with oxygen as oxidant. Using the newly designed trickle bed reactor system was crucial to show that the presence of liquid water enhances methane conversion whilst also improving the selectivity towards C_1 oxygenates. However, the role of liquid water is still very unclear and further studies on this subject are still needed in order to improve methane conversion, as well as yield for selective oxidation products.

8. Recommendations

The two experiments in this study were performed at the same set of reactor conditions with only the inlet flowrate of liquid water allowed to vary with time on stream. Further experiments should be conducted to evaluate the effects of reactor conditions such as temperature, pressure, feed composition and linear gas velocity have on methane conversion, yield and selectivity of reaction products. For example, during the pressure build-up scenarios, high yields of methanol could be obtained even when operating at a liquid feed flowrate of 0.04 ml/min. Thus, it is recommended that experiments should be performed at a higher reaction pressure to potentially improve methanol selectivity. This would mean that the trickle bed reactor would no longer be able to get its supply of high-pressure argon from the centralised house gas line, thus requiring its own argon cylinder.

In addition, the experiments conducted over the pure platinum catalysts supported on titania only provide a base case performance. It would be interesting to add promoters such as metals Ag, Ni, Pd, Mo, Co and Cu to the platinum catalysts and compare their performances in the selective oxidation of methane in the trickle bed reactor set-up. Increasing the dispersion of platinum in the catalyst may also aid in improving the activity and therefore achieving higher turnover frequencies.

Although the GC-Polyarc™-FID system is reliable and sensitive for quantitative analysis, i.e., it is efficient in separating and quantifying the reaction products, it cannot identify all of them. For instance, during the pressure build-up scenario over the Pt/TiO_2(P25) catalyst, trace amounts of products were detected at a retention time of 9.3 minutes but have not been clearly identified yet. Therefore, instead of conducting separate individual trial-and-error experiments for product identification, using a gas chromatography-mass spectrometry (GC-MS) in parallel with the GC-Polyarc™-FID system can make it much easier and less time-consuming in providing definite qualitative information on the products formed in the reactor.

The hydrodynamics of the co-current catalytic trickle bed reactor involving the complex interactions of gas-liquid-solid phases has not been explicitly explored in this research. Knowledge about the hydrodynamics characteristics (such as the flow regime transitions, two-phase flow pressure drop, liquid hold-up and catalyst wetting efficiency) and accurate understanding of how they change with design and operating parameters are however essential as it can immensely help in optimising the performance of the reactor. Hence, thorough hydrodynamics studies which aim at determining these key characteristics should be carried out in the high-pressure trickle bed reactor.

9. References

[1] S. Dale, “BP statistical review of world energy,” London, United Kingdom, 2020. [Online]. Available: https://www.bp.com/content/dam/bp/business-sites/en/global/corporate/pdfs/energy-economics/statistical-review/bp-stats-review-2020-full-report.pdf

[2] Enerdata, “Natural gas domestic consumption,” 2020. https://yearbook.enerdata.net/natural-gas/gas-consumption-data.html (accessed Jun. 06, 2020).

[3] IEA, “Gas market report Q3-2021,” 2021. [Online]. Available: https://www.iea.org/reports/gas-market-report-q3-2021

[4] M. J. da Silva, “Synthesis of methanol from methane: Challenges and advances on the multi-step (syngas) and one-step routes (DMTM),” *Fuel Process. Technol.*, **145**, 42–61, 2016.

[5] Q. Zhang, D. He, and Q. Zhu, “Recent progress in direct partial oxidation of methane to methanol,” *J. Nat. Gas Chem.*, **12**, no. 2, 81–89, 2003.

[6] K. A. Ali, A. Z. Abdullah, and A. R. Mohamed, “Recent development in catalytic technologies for methanol synthesis from renewable sources: A critical review,” *Renew. Sustain. Energy Rev.*, **44**, 508–518, 2015.

[7] P. Khirsariya and R. K. Mewada, “Single step oxidation of methane to methanol - towards better understanding,” *Procedia Eng.*, **51**, 409–415, 2013.

[8] Z. Zakaria and S. K. Kamarudin, “Direct conversion technologies of methane to methanol: An overview,” *Renew. Sustain. Energy Rev.*, **65**, 250–261, 2016.

[9] T. L. Theis and A. Hicks, “Methanol use in wastewater denitrification,” Alexandria, USA, 2012.

[10] Inkwood Research, “Global methanol market forecast 2019-2027,” 2019. https://www.inkwoodresearch.com/reports/global-methanol-market/

[11] K. Aasberg-Petersen, J. H. Bak Hansen, T. S. Christensen, I. Dybkjaer, P. S. Christensen, C. Stub Nielsen, S. E. L. Winter Madsen, and J. R. Rostrup-Nielsen, “Technologies for large-scale gas conversion,” *Appl. Catal. A Gen.*, **221**, no. 1–2, 379–387, 2001.

[12] G. A. Foulds and B. F. Gray, “Homogeneous gas-phase partial oxidation of methane to methanol and formaldehyde,” *Fuel Process. Technol.*, **42**, no. 2–3, 129–150, 1995.

[13] A. I. Olivos-Suarez, À. Szécsényi, E. J. M. Hensen, J. Ruiz-Martinez, E. A. Pidko, and J. Gascon, “Strategies for the direct catalytic valorization of methane using heterogeneous catalysis: challenges and opportunities,” *ACS Catal.*, **6**, no. 5, 2965–2981, 2016.

[14] R. H. Perry, D. W. Green, and J. O. Maloney, *Perry's chemical engineers' handbook*, 7th ed. New York: McGraw-Hill Companies, Inc, 1997.

[15] P. Tang, Q. Zhu, Z. Wu, and D. Ma, "Methane activation: the past and future," *Energy Environ. Sci.*, **7**, no. 8, 2580–2591, 2014.

[16] A. Caballero and P. J. Pérez, "Methane as raw material in synthetic chemistry: the final frontier," *Chem. Soc. Rev.*, **42**, no. 23, 8809–8820, 2013.

[17] S. J. Blanksby and G. B. Ellison, "Bond dissociation energies of organic molecules," *Acc. Chem. Res.*, **36**, no. 4, 255–263, 2003.

[18] F. Dalena, A. Senatore, A. Marino, A. Gordano, M. Basile, and A. Basile, *Methanol production and applications: an overview*. Elsevier, 2018.

[19] B. Cañete, C. E. Gigola, and N. B. Brignole, "Synthesis gas processes for methanol production via CH_4 reforming with CO_2, H_2O, and O_2," *Ind. Eng. Chem. Res.*, **53**, no. 17, 7103–7112, 2014.

[20] G. A. Olah and G. K. Surya Prakash, "The methanol economy project," Los Angeles, CA, 2014. [Online]. Available: http://netl.doe.gov/research/proj?k=FE0000435

[21] R. A. Periana, D. J. Taube, E. R. Evitt, D. G. Löffler, P. R. Wentrcek, G. Voss, and T. Masuda, "A mercury-catalyzed, high-yield system for the oxidation of methane to methanol," *Science (80-.).*, **259**, no. 5093, 340–343, 1993.

[22] C. J. Jones, D. Taube, V. R. Ziatdinov, R. A. Periana, R. J. Nielsen, J. Oxgaard, and W. A. Goddard, "Selective oxidation of methane to methanol catalyzed, with C-H activation, by homogeneous, cationic gold," *Angew. Chemie - Int. Ed.*, **43**, no. 35, 4626–4629, 2004.

[23] R. A. Periana, D. J. Taube, S. Gamble, H. Taube, T. Satoh, and H. Fujii, "Platinum catalysts for the high-yield oxidation of methane to a methanol derivative," *Science (80-.).*, **280**, no. 5363, 560–564, 1998.

[24] A. E. Shilov and G. B. Shul'pin, "Activation of C-H bonds by metal complexes," *Chem. Rev.*, **97**, no. 8, 2879–2932, 1997.

[25] B. L. Conley, W. J. Tenn, K. J. H. Young, S. K. Ganesh, S. K. Meier, V. R. Ziatdinov, O. Mironov, J. Oxgaard, J. Gonzales, W. A. Goddard, and R. A. Periana, "Design and study of homogeneous catalysts for the selective, low temperature oxidation of hydrocarbons," *J. Mol. Catal. A Chem.*, **251**, no. 1–2, 8–23, 2006.

[26] T. Zimmermann, M. Soorholtz, M. Bilke, and F. Schüth, "Selective methane oxidation catalyzed by platinum salts in oleum at turnover frequencies of large-scale industrial processes," *J. Am. Chem. Soc.*, **138**, no. 38, 12395–12400, 2016.

[27] S. Raynes, M. A. Shah, and R. A. Taylor, "Direct conversion of methane to methanol with zeolites: Towards understanding the role of extra-framework d-block metal and zeolite

framework type," *Dalt. Trans.*, **48**, no. 28, 10364–10384, 2019.

[28] R. Palkovits, M. Antonietti, P. Kuhn, A. Thomas, and F. Schüth, "Solid catalysts for the selective low-temperature oxidation of methane to methanol," *Angew. Chemie - Int. Ed.*, **48**, no. 37, 6909–6912, 2009.

[29] M. C. Alvarez-Galvan, N. Mota, M. Ojeda, S. Rojas, R. M. Navarro, and J. L. G. Fierro, "Direct methane conversion routes to chemicals and fuels," *Catal. Today*, **171**, no. 1, 15–23, 2011.

[30] R. S. Hanson and T. E. Hanson, "Methanotrophic bacteria," *Microbiol. Rev.*, **60**, no. 2, 439–471, 1996.

[31] V. C. C. Wang, S. Maji, P. P. Y. Chen, H. K. Lee, S. S. F. Yu, and S. I. Chan, "Alkane oxidation: methane monooxygenases, related enzymes, and their biomimetics," *Chem. Rev.*, **117**, no. 13, 8574–8621, 2017.

[32] C. E. Tinberg and S. J. Lippard, "Dioxygen activation in soluble methane monooxygenase," *Acc. Chem. Res.*, **44**, no. 4, 280–288, 2011.

[33] C. Duan, M. Luo, and X. Xing, "High-rate conversion of methane to methanol by Methylosinus trichosporium OB3b," *Bioresour. Technol.*, **102**, no. 15, 7349–7353, 2011.

[34] V. Uppada, S. Bhaduri, and S. B. Noronha, "Cofactor regeneration - an important aspect of biocatalysis," *Curr. Sci.*, **106**, no. 7, 946–957, 2014.

[35] C. E. Bjorck, P. D. Dobson, and J. Pandhal, "Biotechnological conversion of methane to methanol: evaluation of progress and potential," *AIMS Bioeng.*, **5**, no. 1, 1–38, 2018.

[36] E. V. Kondratenko, T. Peppel, D. Seeburg, V. A. Kondratenko, N. Kalevaru, A. Martin, and S. Wohlrab, "Methane conversion into different hydrocarbons or oxygenates: Current status and future perspectives in catalyst development and reactor operation," *Catal. Sci. Technol.*, **7**, no. 2, 366–381, 2017.

[37] S. S. Verma, "To study the direct transformation of methane into methanol in the lower temperature range," *Energy Convers. Manag.*, **43**, no. 15, 1999–2008, 2002.

[38] K. Tabata, Y. Teng, T. Takemoto, and E. Suzuki, "Activation of methane by oxygen and nitrogen oxides," *Catal. Rev. - Sci. Eng.*, **44**, no. 1, 1–58, 2002.

[39] M. Ravi, M. Ranocchiari, and J. A. van Bokhoven, "The direct catalytic oxidation of methane to methanol—A critical assessment," *Angew. Chemie - Int. Ed.*, **56**, no. 52, 16464–16483, 2017.

[40] Q. Zhang, D. He, J. Li, B. Xu, Y. Liang, and Q. Zhu, "Comparatively high yield methanol production from gas phase partial oxidation of methane," *Appl. Catal. A Gen.*, **224**, no. 1–2, 201–207, 2002.

[41] V. S. Arutyunov, V. I. Vedeneev, S. Y. Klimovetskaya, V. E. Leonov, and L. V. Pavlij, "Influence of pressure on the formation of products of partial oxidation of methane," *Theor. Found. Chem. Eng.*, **28**, no. 6, 563–568, 1994.

[42] H. D. Gesser, N. R. Hunter, and C. B. Prakash, "The direct conversion of methane to methanol by controlled oxidation," *Chem. Rev.*, **85**, no. 4, 235–244, 1985.

[43] K. Otsuka and Y. Wang, "Direct conversion of methane into oxygenates," *Appl. Catal. A Gen.*, **222**, no. 1–2, 145–161, 2001.

[44] G. S. Walker, J. A. Lapszewicz, and G. A. Foulds, "Partial oxidation of methane to methanol-comparison of heterogeneous catalyst and homogeneous gas phase reactions," *Catal. Today*, **21**, no. 2–3, 519–526, 1994.

[45] Q. Zhang, D. He, and Q. Zhu, "Direct partial oxidation of methane to methanol: reaction zones and role of catalyst location," *J. Nat. Gas Chem.*, **17**, no. 1, 24–28, 2008.

[46] G. O. Alptekin, A. M. Herring, D. L. Williamson, T. R. Ohno, and R. L. McCormick, "Methane partial oxidation by unsupported and silica supported iron phosphate catalysts: Influence of reaction conditions and co-feeding of water on activity and selectivity," *J. Catal.*, **181**, no. 1, 104–112, 1999.

[47] S. Grundner, M. A. C. Markovits, G. Li, M. Tromp, E. A. Pidko, E. J. M. Hensen, A. Jentys, M. Sanchez-Sanchez, and J. A. Lercher, "Single-site trinuclear copper oxygen clusters in mordenite for selective conversion of methane to methanol," *Nat. Commun.*, **6**, no. May, 1–9, 2015.

[48] B. E. R. Snyder, M. L. Bols, R. A. Schoonheydt, B. F. Sels, and E. I. Solomon, "Iron and copper active sites in zeolites and their correlation to metalloenzymes," *Chem. Rev.*, **118**, no. 5, 2718–2768, 2018.

[49] P. Tomkins, M. Ranocchiari, and J. A. Van Bokhoven, "Direct conversion of methane to methanol under mild conditions over Cu-zeolites and beyond," *Acc. Chem. Res.*, **50**, no. 2, 418–425, 2017.

[50] D. K. Pappas, E. Borfecchia, M. Dyballa, I. A. Pankin, K. A. Lomachenko, A. Martini, M. Signorile, S. Teketel, B. Arstad, G. Berlier, C. Lamberti, S. Bordiga, U. Olsbye, K. P. Lillerud, S. Svelle, and P. Beato, "Methane to methanol: structure–activity relationships for Cu-CHA," *J. Am. Chem. Soc.*, **139**, no. 42, 14961–14975, 2017.

[51] M. H. Groothaert, P. J. Smeets, B. F. Sels, P. A. Jacobs, and R. A. Schoonheydt, "Selective oxidation of methane by the bis (μ-oxo) dicopper core stabilized on ZSM-5 and mordenite zeolites," *J. Am. Chem. Soc.*, **127**, no. 5, 1394–1395, 2005.

[52] M. Dyballa, D. K. Pappas, K. Kvande, E. Borfecchia, B. Arstad, P. Beato, U. Olsbye, and S. Svelle, "On how copper mordenite properties govern the framework stability and activity in the methane-to-methanol conversion," *ACS Catal.*, **9**, no. 1, 365–375, 2019.

[53] K. Narsimhan, K. Iyoki, K. Dinh, and Y. Román-Leshkov, “Catalytic oxidation of methane into methanol over copper-exchanged zeolites with oxygen at low temperature,” *ACS Cent. Sci.*, **2**, no. 6, 424–429, 2016.

[54] P. Tomkins, A. Mansouri, S. E. Bozbag, F. Krumeich, M. B. Park, E. M. C. Alayon, M. Ranocchiari, and J. A. Van Bokhoven, “Isothermal cyclic conversion of methane into methanol over copper- exchanged zeolite at low temperature,” *Angew. Chemie*, **55**, 5557–5561, 2016.

[55] Y. Kwon, T. Y. Kim, G. Kwon, J. Yi, and H. Lee, “Selective activation of methane on single-atom catalyst of rhodium dispersed on zirconia for direct conversion,” *J. Am. Chem. Soc.*, **139**, no. 48, 17694–17699, 2017.

[56] M. H. Ab Rahim, M. M. Forde, R. L. Jenkins, C. Hammond, Q. He, N. Dimitratos, J. A. Lopez-Sanchez, A. F. Carley, S. H. Taylor, D. J. Willock, D. M. Murphy, C. J. Kiely, and G. J. Hutchings, “Oxidation of methane to methanol with hydrogen peroxide using supported gold-palladium alloy nanoparticles,” *Angew. Chemie - Int. Ed.*, **52**, no. 4, 1280–1284, 2013.

[57] M. H. Ab Rahim, R. D. Armstrong, C. Hammond, N. Dimitratos, S. J. Freakley, M. M. Forde, D. J. Morgan, G. Lalev, R. L. Jenkins, J. A. Lopez-Sanchez, S. H. Taylor, and G. J. Hutchings, “Low temperature selective oxidation of methane to methanol using titania supported gold palladium copper catalysts,” *Catal. Sci. Technol.*, **6**, no. 10, 3410–3418, 2016.

[58] S. Al-Shihri, C. J. Richard, H. Al-Megren, and D. Chadwick, “Insights into the direct selective oxidation of methane to methanol over ZSM-5 zeolytes in aqueous hydrogen peroxide,” *Catal. Today*, **353**, 269–278, 2020.

[59] C. Hammond, M. M. Forde, M. H. Ab Rahim, A. Thetford, Q. He, R. L. Jenkins, N. Dimitratos, J. A. Lopez-Sanchez, N. F. Dummer, D. M. Murphy, A. F. Carley, S. H. Taylor, D. J. Willock, E. E. Stangland, J. Kang, H. Hagen, C. J. Kiely, and G. J. Hutchings, “Direct catalytic conversion of methane to methanol in an aqueous medium by using copper-promoted Fe-ZSM-5,” *Angew. Chemie - Int. Ed.*, **51**, no. 21, 5129–5133, 2012.

[60] J. Xu, R. D. Armstrong, G. Shaw, N. F. Dummer, S. J. Freakley, S. H. Taylor, and G. J. Hutchings, “Continuous selective oxidation of methane to methanol over Cu- and Fe-modified ZSM-5 catalysts in a flow reactor,” *Catal. Today*, **270**, 93–100, 2016.

[61] G. I. Panov, V. I. Sobolev, and A. S. Kharitonov, “The role of iron in N_2O decomposition on ZSM-5 zeolite and reactivity of the surface oxygen formed,” *J. Mol. Catal.*, **61**, no. 1, 85–97, 1990.

[62] E. V. Starokon, M. V. Parfenov, L. V. Pirutko, S. I. Abornev, and G. I. Panov, “Room-temperature oxidation of methane by α-oxygen and extraction of products from the FeZSM-5 surface,” *J. Phys. Chem. C*, **115**, no. 5, 2155–2161, 2011.

[63] M. V. Parfenov, E. V. Starokon, L. V. Pirutko, and G. I. Panov, “Quasicatalytic and catalytic oxidation of methane to methanol by nitrous oxide over FeZSM-5 zeolite,” *J. Catal.*, **318**, 14–21, 2014.

[64] Y. Kim, T. Y. Kim, H. Lee, and J. Yi, “Distinct activation of Cu-MOR for direct oxidation of methane to methanol,” *Chem. Commun.*, **53**, no. 29, 4116–4119, 2017.

[65] B. Ipek and R. F. Lobo, “Catalytic conversion of methane to methanol on Cu-SSZ-13 using N_2O as oxidant,” *Chem. Commun.*, **52**, no. 91, 13401–13404, 2016.

[66] A. Bogaerts, E. Neyts, R. Gijbels, and J. Van der Mullen, “Gas discharge plasmas and their applications,” *Spectrochim. Acta Part B At. Spectrosc.*, **57**, no. 4, 609–658, 2002.

[67] T. Nozaki, A. Aĝiral, S. Yuzawa, J. G. E. Han Gardeniers, and K. Okazaki, “A single step methane conversion into synthetic fuels using microplasma reactor,” *Chem. Eng. J.*, **166**, no. 1, 288–293, 2011.

[68] P. Chawdhury, D. Ray, and C. Subrahmanyam, “Single step conversion of methane to methanol assisted by nonthermal plasma,” *Fuel Process. Technol.*, **179**, 32–41, 2018.

[69] L. Chen, X. Zhang, L. Huang, and L. Lei, “Application of in-plasma catalysis and post-plasma catalysis for methane partial oxidation to methanol over a Fe2O3-CuO/γ- Al2O3 catalyst,” *J. Nat. Gas Chem.*, **19**, no. 6, 628–637, 2010.

[70] P. V. L. Reddy, K. H. Kim, and H. Song, “Emerging green chemical technologies for the conversion of CH4 to value added products,” *Renew. Sustain. Energy Rev.*, **24**, 578–585, 2013.

[71] M. A. Gondal, A. Hameed, Z. H. Yamani, and A. Arfaj, “Photocatalytic transformation of methane into methanol under UV laser irradiation over WO_3, TiO_2 and NiO catalysts,” *Chem. Phys. Lett.*, **392**, no. 4–6, 372–377, 2004.

[72] K. Villa, S. Murcia-López, T. Andreu, and J. R. Morante, “Mesoporous WO3 photocatalyst for the partial oxidation of methane to methanol using electron scavengers,” *Appl. Catal. B Environ.*, **163**, 150–155, 2015.

[73] P. S. Yarlagadda, L. A. Morton, N. R. Hunter, and H. D. Gesser, “Direct conversion of methane to methanol in a flow reactor,” *Ind. Eng. Chem. Res.*, **27**, no. 2, 252–256, 1988.

[74] R. Burch, G. D. Squire, and S. C. Tsang, “Direct conversion of methane into methanol,” *J. Chem. Soc. Faraday Trans. 1 Phys. Chem. Condens. Phases*, **85**, no. 10, 3561–3568, 1989.

[75] G. A. Foulds, B. F. Gray, S. A. Miller, and G. S. Walker, “Homogenous gas phase oxidation of methane using oxygen as oxidant in an annular reactor,” *Ind. Eng. Chem. Res.*, **32**, no. 5, 780–787, 1993.

[76] A. S. Chellappa, S. Fuangfoo, and D. S. Viswanath, “Homogeneous oxidation of methane to methanol: effect of CO_2, N_2, and H_2 at high oxygen conversions,” *Ind. Eng. Chem. Res.*,

36, no. 5, 1401–1409, 1997.

[77] C. Okolie, Y. F. Belhseine, Y. Lyu, M. M. Yung, M. H. Engelhard, L. Kovarik, E. Stavitski, and C. Sievers, "Conversion of methane into methanol and ethanol over nickel oxide on ceria–zirconia catalysts in a single reactor," *Angew. Chemie - Int. Ed.*, **56**, no. 44, 13876–13881, 2017.

[78] G. Fratesi, P. Gava, and S. De Gironcoli, "Direct methane-to-methanol conversion: insight from first-principles calculations," *J. Phys. Chem. C*, **111**, no. 45, 17015–17019, 2007.

[79] L. Arnarson, P. S. Schmidt, M. Pandey, A. Bagger, K. S. Thygesen, I. E. L. Stephens, and J. Rossmeisl, "Fundamental limitation of electrocatalytic methane conversion to methanol," *Phys. Chem. Chem. Phys.*, **20**, no. 16, 11152–11159, 2018.

[80] J. K. Nørskov, J. Rossmeisl, A. Logadottir, L. Lindqvist, J. R. Kitchin, T. Bligaard, and H. Jónsson, "Origin of the overpotential for oxygen reduction at a fuel-cell cathode," *J. Phys. Chem. B*, **108**, no. 46, 17886–17892, 2004.

[81] P. L. Cilliers, "Phase diagram for the co-adsorption of O and OH on Pt(100) and Pt(111) as determined by DFT," University of Cape Town, 2017.

[82] A. Dianat, N. Seriani, L. C. Ciacchi, W. Pompe, G. Cuniberti, and M. Bobeth, "Dissociative adsorption of methane on surface oxide structures of Pd-Pt alloys," *J. Phys. Chem. C*, **113**, no. 50, 21097–21105, 2009.

[83] M. F. Fellah and I. Onal, "C-H bond activation of methane on M- and MO-ZSM-5 (M = Ag, Au, Cu, Rh and Ru) clusters: a density functional theory study," *Catal. Today*, **171**, no. 1, 52–59, 2011.

[84] L. Qi and J. Li, "Adsorbate interactions on surface lead to a flattened Sabatier volcano plot in reduction of oxygen," *J. Catal.*, **295**, 59–69, 2012.

[85] T. Mallat and A. Baiker, "Oxidation of alcohols with molecular oxygen on platinum metal catalysts in aqueous solutions," *Catal. Today*, **19**, no. 2, 247–283, 1994.

[86] M. Besson, F. Lahmer, P. Gallezot, patrick Fuertes, and G. Fleche, "Catalytic oxidation of glucose on bismuth-promoted palladium catalysts," *Journal of Catalysis*, **152**, no. 1. 116–121, 1995.

[87] Z. Zuo, P. J. Ramírez, S. D. Senanayake, P. Liu, and J. A. Rodriguez, "Low-temperature conversion of methane to methanol on CeO_x/Cu_2O catalysts: water controlled activation of the C–H bond," *J. Am. Chem. Soc.*, **138**, no. 42, 13810–13813, 2016.

[88] A. A. Latimer, A. Kakekhani, A. R. Kulkarni, and J. K. Nørskov, "Direct methane to methanol: the selectivity–conversion limit and design strategies," *ACS Catal.*, **8**, no. 8, 6894–6907, 2018.

[89] P. G. Lustemberg, R. M. Palomino, R. A. Gutiérrez, D. C. Grinter, M. Vorokhta, Z. Liu, P. J. Ramírez, V. Matolín, M. V. Ganduglia-Pirovano, S. D. Senanayake, and J. A. Rodriguez, "Direct conversion of methane to methanol on Ni-Ceria surfaces: metal–support interactions and water-enabled catalytic conversion by site blocking," *J. Am. Chem. Soc.*, **140**, no. 24, 7681–7687, 2018.

[90] M. Yan, Z. Q. Huang, Y. Zhang, and C. R. Chang, "Trends in water-promoted oxygen dissociation on the transition metal surfaces from first principles," *Phys. Chem. Chem. Phys.*, **19**, no. 3, 2364–2371, 2017.

[91] P. R. Gunjal, M. N. Kashid, V. V. Ranade, and R. V. Chaudhari, "Hydrodynamics of trickle-bed reactors: experiments and CFD modeling," *Ind. Eng. Chem. Res.*, **44**, no. 16, 6278–6294, 2005.

[92] D. Durante, T. Kilpiö, P. Suominen, V. S. Herrera, J. Wärnå, P. Canu, and T. Salmi, "Modeling and simulation of a small-scale trickle bed reactor for sugar hydrogenation," *Comput. Chem. Eng.*, **66**, 22–35, 2014.

[93] V. Degirmenci and E. V. Rebrov, "Design of catalytic micro trickle bed reactors," *Phys. Sci. Rev.*, **1**, no. 4, 2016.

[94] J. P. Reynier and J. . Charpentier, "Hold-up prediction in packed columns for co-current gas-liquid downflow," *Chem. Eng. Sci.*, **26**, no. 10, 1781–1783, 1971.

[95] W. J. A. Wammes and K. R. Westerterp, "Hydrodynamics in a pressurized cocurrent gas-liquid trickle-bed reactor," *Chem. Eng. Technol. Ind. Chem. Equipment-Process Eng.*, **14**, no. 6, 406–413, 1991.

[96] A. E. Sáez and R. G. Carbonell, "Hydrodynamic parameters for gas-liquid cocurrent flow in packed beds," *AIChE J.*, **31**, no. 1, 52–62, 1985.

[97] V. V. Ranade, R. V. Chaudhari, and P. R. Gunjal, *Trickle bed reactors: Reactor engineering & applications*. Elsevier, 2011.

[98] J. Hanika, "Safe operation and control of trickle-bed reactor," *Chem. Eng. Sci.*, **54**, no. 20, 4653–4659, 1999.

[99] M. H. Al-Dahhan, F. Larachi, M. P. Dudukovic, and A. Laurent, "High-pressure trickle-bed reactors: a review," *Ind. Eng. Chem. Res.*, **36**, no. 8, 3292–3314, 1997.

[100] W. P. M. van Swaaij, "Residence time distributions in Raschig ring columns at trickle flow," Technische Hogeschool Eindhoven, 1967.

[101] W. J. A. Wammes, S. J. Mechielsen, and K. R. Westerterp, "The influence of pressure on the liquid hold-up in a cocurrent gas-liquid trickle-bed reactor operating at low gas velocities," *Chem. Eng. Sci.*, **46**, no. 2, 409–417, 1991.

[102] M. I. Urseanu, J. G. Boelhouwer, H. J. M. Bosman, J. C. Schroijen, and G. Kwant,

"Estimation of trickle-to-pulse flow regime transition and pressure drop in high-pressure trickle bed reactors with organic liquids," *Chem. Eng. J.*, **111**, no. 1, 5–11, 2005.

[103] I. Iliuta, B. P. A. Grandjean, and F. Larachi, "New mechanistic film model for pressure drop and liquid holdup in trickle flow reactors," *Chem. Eng. Sci.*, **57**, no. 16, 3359–3371, 2002.

[104] C. N. Satterfield, "Trickle-bed reactors," *AIChE J.*, **21**, no. 2, 209–228, 1975.

[105] J. Guo, "Design , construction and commissioning of a packed bed reactor system for methane to methanol conversion," University of Cape Town, 2018.

[106] M. J. A. AL-Zuraiji, J. Zanganeh, and B. Moghtaderi, "Application of flame arrester in mitigation of explosion and flame deflagration of ventilation air methane," *Fuel*, **257**, 115985, 2019.

[107] L. Wang, H. Ma, and Z. Shen, "The quenching of propane deflagrations by crimped ribbon flame arrestors," *J. Loss Prev. Process Ind.*, **43**, 567–574, 2016.

[108] B. Walker, "Deepwater horizon oil spill," *J. Environ. Health*, **73**, no. 4, 49, 2010.

[109] G. A. Melhem, "A detailed method for estimating mixture flammability limits using chemical equilibrium," *Process Saf. Prog.*, **16**, no. 4, 203–218, 1997.

[110] W. A. Muth, "Effect of pressure on the flammable limits of some hydrocarbon-air mixtures," Iowa State University of Science and Technology, 1963. [Online]. Available: https://lib.dr.iastate.edu/cgi/viewcontent.cgi?article=3547&context=rtd

[111] M. G. Zabetakis, "Flammability characteristics of combustible gases and vapors," 1965.

[112] M. Molnarne, P. Mizsey, and V. Schröder, "Flammability of gas mixtures: Part 2: Influence of inert gases," *J. Hazard. Mater.*, **121**, no. 1–3, 45–49, 2005.

[113] S. Besnard, "Full flammability test of gases and gas mixtures in air," 1996.

[114] V. S. Arutyunov, V. M. Rudakov, V. I. Savchenko, E. V. Sheverdenkin, O. G. Sheverdenkina, and A. Y. Zheltyakov, "Partial alkane oxidation kinetics at high pressures: methane oxidation in stainless steel and quartz reactors," *Theor. Found. Chem. Eng.*, **36**, no. 5, 472–476, 2002.

[115] S. Ergun, "Fluid through packed columns," *Chem. Eng. Prog.*, **48**, no. 2, 89–94, 1952.

[116] M. Winterberg and E. Tsotsas, "Impact of tube-to-particle-diameter ratio on pressure drop in packed beds," *AIChE J.*, **46**, no. 5, 1084–1088, 2000.

[117] R. Pešić, T. K. Radoičić, N. Bošković-Vragolović, Z. Arsenijević, and Ž. Grbavčić, "Pressure drop in packed beds of spherical particles at ambient and elevated air temperatures," *Chem. Ind. Chem. Eng. Q.*, **21**, no. 3, 419–427, 2015.

[118] O. Levenspiel, *Chemical reaction engineering*, 3rd ed. John Wiley & Sons Inc., 1999.

[119] R. S. Abdulmohsin and M. H. Al-Dahhan, "Axial dispersion and mixing phenomena of the gas phase in a packed pebble-bed reactor," *Ann. Nucl. Energy*, **88**, 100–111, 2016.

[120] H. L. Shulman, C. F. Ullrich, A. Z. Proulx, and J. 0. Zimmerman, "Performance of packed columns. I. Total, static, and operating holdups.," *AIChE J.*, **1**, no. 2, 247–253, 1955.

[121] S. Maduskar, A. R. Teixeira, A. D. Paulsen, C. Krumm, T. J. Mountziaris, W. Fan, and P. J. Dauenhauer, "Quantitative carbon detector (QCD) for calibration-free, high-resolution characterization of complex mixtures," *Lab Chip*, **15**, no. 2, 440–447, 2015.

[122] C. A. Beach, C. Krumm, C. S. Spanjers, S. Maduskar, A. J. Jones, and P. J. Dauenhauer, "Quantitative carbon detector for enhanced detection of molecules in foods, pharmaceuticals, cosmetics, flavors, and fuels," *Analyst*, **141**, no. 5, 1627–1632, 2016.

[123] C. S. Spanjers, C. A. Beach, A. J. Jones, and P. J. Dauenhauer, "Increasing flame ionization detector (FID) sensitivity using post-column oxidation–methanation," *Anal. Methods*, **9**, no. 12, 1928–1934, 2017.

[124] Swagelok, "Tubing Data," 2017. https://www.swagelok.com/downloads/webcatalogs/en/MS-01-107.PDF (accessed Jul. 14, 2020).

[125] S. V. L. Mahlaba, "Personal communication," 2021.

[126] M. M. Shirolkar, D. Phase, V. Sathe, J. Rodrguez-Carvajal, R. J. Choudhary, and S. K. Kulkarni, "Relation between crystallinity and chemical nature of surface on wettability: A study on pulsed laser deposited TiO_2 thin films," *J. Appl. Phys.*, **109**, no. 12, 2011.

[127] V. Bolis, C. Busco, M. Ciarletta, C. Distasi, J. Erriquez, I. Fenoglio, S. Livraghi, and S. Morel, "Hydrophilic/hydrophobic features of TiO2 nanoparticles as a function of crystal phase, surface area and coating, in relation to their potential toxicity in peripheral nervous system," *J. Colloid Interface Sci.*, **369**, no. 1, 28–39, 2012.

[128] A. E. Muslimov, M. K. Gadzhiev, and V. M. Kanevsky, "New approaches to increasing the superhydrophobicity of coatings based on ZnO and TiO_2," *Coatings*, **11**, no. 11, 1–12, 2021.

[129] E. van Steen, "Platinum catalyzes selective aerobic oxidation of methane to formaldehyde in the presence of liquid water", unpublished manuscript, 2022.

[130] A. M. Bahmanpour, A. Hoadley, and A. Tanksale, "Critical review and exergy analysis of formaldehyde production processes," *Rev. Chem. Eng.*, **30**, no. 6, 583–604, 2014.

[131] M. Watanabe, M. Osada, H. Inomata, K. Arai, and A. Kruse, "Acidity and basicity of metal oxide catalysts for formaldehyde reaction in supercritical water at 673 K," *Appl. Catal. A Gen.*, **245**, no. 2, 333–341, 2003.

Appendix A: Instrumentation and control

A.1 Pressure control

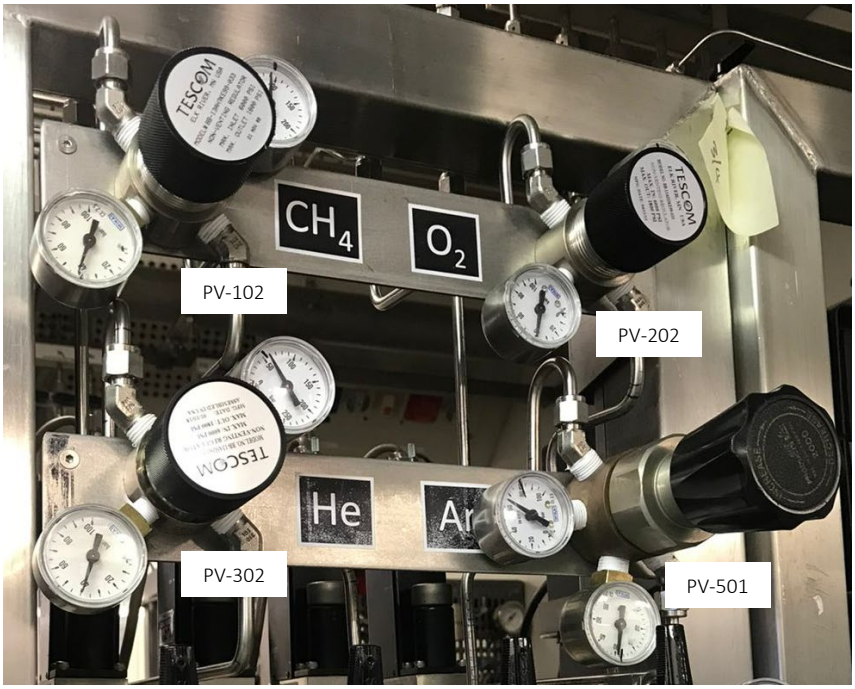

Figure A-1: Miniature BB-1 series Tescom™ piston-sensed pressure regulators for methane, oxygen and helium and Air Products diaphragm-sensed pressure regulator for argon with Wika analogue pressure gauges

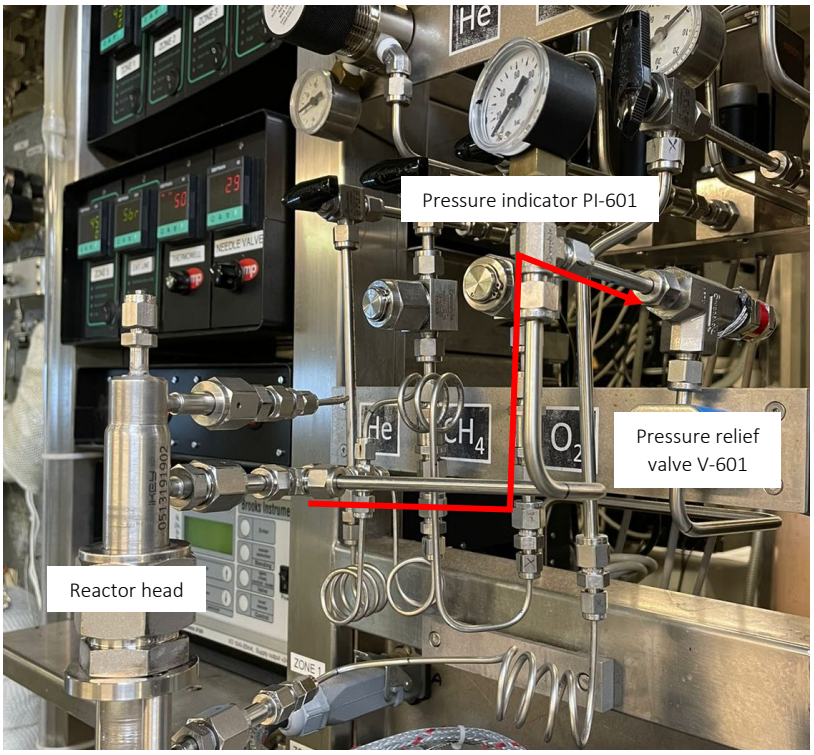

Figure A-2: Branched line after methane-oxygen-helium mixing point connecting the reactor head to the pressure relief valve V-601 and pressure indicator PI-601

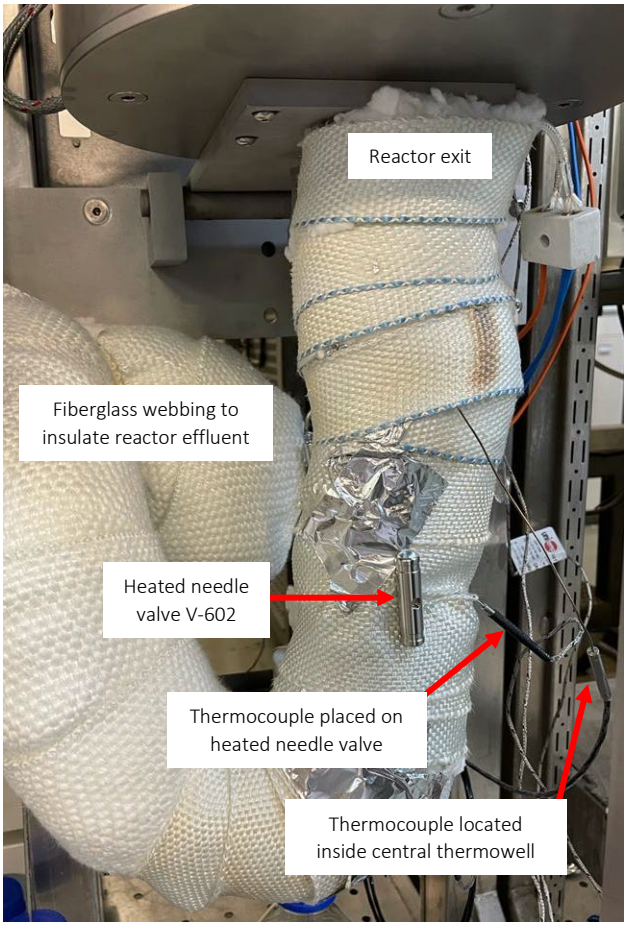

Figure A-3: Heated expansion valve V-602 used to control the pressure in the reactor and to reduce the pressure down close to atmospheric conditions

A.2 Flow control

Brooks flow control module and MFCs

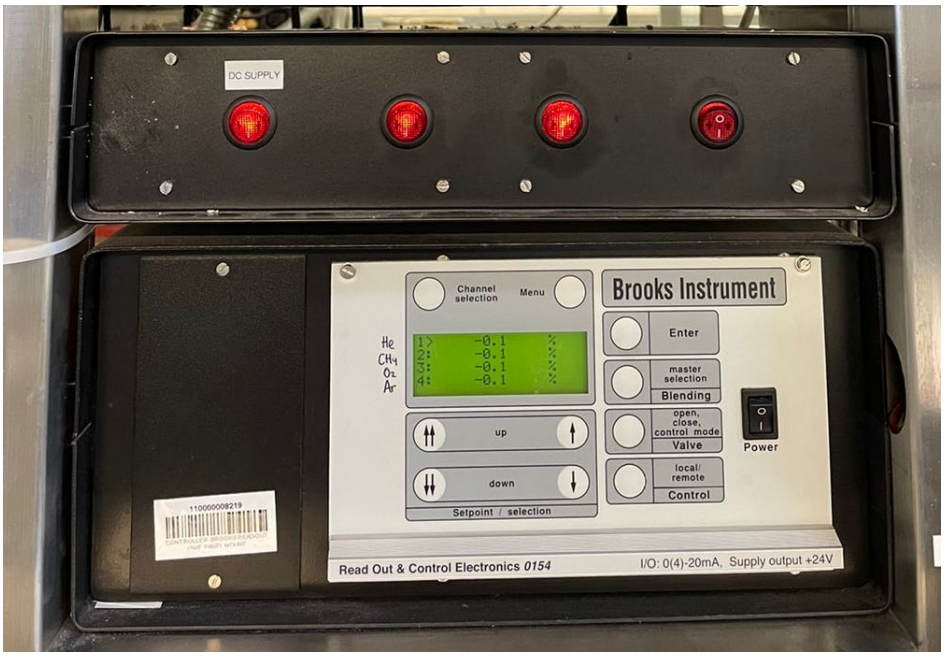

Figure A-4: Four-channel Brooks flow control module for methane, oxygen, helium and argon

Figure A-5: Brooks mass flow controllers for methane, oxygen, helium and argon

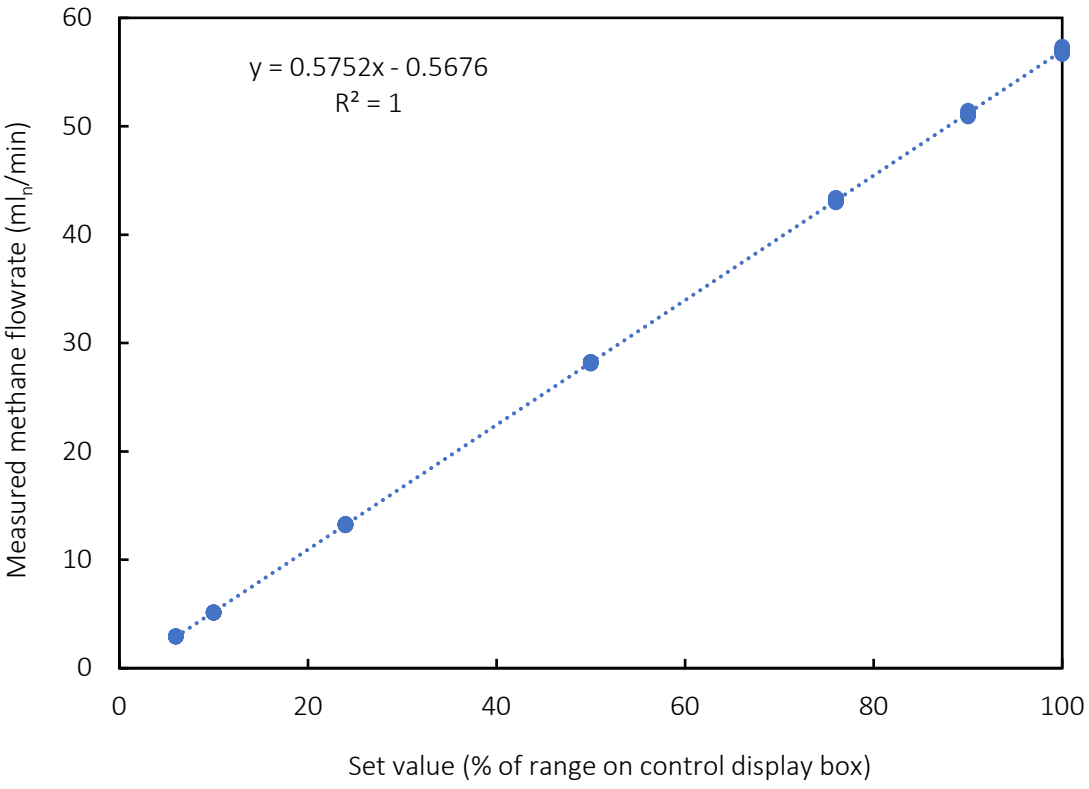

Figure A-6: Calibration curve for methane mass flow controller FV-101

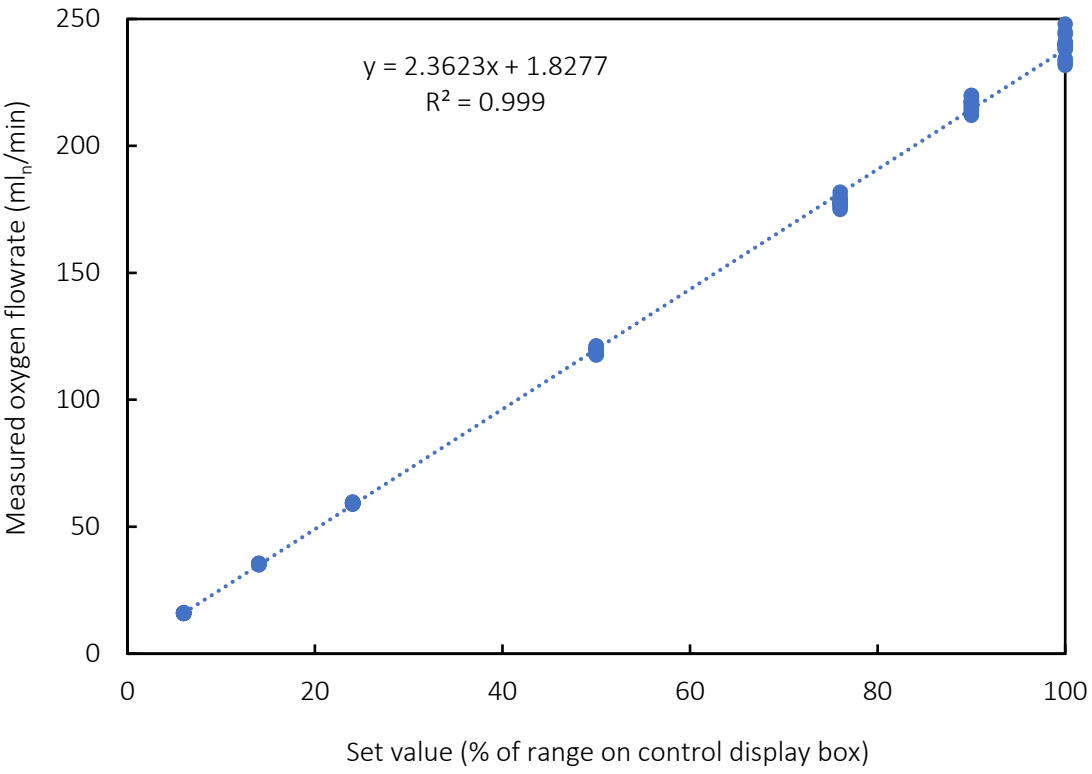

Figure A-7: Calibration curve for oxygen mass flow controller FV-201

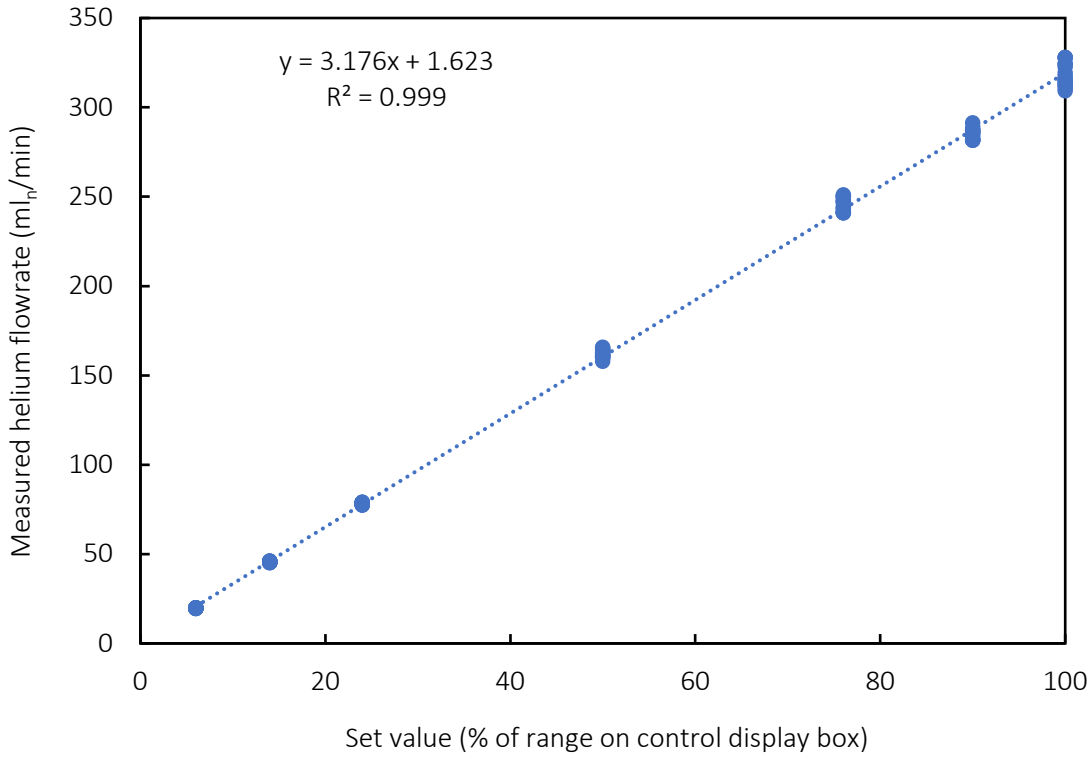

Figure A-8: Calibration curve for helium mass flow controller FV-301

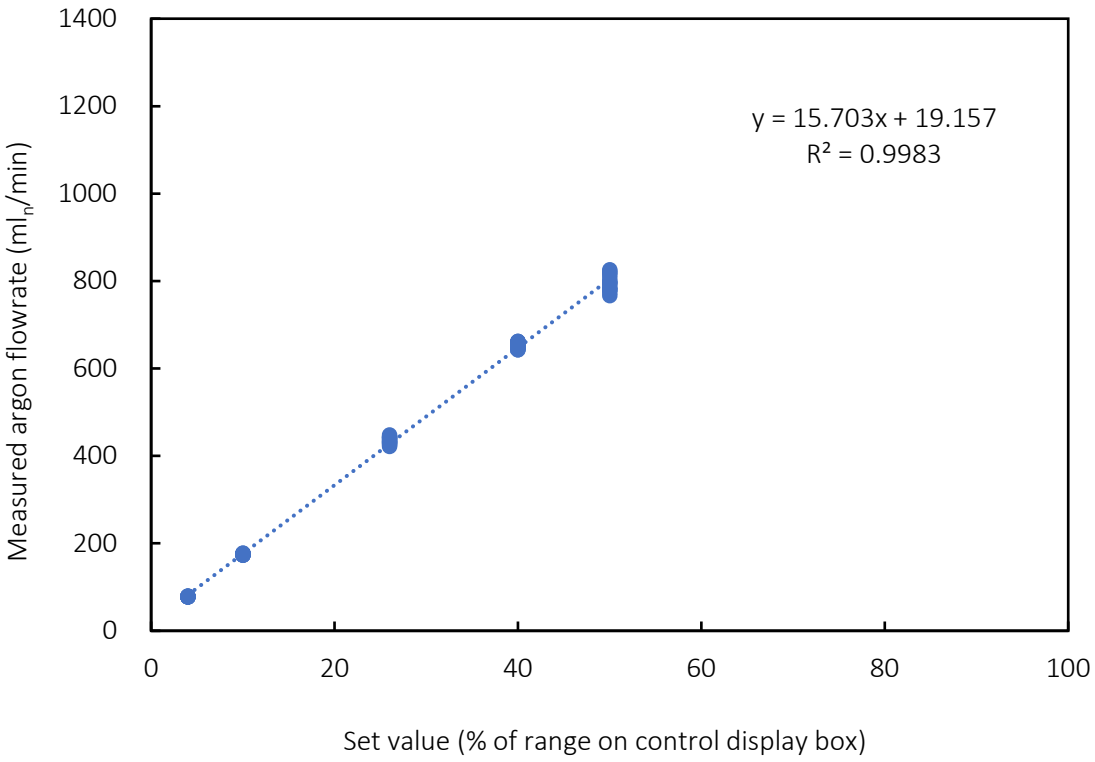

Figure A-9: Calibration curve for argon mass flow controller FV-501

Flow controller and indicator for liquid water

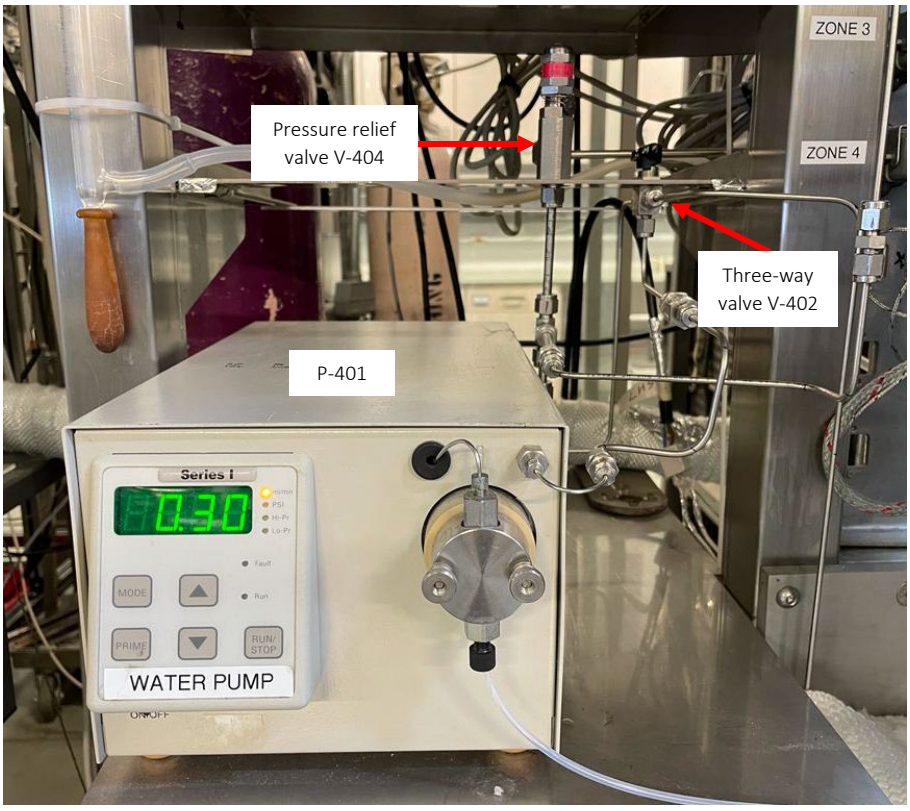

Figure A-10: Lab Alliance Series I HPLC pump P-401 to control the liquid water flowrate

A.3 Temperature control

Figure A-11: Six Gefran 600 temperature-controllers for the 5-zone furnace (TIC-601, TIC-602, TIC-603, TIC-604, TIC-605) and first heating loop of reactor effluent line (TIC-606); two Gefran 40 temperature-indicators for the thermocouple placed inside the central thermowell (TI-601) and the other thermocouple positioned on the heated needle valve V-602 (TI-602)

Figure A-12: Two Gefran 600 temperature-controllers for second heating loop of reactor effluent line (TIC-701) and for heating 6-port injection valve of GC-Polyarc®-FID system

Appendix B: Experimental data

B.1 Pt/TiO_2(P25) catalyst

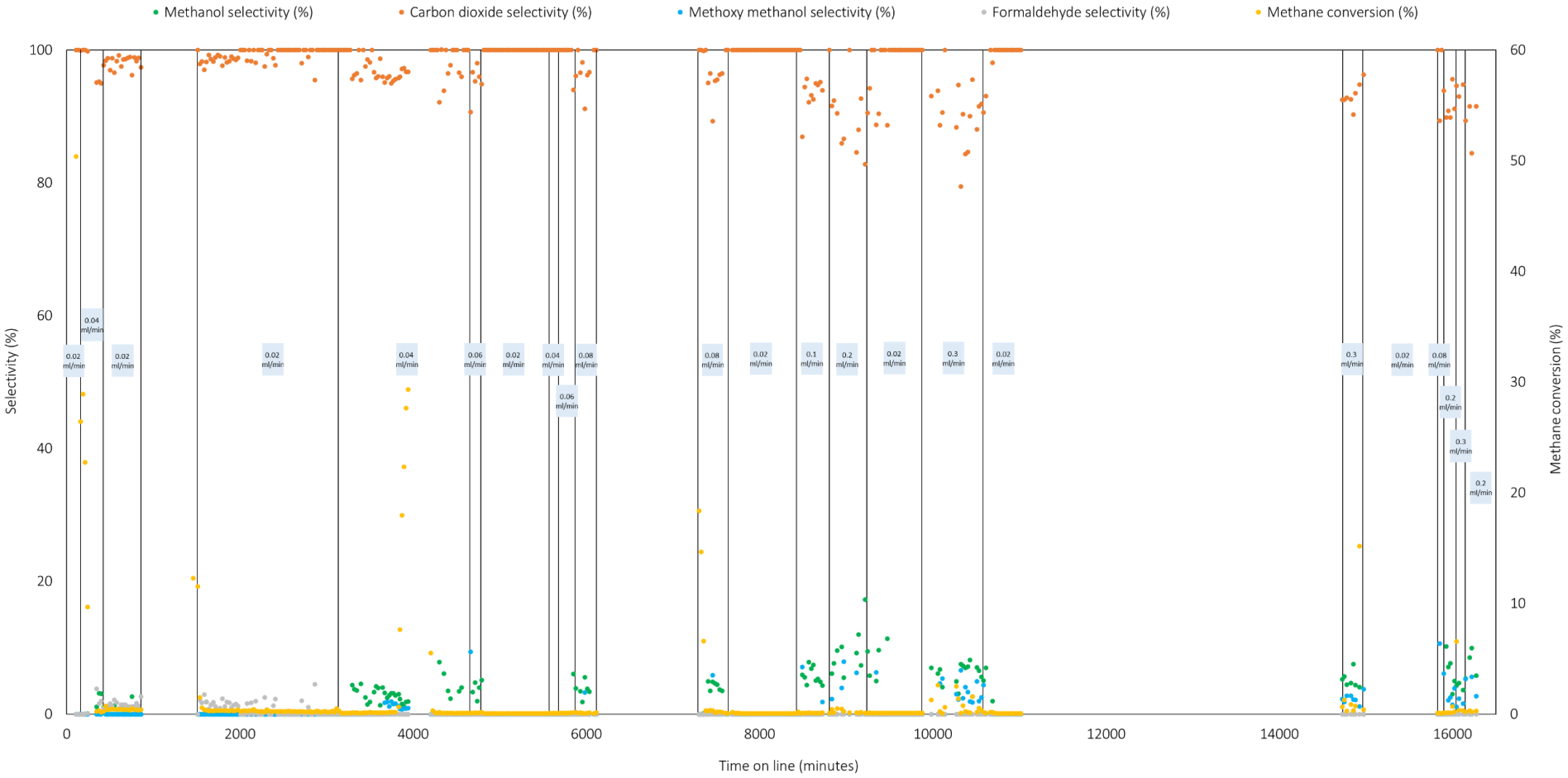

Figure B-1: Conversion of methane and product selectivity as a function of time on line over 10 wt.% Pt/TiO_2(P25) in presence of liquid water at 220 °C and 30 bar (inlet partial pressures P_{CH_4} = 0.5 bar, P_{O_2} = 1.5 bar, P_{sat,H_2O} = 23.1 bar, $F_{CH_4,o}/W$ = 3.1 mmol/g_{cat}.h; black lines indicating changes in water feed rate)

B.2 Pt/TiO_2(rutile) catalyst

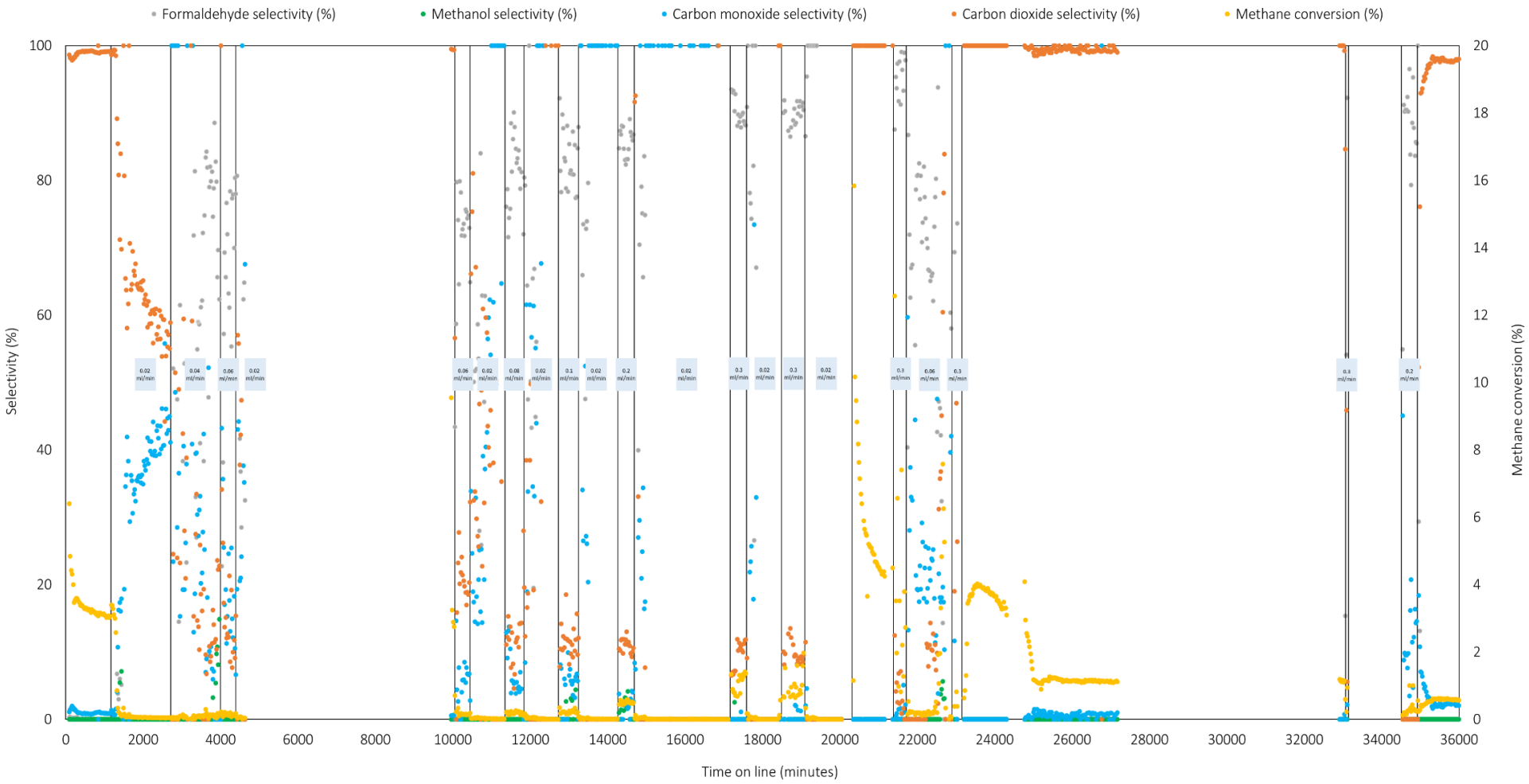

Figure B-2: Conversion of methane and product selectivity as a function of time on line over 10 wt.% Pt/TiO_2(rutile) in presence of liquid water at 220 °C and 30 bar (inlet partial pressures P_{CH_4} = 0.5 bar, P_{O_2} = 1.5 bar, P_{sat,H_2O} = 23.1 bar, $F_{CH_4,o}/W$ = 3.2 mmol/g_{cat}.h; black lines indicating changes in water feed rate